Imbibition into a thin porous medium: an experimental and pore-scale modeling study of coated paper

Hamed Aslannejad

Reading Committee:

Prof.dr. Michael A. Celia
Princeton University

Prof.dr.ir. H.M.A. Wijshoff
Eindhoven University of Technology

Prof.dr. Harald van Brummelen
Eindhoven University of Technology

Prof.dr. Patrick Gane
Aalto University

Dr. Daniel Markl
University of Strathclyde Glasgow

ISBN 978-90-6266-525-9

Printed in the Netherlands by proefschriften.net.

Imbibition into a thin porous medium: an experimental and pore-scale modeling study of coated paper

Imbibitie in een dun poreus medium: Een experimentele- en porieschaal modellering studie van gecoat papier

(met een samenvatting in het Nederlands)

PROEFSCHRIFT

ter verkrijging van de graad van doctor aan de Universiteit Utrecht op gezag van de rector magnificus, prof.dr. H.R.B.M. Kummeling, ingevolge het besluit van het college voor promoties in het openbaar te verdedigen op maandag 28 januari 2019 des middags te 4.15 uur
op dag 00 maand 2011 des ochtends te 10.30 uur

door

Hamed Aslannejad
geboren op 2 juni 1985 te Sarab, Iran

Promotor:
Prof.dr. S. M. Hassanizadeh

Copromotoren:
Dr. A. Raoof
Dr. N. Tomozeiu

This thesis was accomplished with financial support from Océ-Technologies B.V. and European Research Council (ERC) under Grant Agreement no. 341225.

To my wife who is my secret of happiness and success

Acknowledgments

Firstly, I would like to express my sincere gratitude to my supervisor Prof. Majid Hassanizadeh. He has been a tremendous mentor to me. I would like to thank him for encouraging my research and for allowing me to grow as a research scientist. His advice on both research as well as on my career have been priceless. I could not have imagined having a better advisor and mentor for my Ph.D. study.

Besides my supervisor, I would like to thank the rest of my thesis committee: Dr. Amir Raoof and Dr. Nicolae Tomozeiu for their insightful comments and encouragement, but also for the hard questions, which incented me to widen my research from various perspectives. I would like to thank Prof. Ruud Schotting for accepting me as his teaching assistant for several courses; that was absolutely a valuable opportunity.

I thank my colleagues in Utrecht University for the stimulating discussions and for all the fun we have had in the last four years. I truly enjoyed not only our scientific discussion with Niels Hartog but also the Words of the Week lessons, which helped me to improve my Dutch language skills. I would like to than you Jan van Lopik to be a nice friend and invite me several times to the experimental site located outside of the campus, I enjoyed our chats and all the practical measurement techniques he was using at that site.

During last year of my PhD, I had the chance to meet Johan van Leeuwen more often than before, which helped me to know how to find my way in future career. I would like to thank all of my friends who supported me in writing, and incented me to strive towards my goal; Enno de Vries, Luwen Zhuang, Suzanne Faber, Gilian Schout, Amir Hossein Tavangarrad, Lifei Yan, Vahid Nikpeyman and Ioannis Zarikos .

Many thanks to my office mate Matthijs de Winter, who I met at first year of my PhD when I needed to use FIB-SEM imaging technique. He was so kind and helpful and we ended up with writing my first publication. Later on at my last year, he started his postdoc in our group and I had the chance to spend more time with him and enjoy our coffee breaks talking about all various topics. I am also grateful to my old office mate Thomas Sweijen; I enjoyed not only our coffee breaks but also our scientific collaboration.

Thanks to Annuska Exel and Margreet Evertman to be a very kind and patient secretaries of our group, they were always happy to help me with administrative works.

In addition, I thank my fellow scientists from Oce and Omya companies for providing facilities and valuable discussions. I want to thank Prof. Patrick Gane and Dr. Cathy Ridgway from Omya for their excellent collaboration and for all of the opportunities I was given to conduct my research and finish my dissertation. Thanks to people from Oce; Dr. Richard van Hameren, Prof. Herman Wijshoff, Dr. Louis Saes, Dr. Jurriaan Luiken, Sjors Schellekens and Tiny Ritzen. They definitely provided me with the tools and advices that I needed to choose the right direction and successfully complete my dissertation.

Above all I would like to thank my wife Maryam for her love and constant support and for keeping me sane over the past few months. Thank you for being my editor, proofreader and sounding board. But most of all, thank you for being my best friend. I owe you everything.

Hamed Aslannejad

Contents

LIST OF PUBLICATIONS RELATED TO PHD THESIS (UPDATED ON 18TH DECEMBER 2018)

Title	Cited By	Year
Characterizing the hydraulic properties of paper coating layer using FIB-SEM tomography and 3D pore-scale modeling, H Aslannejad, SM Hassanizadeh, A Raoof, DAM de Winter, N Tomozeiu, Chemical Engineering Science 160, 275-280	13	2017
Capillary pressure–saturation relationships for porous granular materials: Pore morphology method vs. pore unit assembly method T Sweijen, H Aslannejad, SM Hassanizadeh Advances in Water Resources 107, 22-31	9	2017
Heat release at the wetting front during capillary filling of cellulosic micro-substrates, A Terzis, E Roumeli, K Weishaupt, S Brack, H Aslannejad, J Groß, Journal of colloid and interface science 504, 751-757	5	2017
Study of hydraulic properties of uncoated paper: image analysis and pore-scale modeling, H Aslannejad, SM Hassanizadeh,Transport in Porous Media 120 (1), 67-81	5	2017
Occurrence of temperature spikes at a wetting front during spontaneous imbibition, H Aslannejad, A Terzis, SM Hassanizadeh, B Weigand Scientific reports 7 (1), 7268	4	2017
Grain-scale modelling of swelling granular materials using the discrete element method and the multi-sphere approximation T Sweijen, SM Hassanizadeh, H Aslannejad, S Leszczynski Poromechanics VI, 329-336	3	2017
Modeling water imbibition into coated and uncoated papers AR Behzad Ghanbarian, Hamed Aslannejad, Chemical Engineering Science 189, 33-42	1	2018
Movement of a liquid droplet within a fibrous layer: Direct pore-scale modeling and experimental observations, H Aslannejad, H Fathi, SM Hassanizadeh, A Raoof, N Tomozeiu, Chemical engineering science 191, 78-86		2018
Droplet Imbibition into Paper Coating Layer: Pore-Network Modeling Simulation, X Yin, H Aslannejad, ET de Vries, A Raoof, SM Hassanizadeh Transport in Porous Media 125 (2), 239-258		2018
Water flux reduction in microfiltration membranes: a pore network study SM Abdoli, S Shafiei, A Raoof, A Ebadi, Y Jafarzadeh, H Aslannejad Chemical Engineering & Technology 41 (8), 1566-1576		2018

Introduction

Thin porous coating layers are widely used in industrial products to enhance their performance or to add specific feature to the product. For instance, in case of printing industry, a thin layer of $CaCO_3$ is added to certain type of papers to control ink settlement and enhance the print quality. Other example is thin Gas Distributor Layer (GDL) of fuel cells, which distributes the fuel and oxidant gases and meanwhile conducts the electrons. Thin layers of diaper and membranes are other two examples.

Inkjet and offset printing are two most commonly used printing techniques used for mass production scale. Offset printing is basically contact-based technique since paper and print roller touch each other during print process. However, inkjet printing is a contactless technique where ink droplets are jetted from a distance onto the surface of the printing substrate. In both printing techniques, water is involved: inkjet aqueous ink and offset fountain solution.

Inkjet printing is attracting much attention due to its potential in the printing of graphics, 3D objects, medical applications, paper-based diagnostic devices and electronics (de Gans et al. 2004), (López-Marzo and Merkoçi 2016), (Suffield and Jokar 2008), (Gambaryan-Roisman 2014). In most of the cases, paper is used as substrate and droplets are jetted on its surface. The surface of paper substrate can be treated to deliver specific characteristics. For instance, in inkjet printing of graphics, a thin layer is added on surfaces of paper in order to confine ink spreading and result in better print quality.

In this chapter, a brief understanding of printing processes, ink types, and paper manufacturing will be provided. At the end of the chapter, main research question and a road-map toward answering them will be provided.

1.1 Inkjet printing

Inkjet printing is a liquid phase deposition technique. The liquid phase consists of a solute dissolved or dispersed in a solvent. The inkjet printing involves ejection of a fixed amount of liquid phase from a nozzle onto a substrate. The ejected droplet falls due to gravity. The impinged droplet spreads and penetrates into paper due to surface tension aided flow (Singh et al. 2010).

Inkjet printer have been used for graphics printing, such as books, flyers, and photos. They include not only office-size printers but also mass production printers which are able to print 300 pages per minute (Oce 2016). Fig. 1.1. Shows an example of a mass production inkjet printer.

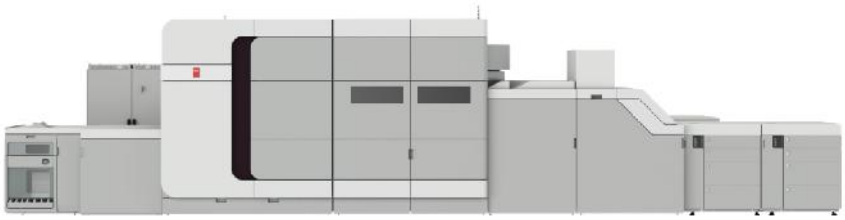

Figure 1.1 A general view of Oce VARIO PRINT I300 inkjet printer

Inkjet printing of the graphic arts can be adapted to produce large volume of organic electronics. The main advantages of the printing technique are contact-less, additive patterning, and mask-less approach. Other attractive features are low costs, scale up and mass production ability. In recent years, inkjet printing has been used in several areas like

- organic thin-film transistors
- light-emitting device
- printing of magnetic nanoparticles
- organic thin film transistors i.e. LEDs, solar cells

Depending on the application, different printers may use a variety of ink compositions, curing methods, and substrate structure (Kettle et al. 2010).

There are mainly two types of dispensers used in inkjet printing; drop on demand (DOD) and continuous inkjet (CIJ). DOD type is the most common type used in office inkjet printers. In DOD type, ink droplets are jetted only when needed. The DOD printing head is usually thermal or piezoeectric type. Although DOD types are usually smaller, cheaper and able to induce very tiny droplets to produce higher

print resolution, they need intensive maintenance during operation. DOD dispensers may use water-based, non-aqueous, phase change, and UV-curable inks (Le 1998).

Since the droplet formation is a continuous process in CIJ printers, they are usually faster than DOD types. They use water-based ink and produce larger droplets (compared with DOD) and, consequently, have lower resolution (Kettle et al. 2010).

There are two types of dryers being used in inkjet printers; drum air and UV dryer; the latter used when UV ink is applied. The temperature of the air dryer and power of the UV light can determine the moisture content of the final print.

As inkjet printing is a non-contact method, the droplets are jetted from the nozzle and they settle on the surface of paper and slightly penetrate into the paper layer. Pore size distribution of the paper layer, its chemistry and connectivity of pores determine the optimal absorption of ink.

During inkjet printing, once an ink droplet reaches the paper surface, spreading and evaporation processes determine overall ink penetration. The dynamics of these processes affect the final print quality. In order to optimize ink penetration during inkjet printing, paper is often coated with a layer of ultra-fine mineral particles, usually composed of kaolin or calcium carbonate and bound together with an adhesive. Surface-modified calcium carbonate and clays, colloidal-precipitated calcium carbonate, alumina silicate, and zeolite are considered to be among the most promising pigments (Malla and Devisetti 2005) and (Vikman and Vuorinen 2004). The extent of ink penetration depends on the structure of this coating layer as well as fluid properties of the employed ink (Heard et al. 2004).

The porosity and pore size distribution of a coating determines the extent, speed, and final distribution of the jetted ink. Figure 1.2 shows an overview of the processes that occur during inkjet printing (Kettle et al. 2010). The specified times indicate the approximate moment at which various phenomena are expected to start. The forces that cause lateral spreading of a droplet on the paper surface compete with the capillary suction of liquid into the paper (Girard et al. 2006). Capillarity is the dominant force drawing ink into the pore structure. Micro capillary penetration starts typically within 0.1 ms after the droplet arrives (Ridgway and Gane 2002), (Desie et al. 2004).

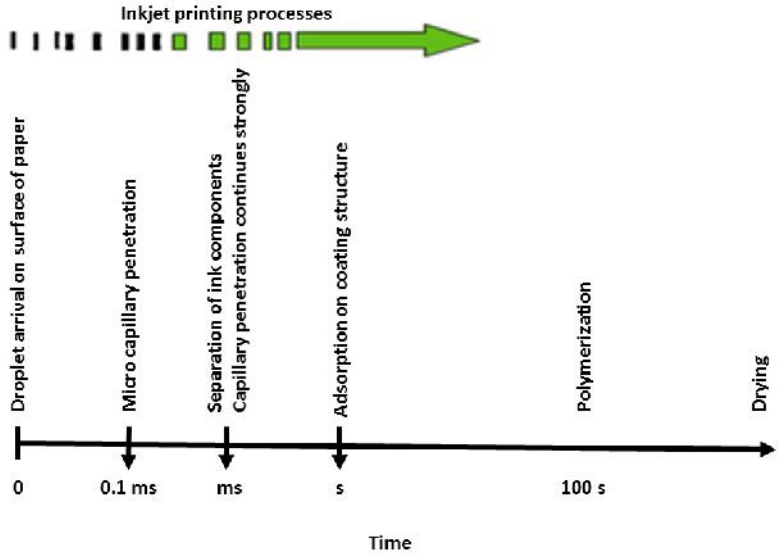

Figure 1.2 An overview of the processes that occur during inkjet printing (Kettle et al. 2010)

1.2 Offset printing

Offset printing is a commonly used printing technique in which the print pattern is first transferred to a rubber blanket and then to the printing surface (Hird 2000). This is an indirect printing technique where due to chemical surface treatment, image area receives ink and non-image area gets water-based film (called fountain solution). The roller containing image and non-image area transfers ink onto the paper. Despite the inkjet printing, offset printing is contact-based printing technique and paper is pressed during printing (Tåg et al. 2007).

1.3 Ink

The ink used in inkjet printing process can be categorized based on its physical properties or based on its colorant part. The most common types are water-based, non-aqueous, UV-curable, phase change or dye-based and pigment-based inks. The main parameters of the ink are viscosity, density, surface tension, stability of ink, and jet stability (Kettle et al. 2010).

In order to modify ink properties, an additive may be used. For instance, biocides may be added to control microbial growth, buffer to adjust the pH, surface active agents to define droplet stability and accelerate surface wetting, and binders

to pigment-based ink in order to bind them to the surface of paper. In total the additives comprise 4-10% of the ink (Le 1998).

For a typical inkjet printer, the water-based ink consists of 2-5% weight of dye or pigment, 2-5% surfactants, 30% humectant (ethylene glycol), and 60% water (Lee et al. 2002). The most important properties of the ink are represented by surface tension, viscosity and density. Figure 1.3 illustrates main components of printing paper and ink.

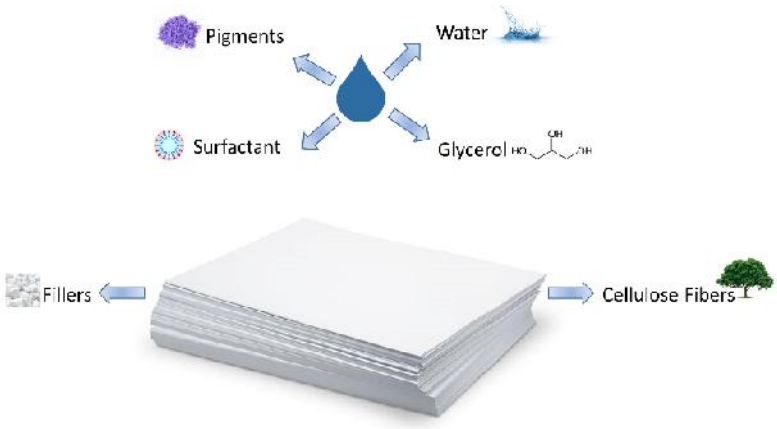

Figure 1.3 Printing paper and main components of ink

1.4 Paper and paper manufacturing

Paper is a thin fibrous porous medium consisting of cellulose fiber, which is oriented in different directions. Fibres diameter and length varies and depends on source, which could be:

- Deciduous trees: Birch, poplar, beech, eucalyptus
- Conifer trees: Spruce, fir, pine

As a result of manufacturing, fibers usually lie in two main directions, machine direction (the direction that the calender rollers press on paper layer) and perpendicular to machine direction. The fibers are bonded to each other due to hydrogen bonding, which occurs during the drying step.

Here, as an example, the paper manufacturing steps taken by Sappi company will be explained (Sappi 2012). Paper manufacturing starts with bark removal and chopping the logs. Then entering digester columns, lignin is removed and plant

fibers are separated. Then, during a washing step the leftover lignin and dirt are removed, and finally, in the bleaching step, the colour of fibers is turned to white. Figure 1.4 shows the aforementioned steps.

Figure 1.4 Paper manufacturing steps, from tree to white fiber

After the bleaching step, the treated fiber is transported to paper mills. There water is added. So far, water is the main process material in paper mill plants. There, after adding water, the mixture of water and fibers is refined and then calcium carbonate and clay are added to reach the required mechanical properties. Then, the mixture enters the paper machine and excess water is removed as it goes between press rollers. At the end of the paper machine, papers go through long drying tray and there the drying process continues until a desired moisture content is reached. At the end of the drying step, the paper has enough strength to support itself. In the next step, the paper sheet passes between two finely polished calender rollers in order to have thickness consistency.

Figure 1.5 shows the processes taking place in a paper machine.

Figure 1.5 Paper manufacturing steps, from white fiber sheets to calendered fibrous layers

In order to add some specific characteristics to the paper, the uncoated paper form the previous section enters a "sizing and coating" process. There a coating layer is applied on the fibrous layer in two steps:

- First, a coating material made of course grains is applied on the fibrous layer using a film transport technique. In this technique, the coating pigments and starch are sprayed on an elastic layer and then the layer transfers the material onto the fibrous web. Figure 1.6 shows the first step.

In the second step, coating material of finer grains is applied under pressure in a continuous stream and then excess coating material is removed by special steel blades. Figure 1.7 shows the process of second coating deposition.

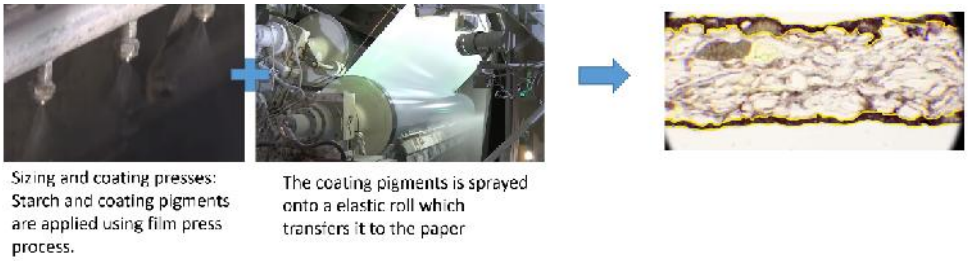

Figure 1.6 First paper coating layer addition on the fibrous layer

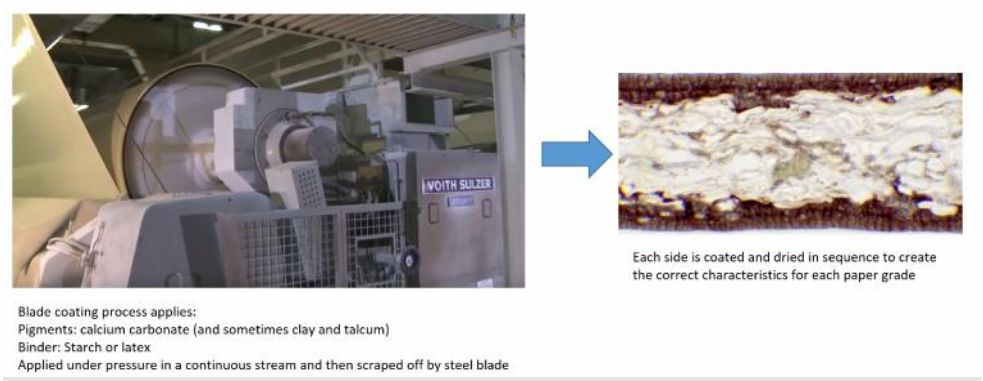

Figure 1.7 Second step of paper coating layer addition

At the last stage of paper fabrication, jumbo reels are fed into a rotary cutter in order to cut them to narrower reels. They are then sent to the sheeter unit, which cuts them into standard sizes and stacks them.

1.5 Objectives and Outline of this thesis

This study will look at an uncoated paper versus the structure of the coating layer of coated paper. In order to investigate water-based ink imbibition into printing paper samples (coated and uncoated), one first needs to characterize the layer, onto which the liquid drops arrive (substrate layers) and to extract their hydraulic properties. Therefore, this research will be started by the characterization of the coating layer (in the case of coated paper), the fibrous layer, and the interfacial region between the two layers (the coating and fibrous layers).

In order to characterize the layers and interfacial region between them, suitable imaging techniques are needed. For the fibrous layer, since pores in the range of few micrometers are present, a micro computed tomography (µCT) is needed. Using the µCT-imaging technique, the three-dimensional (3D) geometry of pores can be extracted. The geometry will include detail information about pore sizes, location, and their connectivity.

Since µCT is not able to capture pores of nano-scale size, a higher resolution imaging technique is needed to extract pore network information of the coating layer of paper. The coating layer is very thin and contains fine grains with sub-micrometers diameters. We will use Focused Ion Beam Scanning Electron Microscopy (FIB-SEM) to image the coating layer of paper.

FIB-SEM is also the right tool for imaging of the interfacial region of coating and fibrous layers, which include both fibers (size in order of micrometers) and the primary coating material (within the nanometer size range).

Having imaging results of the layers, image analysis methods can be used to reconstruct the pore space of layers. Within the reconstructed layer, one can use pore-scale modeling tools to extract hydraulic properties of the layer. In chapters two, three, and four, characterization of the coating layer, fibrous layer, and interfacial region will be presented, respectively. Results are then used in fluid dynamics simulation pursued in the following chapters.

In chapter 5, droplet imbibition into the coating and fibrous layer will be modelled and studied. Results of such a modeling work can be used in order to better understand ink imbibition into the paper layer and to optimize characteristic properties of the ink and paper substrate.

Finally, in chapter six, an interesting phenomenon, which occurs during water-based ink imbibition into paper layers, will be studied. In this chapter the temperature rise during imbibition and mechanisms behind it are explained. The extent of temperature rise in a paper layer during printing is discussed.

At the end, a summary of the work will be presented and suggestions for further research will be provided.

1.6 References:

de Gans, B.-J., Duineveld, P. C. & Schubert, U. S. Inkjet Printing of Polymers: State of the Art and Future Developments. Adv. Mater. 16, 203–213 (2004).

López-Marzo, A. M. & Merkoçi, A. Paper-based sensors and assays: A success of the engineering design and the convergence of knowledge areas. Lab on a Chip 16, 3150–3176 (2016).

Suffield, S. & Jokar, A. Modeling the Flow of a Liquid Droplet Diffusing Into Various Porous Media for Inkjet Printing Applications. in Volume 10: Heat Transfer, Fluid Flows, and Thermal Systems, Parts A, B, and C 1013–1022 (ASME, 2008). doi:10.1115/IMECE2008-68151

Gambaryan-Roisman, T. Liquids on porous layers: wetting, imbibition and transport processes. Curr. Opin. Colloid Interface Sci. 19, 320–335 (2014).

Singh, M., Haverinen, H. M., Dhagat, P. & Jabbour, G. E. Inkjet Printing-Process and Its Applications. Adv. Mater. 22, 673–685 (2010).

Specificaties Océ VarioPrint i300 - Canon Nederland. Available at: https://www.canon.nl/business-printers-and-faxes/cut-sheet-colour-printers/varioprint-i300/specifications/. (Accessed: 22nd October 2018)

Kettle, J., Lamminmäki, T. & Gane, P. A review of modified surfaces for high speed inkjet coating. Surf. Coatings Technol. 204, 2103–2109 (2010).

Le, H. P. Progress and trends in ink-jet printing technology. J. Imaging Sci. Technol. 42, 49–62 (1998).

Malla, Prakash B. Devisetti, S. Novel kaolin pigment for high solids ink jet coating. Pap. Technol. 46, 17–27 (2005).

Vikman, K. & Vuorinen, T. Water fastness of ink jet prints on modified conventional coatings. 48, 138–147 (2004).

Heard, P. J., Preston, J. S., Parsons, D. J., Cox, J. & Allen, G. C. Visualisation of the distribution of ink components in printed coated paper using focused ion beam techniques. Colloids Surfaces A Physicochem. Eng. Asp. 244, 67–71 (2004).

Girard, F., Attané, P. & Morin, V. A new analytical model for impact and spreading of one drop: Application to inkjet printing. Tappi J. 5, 24–32 (2006).

Ridgway, C. J. & Gane, P. A. C. Controlling the absorption dynamic of water-based ink into porous pigmented coating structures to enhance print performance. Nord. Pulp Pap. Res. J. 17, 119–129 (2002).

Desie, G., Deroover, G., De Voeght, F. & Soucemarianadin, A. Printing of dye and pigment-based aqueous inks onto porous substrates. J. Imaging Sci. Technol. 48, 389–397 (2004).

Lee, H. K., Joyce, M. K., Fleming, P. D. & Cameron, J. H. Production of a single coated glossy inkjet paper using conventional coating and calendering methods. (2002).

Sappi. The Paper Making Process. (2012). Available at: https://www.youtube.com/redirect?redir_token=VEjJPq2aJlcjBgVBNfN_Rc4CZfl8MTU0MDIxMjEyMkAxNTQwMTI1NzIy&event=video_description&v=E4C3X26dxbM&q=http%3A%2F%2Fwww.na.sappi.com%2Feducation%2Flifecycle.

Characterizing the hydraulic properties of a porous coating of paper using FIB-SEM tomography and 3D pore-scale modeling

Abstract

Paper used in the printing industry generally contains a relatively thin porous coating covering a thicker fibrous base layer. The three-dimensional pore structure of coatings has a major effect on fluid flow patterns inside the paper medium. Understanding and quantifying the flow properties of thin coating layers is hence crucial. Pore spaces within the coating have an average size of about 180 nm. We used scanning electron microscopy combined with focused ion beam (FIB-SEM) methods to visualize the nano-scale pore structure of the paper coating layer. Post-processing of the FIB-SEM images allowed us to reconstruct the three-dimensional pore space of the coating. The 3D FIB-SEM images were analysed in detail to obtain pore size distribution and porosity values. The permeability was estimated using the GeoDict software, based on solutions of the Stokes equation. By determining the porosity and permeability of increasingly larger domain sizes, we estimated the size of a representative elementary volume (REV) for the coating layer to be 60 μm^3, which is well within the volume analysed using FIB-SEM. The estimated porosity and permeability of the REV domain were 0.34 and 0.09 mDarcy, respectively, relatively close to previous literature values for coatings. Using the pore morphology method, capillary pressure-saturation (*Pc-S*) and relative permeability curves of the REV domain could be constructed next. The *Pc-S* curves showed that the coating had a high air entry suction, which is very favourable for printing in that ink will invade the coating as soon as it is applied to the coating. Our results are essential for macroscale modelling of ink penetration into a coating layer during inkjet printing. Macroscopic models can be valuable tools for optimization of the penetration depth and the spreading of ink on and within paper substrates.

Published as: H Aslannejad, SM Hassanizadeh, A Raoof, DAM de Winter, N Tomozeiu, M Th van Genuchten. Characterizing the hydraulic properties of paper coating layer using FIB-SEM tomography and 3D pore-scale modeling- *Chemical Engineering Science 160 (2017), 275-280*

2.1 Introduction

During inkjet printing, once an ink droplet reaches the paper surface, spreading and evaporation processes determine overall ink penetration. The dynamics of these processes affect the final print quality. In order to optimize ink penetration during inkjet printing, paper is often coated with a layer of ultra-fine mineral particles, usually composed of kaolin or calcium carbonate and bound together with an adhesive. Surface-modified calcium carbonate and clays, colloidal-precipitated calcium carbonate, alumina silicate, and zeolite are considered to be among the most promising pigments (Malla and Devisetti 2005) and (Vikman and Vuorinen 2004). The extent of ink penetration depends on the structure of this coating as well as on the fluid properties of the employed ink (Heard et al. 2004).

The porosity and pore size distribution of a coating determines the extent, speed, and final distribution of the injected ink. Figure 1.2 shows an overview of the processes that occur during inkjet printing (Kettle et al. 2010). The specified times indicate the approximate moment at which various phenomena are expected to start. The forces that cause lateral spreading of a droplet on the paper surface compete with the capillary suction of liquid into the paper (Girard et al. 2006). Capillarity is the dominant force drawing ink into the pore structure. Micro capillary penetration starts typically within 0.1 ms after the droplet arrives (Ridgway and Gane 2002), (Desie et al. 2004).

Several studies have been conducted to explore the performance of ink on different papers. For example, Dalton et al. (Dalton et al. 2002) used secondary ion mass spectrometry and X-ray photoelectron spectroscopy (XPS) to determine the final distribution of ink in a cross section of paper samples. Alam et al. (Alam et al. 2009) used computational fluid dynamics simulations in order to calculate the permeability of three packing structures representing the coating layer of paper. Calculated permeability values were within one order of magnitude of reported experimental equivalents. Matilainen et al. (Matilainen et al. 2012) studied the spreading and penetration of bio-based ink, which contained laccase enzyme and its substrate ABTS (2,2'-Azinobis [3-ethylbenzothiazoline-6-sulfonic acid]-dimmonium salt), on three different coated printing papers. Optical and confocal microscopy techniques were used, together with a tape laminating method (Matilainen et al. 2012). The pore size distribution of the printing substrate was further explored using mercury porosimetry. Pore sizes were found to be 1–5 µm for the base layer, and 0.05–0.5 µm for the coating pores.

Lamminmäki et al. (Lamminmäki et al. 2012) studied the coupled effects of pore structure and swelling of the binder of a coating layer on ink imbibition in terms of its penetration and spreading. The coating structure was studied with respect to its absorption behavior for polar and non-polar liquids. The measurements were performed on compressed tablets (having thicknesses of about 200 µm) containing polyvinyl alcohol (PVOH) or Styrene Acrylic latex (SA) as the binder. Results indicated that small pores play a dominant role in the ink imbibition process during the first two seconds. Simultaneously, water diffusion into the hydrophilic PVOH binder caused its swelling. This swelling reduced the diameters of the remaining pores, thus decreasing capillary flow. In contrast, the SA latex binder did not absorb water, which hence indicates capillary absorption was the dominant process.

Short-time processes during the early stages of ink penetration cannot be described using equilibrium fluid flow simulation methods. The liquid advance in a porous structure is usually simulated using some approximate method, e.g. as described in Lamminmäki et all (Lamminmäki et al. 2012). A well-known method is based on the Lucas–Washburn equation, which assumes that the coating consists of a collection of vertical capillary tubes. The method was improved later by Schoelkopf et al. (Schoelkopf et al. 2002) and Ridgway and Gane (Ridgway et al. 2002), who employed the Bosanquet equation (Bosanquet 1923) to show the role of pore size and viscous drag (Ridgway et al. 2002).

The spreading and penetration of ink is generally very much affected by such paper bulk properties as porosity, permeability, thickness, moisture content, temperature, and layer structure. Gane et al. (Gane et al. 2008) showed that standard ground calcium carbonate coatings, because of their relatively broad particle size distributions and low permeability, produce slower initial rates of absorption of ink than more refined coating having a narrower pore size distribution and higher permeability. They found that coatings with a higher specific surface area and permeability have a faster initial moisture uptake.

The aim of this work is to obtain the detailed pore structure of a coating layer at a very high resolution, and from this its hydraulic properties using a pore-scale computational method. We first introduce a visualization method of extracting the 3D structure of the layer by using FIB-SEM imaging. The approach allowed a resolution of down to three nanometers. The method involved many cycles of removing a very thin cross-sectional layer by ion beam, and imaging by electron microscopy. Image analysis was used to obtain pore morphological information about the coating layer. Finally, using the pore morphology method, pore-scale

simulations were carried out to estimate the effective hydraulic properties of the coating. Such estimates are required for continuum scale-models of ink movement in the coating layer.

2.2 Material and Methods

2.2.1 Paper sample

The paper samples used in this study (i.e., Sappi Magno Gloss paper) were made of a fibrous layer covered on both sides with coating material. The total thickness of the samples was 83 µm, with a basis weight of 115 g/m^2 and a porosity of 0.34. The coatings, which had a thickness of 12.8 µm on each side of the paper, consisted mostly of $CaCO_3$ along with a small amount of binder. All samples were kept under room conditions (21°C and relative humidity of 88%). A typical image of the surface and a vertical cross section of the coating are shown in Figure 2.1.

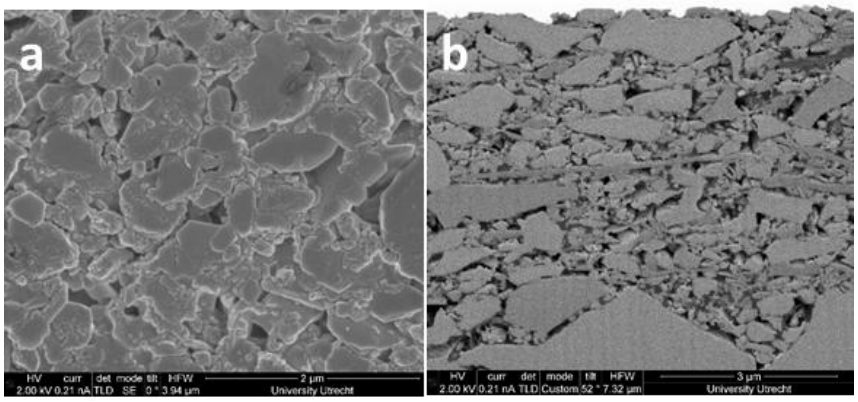

Figure 2.1 Surface (a) and cross-sectional (b) views of the paper coating

2.2.2 FIB-SEM imaging

Samples for imaging were prepared by attaching a small piece (1 cm^2) of coated paper to a standard aluminum SEM stub with a conductive carbon sticker. The paper was sputter coated with approximately 5 nm of platinum (HQ280; Cressington Scientific Instruments Ltd, Watford, UK). The samples were placed in the vacuum chamber of a Nova Nanolab 600 focused ion beam scanning electron microscope (FIB-SEM) (FEI Company, Eindhoven, Netherlands). SEM imaging conditions were kept low to prevent potential damage of the layer by the beam. Typical imaging conditions were 2 kV and 0.21 nA. The FIB acceleration voltage was 30 kV for all processes (e.g., deposition, rough cutting, polishing); the current density was varied according to the required process.

Standard FIB-SEM tomography preparation procedures were used (Karwacki et al. 2011). An additional layer of Platinum (about 100 nm) was deposited over the area of interest to prevent damage from the FIB and to improve the finish (smoothness) of cross sections. Also, a very thin layer of platinum was deposited over a small square to the left of the area of interest, to be used as a fiducial marker for aligning both the FIB and the SEM during the FIB-SEM tomography process. Two trenches were subsequently milled alongside the area of interest (see Figure 2.2) to create sufficient space for redepositing material that was removed by the FIB during tomography. A large pit (10 µm in each direction) was milled in front of the region of interest, to allow the SEM to view consecutive vertical cross sections (Figure 2.2). In order to smoothen the first vertical cross section, the pit was polished with a moderate FIB current. After imaging the first cross section, FIB with a current of 0.3 nA was used to remove a 25-nm thick vertical slice and thus to expose the next cross section for electron microscopy.

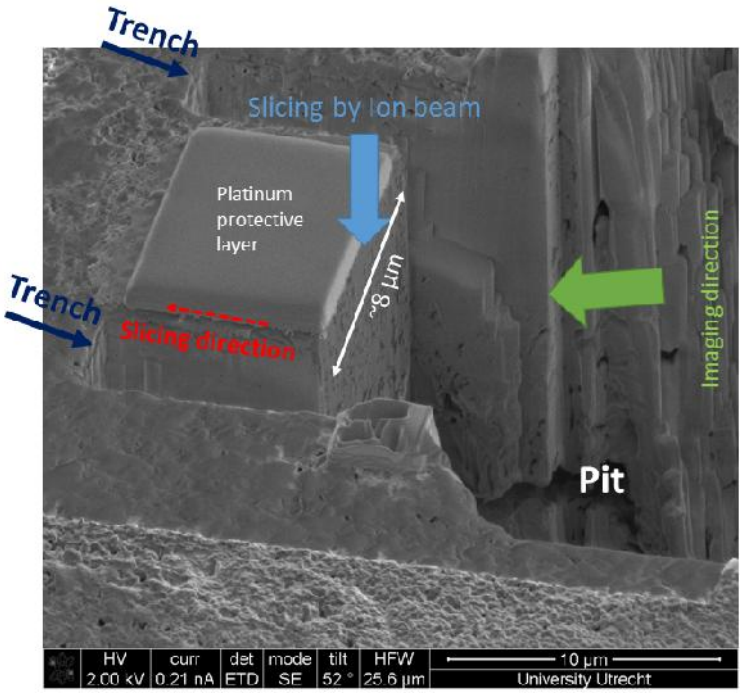

Figure 2.2 An image of the coating layer under FIB-SEM tomography, showing the pit and two trenches made by the ion beam

The tomography measurements were carried out with the SEM recording images at 2 kV and 0.21 nA in BSE mode, with the immersion lens switched on. The scan resolution was 2048x1768 pixels and the pixel width 3.5 nm. The dwell time was 4 µs, and the line integration two times, resulting in a frame time of approximately 35 seconds. A total of 678 cross sections were recorded.

2.2.3 Three-dimension tomography data analysis

We used Avizo Fire software 9.0 (FEI, Oregon, US) for the 3D tomography data analysis of the images. Figure 2.3a shows the image of one slice. The full stack of images (Figure 2.3b) was first smoothened using a median filter, with a neighborhood of 6, using 5 iterations. Watershed segmentation was used next to distinguish and separate pores from the solid structures (Figure 2.3c). The threshold values for the solid phase were manually chosen by comparing real gray scale images with the segmented images. With the above segmentations, the 3D structure of the coating layer could be reassembled and visualized (Figure 2.3d).

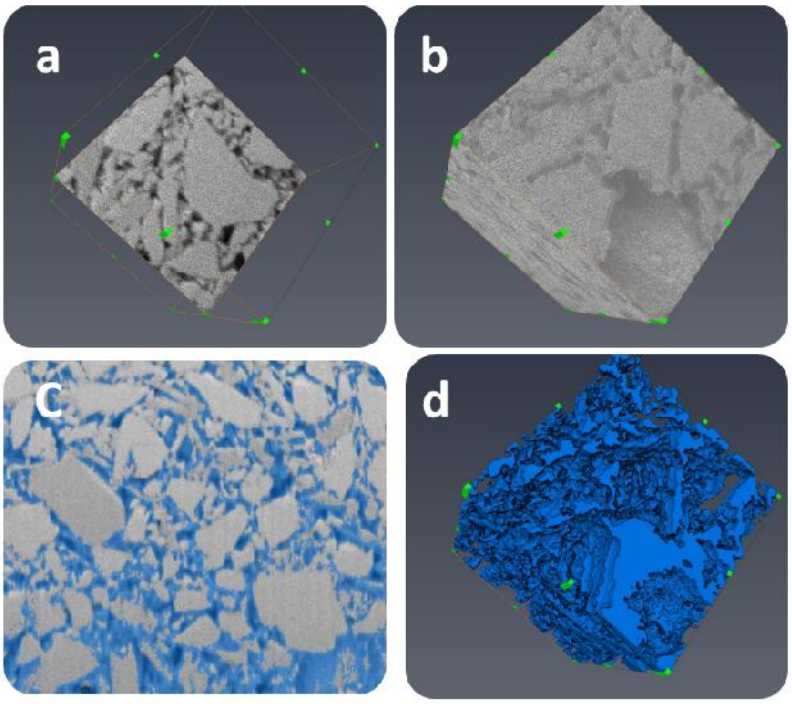

Figure 2.3 Reconstructed FIB-SEM results showing (a) one layer of the scanned stack, (b) volume rendering of the entire scanned domain, (c) the segmented domain, and (d) labelled pores using the "Label analysing" module

The Avizo label analysis module was used to calculate the volume of pores. This module performs a connectivity analysis of individual pores within the entire 3D volume. The calculated volumes were needed for the porosity calculations.

2.2.4 Pore-scale contact angle

The contact angle, ψ, is one of the key parameters affecting fluid retention and movement. We note that the contact angle is different from the spreading angle, which is measured as the edge angle of a droplet lying on the paper surface. This angle decreases with time as the liquid penetrates into the substrate. The contact angle, on the other hand, is the angle that a fluid-fluid interface inside a capillary forms with the pore wall. Under static isothermal conditions, this is a constant property of the two fluids involved (air, water) and the solid. Practical limitations of the microscopy techniques make it difficult to measure the real contact angle of liquids inside a single pore (in our case having an average diameter of only about 180 nm). Nevertheless, various approaches have been employed to estimate the

contact angle. Here we used an average value of 45° for the contact angle based on studies by (Järnström et al. 2010).

2.2.5 Determination of hydraulic properties

Upon arrival of an ink droplet, fluid will start moving into the pore network of dry paper (initially filled completely with air). Replacement of air by the invading liquid during ink setting constitutes an imbibition (wetting) process. Full characterization and simulations of the imbibition process requires information about several key parameters such as the pore size distribution, the porosity, and the capillary pressure – saturation (P_c-S) curve (Song et al. 2016). The 3D pore structure of the coating layer was used as input of the GeoDict software (Math2Market, Kaiserslautern, Germany) to obtain estimates of the capillary pressure (P_c-S) and relative permeability (K_r-S) curves. GeoDict uses for this purpose the pore morphology method (Schulz et al. 2014), which calculates the stationary distributions of the wetting and non-wetting phases at a given capillary pressure (Figure 2.4). This approach neglects gravity effects and requires a known value for the contact angle.

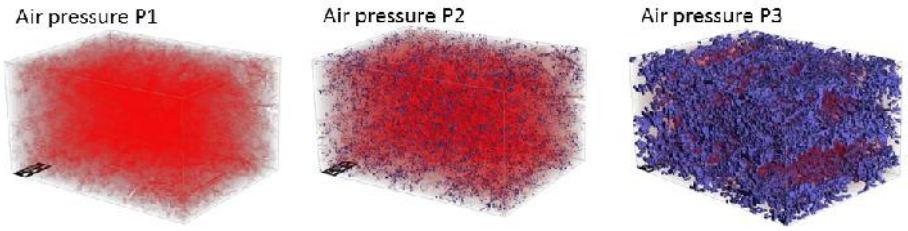

Figure 2.4 Images of the sample at three different air pressures during imbibition, with pressures P1>P2>P3. The red and blue colours represent air and water filled pores, respectively.

For any given capillary pressure, a critical pore size is calculated based on the Young- Laplace equation:

$$r = \frac{2\sigma}{P_c} c \quad \psi \qquad 2\text{-}1$$

where σ is surface tension, ψ the contact angle, and P_c the capillary pressure. For imbibition, initially all pores are filled by the non-wetting phase. We then search

for all pores whose size is equal to or smaller than the critical pore size r_c and are connected to the wetting phase reservoir. All those pores are assumed to become filled with the wetting phase (Hilpert et al. 2001). For drainage, all pores are at first filled with the wetting phase and we search for all pores whose size is equal to or larger than the critical pore size r_c and are connected to the non-wetting phase reservoir. All those pores are assumed to become invaded by the non-wetting phase. At the end of the drainage process, a certain part of the wetting phase may remain trapped in some pores, which leads to irreducible wetting saturation. Similarly, at the end of an imbibition process, the non-wetting phase may remain trapped in some pores, thus producing residual non-wetting saturation.

The relative permeability under imbibition was determined based on the distribution of phases obtained with the pore morphology method during imbibition. Thus, in order to calculate the relative permeability at a given saturation, the distribution of the phases (wetting and non-wetting) were determined. A pressure gradient was subsequently imposed on each phase and flow was simulated by solving the Stokes equation. Flow of each phase was assumed to be independent of flow of the other phase (i.e., transfer of momentum along the phase interfaces was not considered). The permeability of each phase was then determined by substituting the pressure gradient and total flow rate in Darcy's law. We refer to several previous studies for details (Schulz et al. 2014); (Hilpert et al. 2001); (Cheng et al. 2013).

2.3 Results

2.3.1 Pore size distribution

Properties of the pore structure of the coating layer are listed in Table 2-1. The total porosity of the sample was found to be 0.34 which is in good agreement with independent mercury porosity measurements as well as previous literature (Patrick A. Gane et al. 1996). The pore size distribution showing the probability of the various pore sizes is given in Figure 2.5. The average pore size was 180 nm, which means that the coating has a high capillary suction.

Table 2-1 Pore network parameters of the coating

Total Surface Area (μm²)	Ave. pore eq. diameter (nm)	Total no. pores	Porosity			Pore Volume (nm³)		
			Porosity	Open porosity	Closed porosity	Min.	Max.	Ave.
1273	180	31587	0.34	0.339	0.001	1213	113e6	118e4

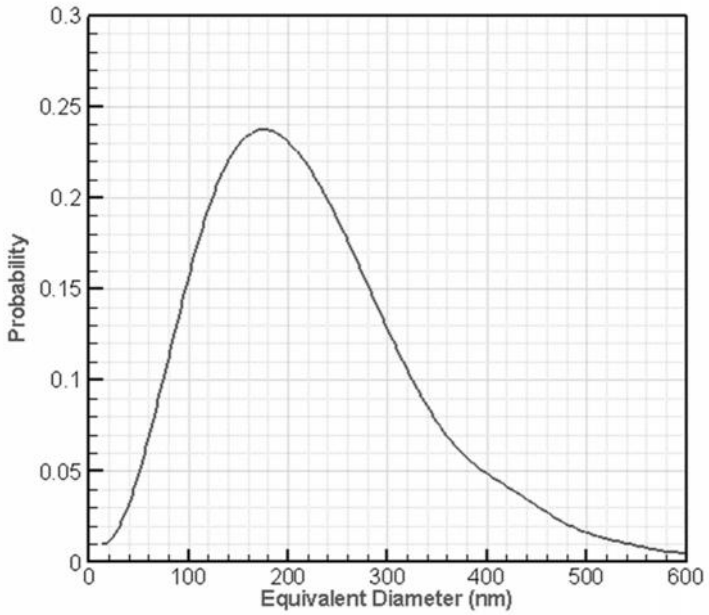

Figure 2.5 The pore size distribution of the paper coating

2.3.2 Hydraulic properties of the coating

2.3.2.1 Representative elementary volume (REV)

An important issue to be considered before performing pore-scale simulations is the minimum domain size that provides statistically meaningful parameter values. Calculated hydraulic properties for such a domain are then relatively insensitive to the pore network size. Such a representative network size will be considered as the REV of the porous medium being modeled. The REV size in our study was determined by calculating values of the porosity and permeability for different domain sizes, and plotting the results versus the domain dimension. Our results in

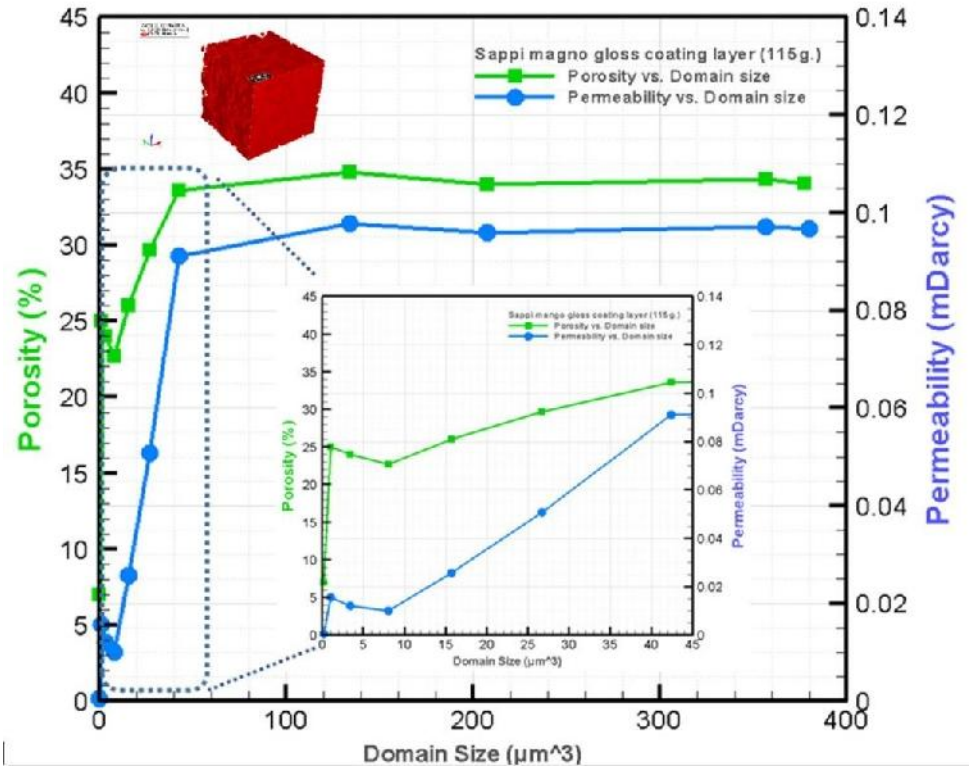

Figure 2.6 show that the porosity and permeability increased with domain size up to a domain of about 60 μm^3, above which they remained essentially constant at values of 0.34 and 0.1 mDarcy, respectively. For domains larger than 60 μm^3, the porosity

and permeability changed less than 3%. Based on these results, we used a domain size of 60 μm^3 as the REV in our study.

2.3.2.2 Capillary pressure- saturation (P_c-S) and relative permeability (K_r-S) curves

The capillary pressure curves associated with drainage and imbibition obtained with the software GeoDict, are shown in Figure 2.7. The plots show that the air entry suction during both drainage and imbibition was very high (about 1 MPa or 10 bar). This feature of the coating is very favorable for printing purposes. Having a high capillary suction means that the ink (or droplet) will invade the coating as soon as the droplet touches the surface of the coating layer. The macroscopic (bulk) hydraulic parameters for fluid movement in a variably-saturated coating layer can be determined by fitting an empirical equation to the simulated P_c-S data. While several equations for the P_c–S curve can be used for this purpose (e.g., (Leij et al. 1997), in this study we use the van Genuchten-Mualem model (van

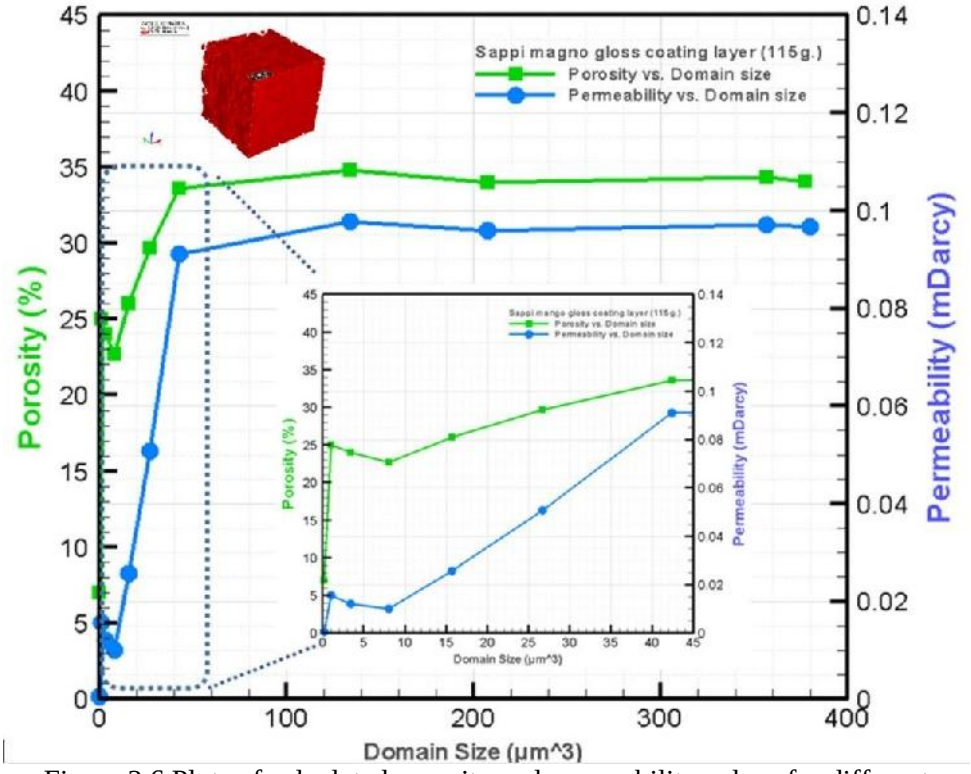

Figure 2.6 Plots of calculated porosity and permeability values for different domain sizes of the coating

Genuchten 1980), which is often used in numerical studies of fluid flow in variably-saturated media. The capillary pressure- saturation relationship is then given by

$$S_e(P_c) = [1 + (\alpha P_c)^n]^{-m} \text{ , } S_e = \frac{S_w(P_c) - S_{ir} - S_r}{1 - S_{ir} - S_r} \qquad 2\text{-}2$$

where S_e, S_r, $S_{ir,}$ and S_w are effective saturation, air residual saturation, irreversible wetting phase saturation, and wetting phase saturation, respectively, P_c is the capillary pressure, α and n are empirical shape parameters reflecting the average pore size and width of the pore-size distribution, respectively, and m=1-1/n. The parameter α is closely related to the inverse of the air-entry capillary pressure of the medium (Luckner et al. 1989); (Oostrom et al. 2002).

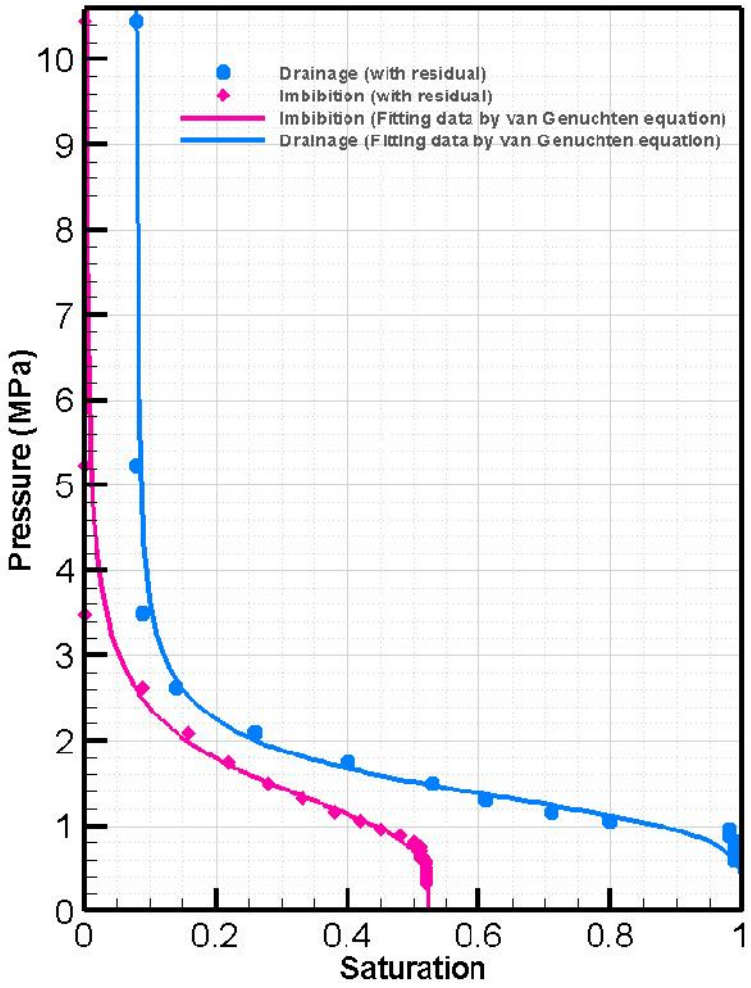

Figure 2.7 Estimated Pc-S curves of the coating of a paper sample. Symbols represent simulation results obtained with the pore morphology method, while solid lines are based on the fitted van Genuchten-Mualem equation

The fitting parameters for the primary imbibition and drainage curves are shown in Table 2-2; they are in good agreement with the hydraulic parameters reported for similar porous materials having relatively narrow pore-size distributions (Carsel and Parrish 1988) and (Ghanbarian-Alavijeh et al. 2010).

Table 2-2 Values of the van Genuchten parameters of the Pc-S curves in Figure 2.7.

	n	α (kPa^{-1})	S_r	S_{ir}
Primary Imbibition	3.96	0.712	0.476	0.000
Primary Drainage	5.00	0.731	0.00	0.082

As explained above, relative permeability at different saturations for both drainage and imbibition were calculated using pore morphology method results. Results for the primary imbibition are shown in Figure 2.8 as symbols. Values are given up to a saturation of 0.534, which was the largest saturation value reached with the Pc- S imbibition curve.

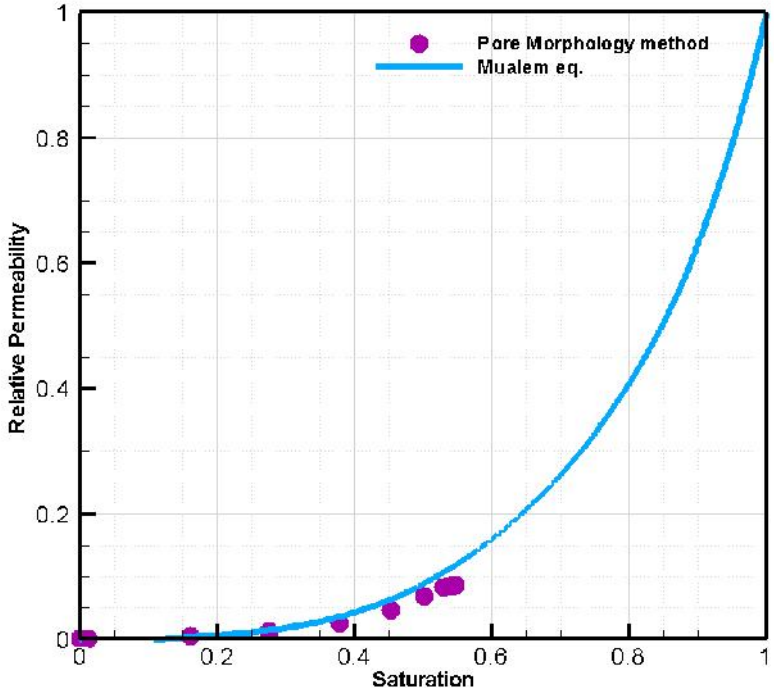

Figure 2.8 Relative permeability curves for the wetting phase

The relative permeability can be also determined based on equation 2-2. On the basis of the van Genuchten- Mualem model (van Genuchten 1980), the relative permeability of the wetting phase (k_{rw}) is given by

$$k_r = s_e^l\{1 - [1 - s_e^m]^{1/m}\}^2 \qquad 2\text{-}3$$

where l is a pore connectivity parameter, generally set equal to 0.5 following the early work by Mualem (1976) and van Genuchten (1980). Sometimes, however, its value is fitted to experimental data in order to have more flexibility in describing observed relative permeability data ((Luckner et al. 1989), (Leij et al. 1997)). Here we kept the original value of 0.5 for l.

The calculated relative permeability curve is shown in Figure 2.8 as a solid line. Good agreement was obtained between the relative permeability values calculated using the pore morphology method and the van Genuchten-Mualem equation as based on the primary drainage curve. Equation (2-3) provided only slightly higher values of the calculated data points. Moreover, differences between the calculated primary drainage and imbibition curves using equation (2-3) with the parameter values in Table 2-1 were found to be negligible, indicating that hysteresis between the primary drainage and imbibition curves can be ignored when plotting results as a function of saturation. This is very much in agreement with many previous studies of flow in variably-saturated porous media.

2.4 Conclusions

The standard focused ion beam scanning electron microscope (FIB-SEM) procedure used in our study was found to be a very effective technique for visualizing the three-dimensional morphology of coating layers of paper. In combination with image analysis methods, the technique was used to extract a 3D pore network of the coating layer. By analyzing segmented images, the pore size distribution and porosity of the coating could be determined. The minimum domain size for obtaining statistically meaningful values for porosity and permeability (REV) was found to be 60 μm^3. Capillary pressure – saturation (P_c- S) and relative permeability (K_r-S) values for the coating were obtained using the GeoDict software, based on the pore morphology method. By fitting the van Genuchten-Mualem equation to the Pc- S data, required parameters for calculation of the relative permeability were determined. The resulting hydraulic functions and its parameters provide a macroscopic characterization of the coating layer. These function can be used in continuum models for simulating ink penetration and spreading inside the coating layers of paper.

2.5 References

Malla, Prakash B. Devisetti, S. Novel kaolin pigment for high solids ink jet coating. Pap. Technol. 46, 17–27 (2005).

Vikman, K. & Vuorinen, T. Water fastness of ink jet prints on modified conventional coatings. 48, 138–147 (2004).

Heard, P. J., Preston, J. S., Parsons, D. J., Cox, J. & Allen, G. C. Visualisation of the distribution of ink components in printed coated paper using focused ion beam techniques. Colloids Surfaces A Physicochem. Eng. Asp. 244, 67–71 (2004).

Kettle, J., Lamminmäki, T. & Gane, P. A review of modified surfaces for high speed inkjet coating. Surf. Coatings Technol. 204, 2103–2109 (2010).

Girard, F., Attané, P. & Morin, V. A new analytical model for impact and spreading of one drop: Application to inkjet printing. Tappi J. 5, 24–32 (2006).

Ridgway, C. J. & Gane, P. A. C. Controlling the absorption dynamic of water-based ink into porous pigmented coating structures to enhance print performance. Nord. Pulp Pap. Res. J. 17, 119–129 (2002).

Desie, G., Deroover, G., De Voeght, F. & Soucemarianadin, A. Printing of dye and pigment-based aqueous inks onto porous substrates. J. Imaging Sci. Technol. 48, 389–397 (2004).

Dalton et al. Investigation into the distribution of ink components throughout printed coated paper. Colloids Surfaces A Physicochem. Eng. Asp. 205, 199–213 (2002).

Alam, P., Byholm, T., Kniivilä, J., Sinervo, L. & Toivakka, M. Calculating the permeability of model paper coating structures comprising incongruent particle shapes and sizes. Microporous and Mesoporous Materials 117, (2009).

Matilainen, K. et al. Performance and penetration of laccase and ABTS inks on various printing substrates. Colloids Surfaces B Biointerfaces 90, 119–128 (2012).

Lamminmäki, T. T., Kettle, J. P., Puukko, P. J. T., Ridgway, C. J. & Gane, P. A. C. Short timescale inkjet ink component diffusion: an active part of the absorption mechanism into inkjet coatings. J. Colloid Interface Sci. 365, 222–235 (2012).

Schoelkopf, J., Gane, P. A. ., Ridgway, C. J. & Matthews, G. P. Practical observation of deviation from Lucas–Washburn scaling in porous media. Colloids Surfaces A Physicochem. Eng. Asp. 206, 445–454 (2002).

Ridgway, C. J., Gane, P. A. C. & Schoelkopf, J. Effect of capillary element aspect ratio on the dynamic imbibition within porous networks. J. Colloid Interface Sci. 252, 373–382 (2002).

Bosanquet, C. H. LV. On the flow of liquids into capillary tubes. Philos. Mag. Ser. 6 45, 525–531 (1923).

Gane, P. A. C., Salo, M., Kettle, J. P. & Ridgway, C. J. Comparison of Young-Laplace pore size and microscopic void area distributions in topologically similar structures: a new method for characterising connectivity in pigmented coatings. J. Mater. Sci. 44, 422–432 (2008).

Karwacki, L. et al. Architecture-Dependent Distribution of Mesopores in Steamed Zeolite Crystals as Visualized by FIB-SEM Tomography. Angew. Chemie Int. Ed. 50, 1294–1298 (2011).

Järnström, J. et al. Effect of latex on surface structure and wetting of pigment coatings. Colloids Surfaces A Physicochem. Eng. Asp. 353, 104–116 (2010).

Song, Y., Davy, C. A., Bertier, P. & Troadec, D. Understanding fluid transport through claystones from their 3D nanoscopic pore network. Microporous Mesoporous

Mater. 228, 64–85 (2016).

Schulz, V. P., Wargo, E. A. & Kumbur, E. C. Pore-morphology-based simulation of drainage in porous media featuring a locally variable contact angle. Transp. Porous Media 107, 13–25 (2014).

Hilpert, Markus, Miller & T., C. Pore-morphology-based simulation of drainage in totally wetting porous media. Adv. Water Resour. 24, 243–255 (2001).

Cheng et al. PleatLab. A pleat scale simulation environment for filtration simulation. (2013).

Patrick A. Gane, †, John P. Kettle, ‡, G. Peter Matthews, * and & Ridgway, C. J. Void Space Structure of Compressible Polymer Spheres and Consolidated Calcium Carbonate Paper-Coating Formulations. (1996). doi:10.1021/IE950413M

Leij, F. J., Russell, W. B. & Lesch, S. M. Closed-form expressions for water retention and conductivity data. Ground Water 35, 848–858 (1997).

van Genuchten, M. A closed-form equation for predicting the hydraulic conductivity of unsaturated soils. Soil Sci. Soc. Am. J. 44.5, 892–898. (1980).

Luckner, L., van Genuchten, M. T. & Nielsen, D. R. A consistent set of parametric models for the two-phase flow of immiscible fluids in the subsurface. Water Resour. Res. 25, 2187–2193 (1989).

Oostrom, M., Dane, J. H. & Lenhard, R. J. Fluid Contents. (J.H. Dane and G.C. Topp; Soil Science Society of America , Madison, WI, United States(US)., 2002). doi:AC05-76RL01830

Carsel, R. F. & Parrish, R. S. Developing joint probability distributions of soil water retention characteristics. Water Resour. Res. 24, 755–769 (1988).

Ghanbarian-Alavijeh, B., Liaghat, A., Huang, G.-H. & van Genuchten, M. T. Estimation of the van Genuchten soil water retention properties from soil textural data. Pedosphere 20, 456–465 (2010).

Study of hydraulic properties of uncoated paper: image analysis and pore-scale modeling

Abstract

In this study, uncoated paper was characterized. Three-dimensional structure of the layer was reconstructed using imaging results of micro CT scanning with a relatively high resolution (0.9 µm). Image analysis provided the pore space of the layer, which was used to determine its porosity and pore size distribution. Representative elementary volume (REV) size was determined by calculating values of porosity and permeability values for varying domain sizes. We found that those values remained unchanged for domain sizes of 400x400x150 μm^3 and larger; this was chosen as the REV size. The determined REV size was verified by determining capillary pressure-saturation (Pc-S) imbibition curves for various domain sizes. We studied the directional dependence of Pc-S curves by simulating water penetration into the layer from various directions. We did not find any significant difference between Pc-S curves in different directions. We studied the effect of compression of paper on Pc-S curves. We found that up to 30% compression of the paper layer had very small effect on the Pc-S curve. Relative permeability as a function of saturation was also calculated. Water penetration into paper was visualized using confocal laser scanning microscopy. Dynamic visualization of water flow in the paper showed that water moves along the fibers first and then fills the pores between them.

Published as: H Aslannejad, SM Hassanizadeh. Study of hydraulic properties of uncoated paper: image analysis and pore-scale modeling- *Transport in Porous Media1120 (2017), 37-81.*

3.1 Introduction

Paper sheets and paper-based products like tissues and packing materials are commonly used in everyday life. Special fluid flow properties are required in such materials to achieve desired results; For instance, in the case of printing, penetration of ink into the paper affects the print quality significantly. Uncontrolled ink movement on/in paper layer potentially will cause poor print qualities like; color bleeding and print contamination on the other side of paper. So, in order to achieve the desired print quality, by controlling ink spreading and penetration, we need to understand ink flow inside the porous structure of paper. A valuable tool in this regard is the macroscale simulation of ink penetration into paper. For macroscale model of ink movement in paper, values of hydraulic properties, such as porosity, permeability, capillary pressure-saturation curves, and relative permeability curves are needed. In the absence of appropriate experimental methods, we obtain values of hydraulic properties by means of image analysis and a pore-scale model.

Normal plain paper is a fibrous layer consisting of cellulose fibers, which form a special type of pore network (different from pore network of a granular porous medium). For a granular porous medium, there is a clear distinction between pore body and pore throat. A fibrous layer, however, has a complex structure with the surface of a fiber as the solid part of the domain. In order to model fluid flow inside such a material, we need to characterize the three-dimensional structure of the layer in detail. This is usually done by means of imaging techniques.

Various imaging techniques have been used for papers like: X-ray tomography, focused ion beam secondary electron microscopy, and confocal microscopy. Aronsson et al. (Aronsson et al. 2001) acquired two-dimensional SEM images of cardboard paper. They reconstructed 3D structure of paper using a micro-tomography destructive method to slice layers of paper and acquire stacks of 2D images. (Samuelsen et al. 2001) obtained 3D images of paper using non-destructive synchrotron X-ray micro tomography. They used the images for the study of mechanical properties of paper. (Rolland du Roscoat et al. 2008) also used synchrotron X-ray micro tomography to study two different types of paper, Eucalyptus pulp handsheet and Blotting paper. They carried out pore-scale calculations and determined values of thermal conductivity and permeability. They also analyzed synchrotron results in order to determine the variation of porosity over the paper thickness, and checked anisotropy and heterogeneity of the micro structure. (Holmstad 2005) did a comparison study on low and high resolution X-

Ray tomography results of paper samples for obtaining structural information. They concluded that high resolution images are required for research into paper structure.

(Axelsson 2009) demonstrated that digital image analysis of X-ray images is a fast, automatic, and reproducible method for characterizing micro structure of porous materials. In 2010, (Axelsson and Svensson 2010) proposed a new computational method to extract pore network of duplex paper structure from scanned images. They introduced a pore-based skeleton representation of the material which is useful for permeability and tortuosity calculations.

Pore size distribution and porosity determination can be done either experimentally (mercury porosimetry) or by image analysis methods. In case of determination by image analysis, pore space of the domain should be reconstructed. (Delerue et al. 1999) introduced a new skeletization method to obtain the pore space of a porous material from 3D images. (Huang et al. 2002) developed a method for using X-ray micro tomography to determine structural parameters like porosity, pore size distribution, and specific surface area of fibers. They concluded that their results compared favorably with mercury intrusion porosimetry results.

Performing direct numerical simulation on a big domain size usually is prohibitive because of computational cost. So, effective properties of a porous material should be determined for a minimum domain size which is Representative Elementary Volume (REV). The REV size can be determined by analyzing domain size influence on values of physical and hydraulic parameters (Ramaswamy et al. 2001). (Kanit et al. 2003) proposed a REV determination method which is applicable to real three-dimensional images of heterogeneous materials obtained by imaging techniques. (Ramaswamy et al. 2001) determined REV size for a glass bead packing by analyzing the change in porosity and specific surface area values with increasing domain size.

Several studies have been done to determine permeability values for paper samples. (Lindsay 1988) conducted an experimental study of measuring paper permeability. They found that the anisotropy of fibrous layer has influence on permeability values and the ratio of lateral to transverse permeability is less than 2. (Zhu et al. 1995) developed a mechanistic model to describe fluid permeation through fiber beds. Their method was based on the micro-mechanical theories of compressibility of fiber assemblies. First, they determined the porosity profile along thickness. Then they related permeability to the porosity with help of the Davies-Ingmanson equation.

(Das and Ramarao 2002) determined permeability and compressibility relation for filter cakes formed during cake filtration. They showed that permeability for pulp mats is related to the specific surface area and volume of fibers. (Wei and Ramarao 1996) introduced a novel drainage test to determine specific surface area and volume of fibers which are required for permeability calculation.

(Ingmanson et al. 1959) modified Kozeny-Carman equation for calculation of permeability value for paper containing fillers and pulp fibers in the following form:

$$K = \frac{1}{kS_{w,f}^2}\frac{\left(1 - v_{f,f}C\right)^3}{C^2} \quad 3\text{-}1$$

$$C = \frac{m_f + m_p}{v_f + v_p + v_v} \quad 3\text{-}2$$

$$S_{w,f} = S_{0,f}.v_{f,f} \quad 3\text{-}3$$

where k is an empirical constant, $S_{0,f}$ is specific surface area of fibers (m^{-1}), $v_{f,f}$ is specific volume of fibers (m^3kg^{-1}), m_f a m_p are masses of fibers and pigment fillers respectively, v_f, v_p, v_v are volumes of fibers, fillers and void space (m^3), respectively.

In order to understand fluid flow inside a fibrous layer, one needs to know more about the structure of the material and its composition. (Zhao et al. 2007) did a comprehensive study of cellulose fiber structure using SEM, XRD, NMR and acid hydrolysis. Based on their study, each cellulose fiber is composed of micro fibril bundles (diameters of 20–30 nm). (Hirn and Schennach 2015) found out that fibers in a paper bond to each other by six different mechanisms: interdiffusion, mechanical interlocking, capillary forces, Coulomb forces, hydrogen bonding, and van der Waals forces. They concluded that, in contrast to general belief, that favors hydrogen bonding, van der Waals bonds play the most important role.

In this paper, we report on a comprehensive study of pore space and hydraulic properties of an uncoated paper. Through analysis of high-resolution micro-computational tomography (μCT) images, we obtained the pore structure of the fibrous layer. Then, pore space properties including porosity and pore size distribution were obtained. In addition, permeability, capillary pressure- saturation curves and relative permeability curves were determined using pore morphology and solving Stokes and Darcy equations. The REV size for determining average

properties of the layer was determined through investigation of porosity variation, anisotropic permeability, and capillary pressure curves for various domain sizes. Finally, in order to find out more about fluid flow in such a layer, an experimental visualization of ink movement in fibrous layer was performed and analyzed.

3.2 Material and Methods

3.2.1 Paper sample

This study was performed on Ziegler Z-Plot 650, which is an uncoated filler-free fibrous layer. The sample had a thickness of 150 µm and surface roughness of about 35 µm. Samples were kept under room conditions (21°C and relative humidity of 88%) for 24 hours before performing an experiment. Physical properties of the paper are shown in Table 3-1. Cellulose fibers are the only component of the studied paper sample. The layer is made of fibers with various lengths and with a mean diameter of 20 µm. Figure 3.1 shows a SEM image of surface of Ziegler paper.

Table 3-1 Physical properties of paper samples*

Property	Thickness (µm)	Grammage (gsm)**	Smoothness*** * (µm)	Ash content (%)	Surface PH	Relative humidity* ** (%)
value	105	90±2	4.50±0.5	12.0±1	7.3±0.5	40±4

* Data were obtained from www.zieglerpapier.com

** Gram per square meter

*** Product condition before experiment

****Measured by Parker Print-surf method which measures the roughness of paper and paperboard under conditions intended to simulate the nip pressures and backing substrates found in printing processes.

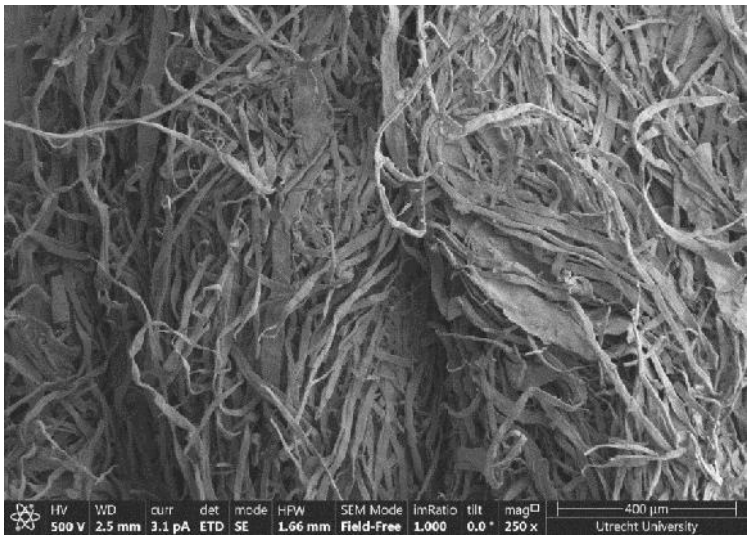

Figure 3.1 SEM image of paper sample surface

3.2.2 Imaging methods

The pore space of the paper was imaged using a Zeiss Xradia Versa 520 micro tomography scanner. The images had a voxel size (resolution) of 0.9 µm. The water movement between the fibers of the paper was studied with a confocal laser scanning microscope (Nikon A1+ confocal microscopy, Tokyo, Japan). Water containing fluorescent salt (Florescein sodium salt, Sigma Aldrich, Nederland), dissolved to a concentration of 1.5 gr/300 ml used as the liquid. Water was provided by a syringe pump (11 Elite, Harvard Apparatus, UK) at a constant flow rate of 0.005 ml/min.

The fibers and ink were visualized using a combination of laser wave lengths of 405, 488, and 561nm. A 637-nm red diode laser was also used to detect fluorescent particle sin the ink. Optimization of imaging parameters yielded a clear distinguish between fibers and ink. Images of water flow in paper were captured using a 10x microscope objective and the view domain was 1.8 x 1.8 mm^2.

3.2.3 Image analysis

µCT Images of the paper samples were analyzed to reconstruct 3D structure of the domain. All image analysis work was done using the software Avizo 9.0 Fire edition (FEI). A stack of two-dimensional high resolution (0.9 µm) images were first filtered using a Gaussian filter module to remove image noise. Then, using the

interactive thresholding module (with intensity range of 32000-46500), the grayscale images were converted to binary images (Figure 3.2).

Figure 3.2 Binary three-dimensional domain of fibrous layer

In order to determine the volume of each pore, the Separation and Labeling modules were used. These modules separate the pores from each other and label them by a distance map based method. Then, analysis of the labeled pores resulted in pore size distribution and porosity of the sample.

3.2.4 Pore-scale simulation

Pore-scale flow properties were obtained using the Pore Morphology method embedded in GeoDict software (Math2Market, Germany). Using this software, we could determine capillary pressure-saturation curves, permeability, and relative permeability. The calculation of saturation and capillary pressure was based on Young-Laplace equation. For an applied capillary pressure, which is the difference between wetting and non-wetting phase pressures, a pore radius is determined:

$$r = \frac{2\sigma}{P_c}\cos\psi \qquad 3\text{-}4$$

where σ is surface tension, ψ is the contact angle, P_c is the capillary pressure. The calculated pore radius determines the smallest pores (and throats) that will be filled with the wetting phase during imbibition, and the largest pores that will be filled with non-wetting phase during drainage (Hilpert et al. 2001); (Schulz et al. 2014); (Aslannejad et al. 2017a).

With the distribution of wetting and non-wetting phases inside the domain determined for a given capillary pressure, the saturation value could be calculated. Both primary imbibition and drainage curves were obtained.

To define, first Stokes equation was solved for steady-state flow of water within the pores at a certain applied pressure gradient. Then, the flow rate across the domain was calculated and Darcy's law was used to obtain permeability (Cheng et al. 2013). The calculated permeability values in combination with porosity values were used in the determination of REV size. The relative permeability- saturation curve was obtained based on primary imbibition results as follows. As mentioned above, for any given imposed capillary pressure, the distribution of wetting and non-wetting phases within the pores were known. Then, a pressure gradient across the REV was imposed on the wetting phase and Stokes equation was solved to calculate flow rate. Therefore, for any imposed pressure, substitution of flow in Darcy's law yielded effective permeability and consequently relative permeability values (Hilpert et al. 2001) (Cheng et al. 2013); (Schulz et al. 2014).

3.2.5 REV size determination

It is preferable to find the smallest REV size which provides representative average macroscale parameters of the domain. The REV size can be determined by calculation and comparison of values of a given hydraulic property for different REV sizes. It is the smallest domain size beyond which no difference in values of the property is found. For this study, ten different averaging domain sizes were selected. As the paper fibrous layer is anisotropic, liquid flow had to be considered in all three directions (*x*, *y*, and *z*). Due to the small number of pores in z (thickness) direction, all averaging domains were chosen to have the same thickness as the paper (150 µm) and their sizes were varied in lateral directions (*x*, *y*) from 50 to 1000 µm.

3.3 Results and discussion

3.3.1 Pore size distribution

The distance map values obtained via image analysis, revealed pores and then pore size distribution of the layer (Figure 3.3). The mean pore size was found to be 12 µm, which is in the same range as reported for similar materials by other researchers (Dodson and Sampson 1996).

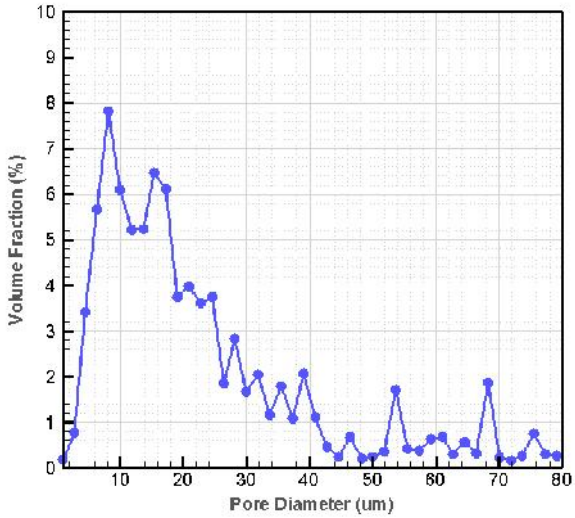

Figure 3.3 Pore size distribution of fibrous layer

3.3.2 Determination of hydraulic properties

The variation of porosity with the size of the averaging domain is shown in Figure 3.4. Based on this figure, we concluded that for domain sizes of 400 x 400 x 150 μm^3 and larger, the calculated porosity values are about 50% and do not vary significantly. For comparison, we recall that the REV size for the coating layer of paper was found to be 4 x 4 x 4 μm^3 (Aslannejad et al. 2017a).

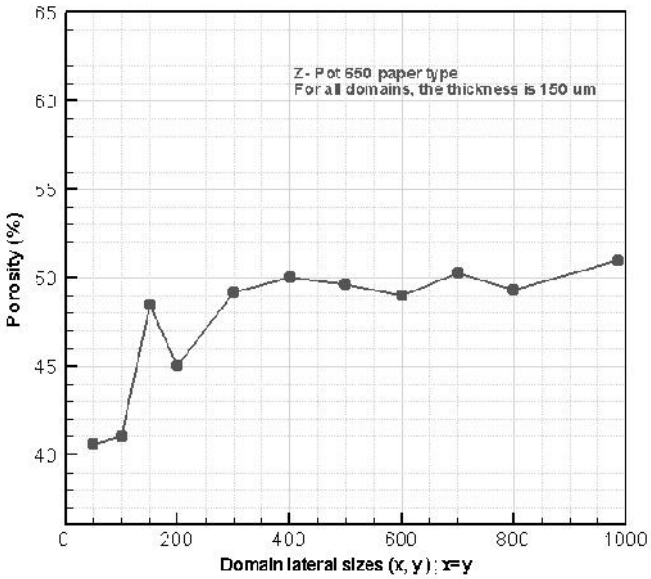

Figure 3.4 Porosity values for different domain sizes (thickness is constant and equal to 150 um)

Increasing the domain size when calculating permeability resulted in higher permeability values. This is because larger domains yielded bigger mean pore sizes. We found that the correlation of higher permeability value for larger mean pore size just stands till reaching REV size. Permeability values for different domain sizes in three directions are plotted in Figure 3.5. The variation of permeability value with changing domain size also gives an REV size of 400 µm (400 x 400 x 150 μm^3). In the case of a paper coating layer, the permeability value was found to be about 50 times smaller (Aslannejad et al. 2017a).

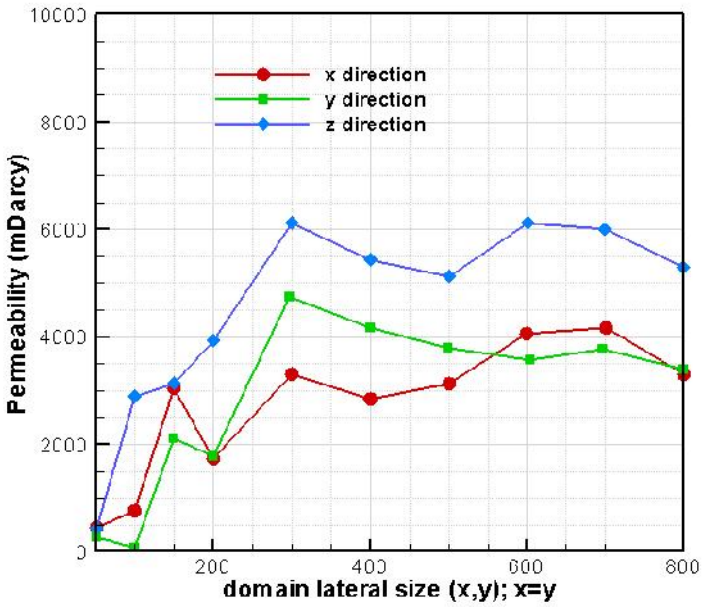

Figure 3.5 Permeability values for ten different domain sizes (*x, y; x=y* and thickness is constant 150 µm for all domains)

Permeability values in z direction (in thickness direction) were larger in comparison with lateral directions (see Figure 3.5). This could be due to bigger pore sizes (and/ or) shorter pathways in connected pores in z direction. By fitting spheres in pores in three different directions, percolation paths were determined. The biggest particle size that could pass from one side to the opposite side in each direction was determined. Also, the path length divided by the length of a straight line in the selected direction was calculated. As shown in Table 2-2, larger particles could pass in the *z* direction. This explains why we found a larger permeability value in the *z* direction in comparison with the other two directions. Figure 3.6 shows the relative permeability-saturation curve for the studied fibrous layer.

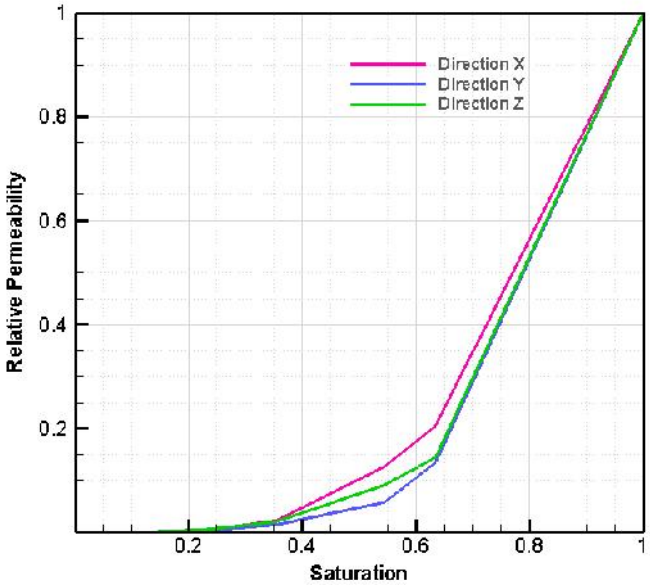

Figure 3.6 Relative permeability curve based on imbibition phase distribution

Plots of capillary pressure versus saturation (P_c-S) for different averaging domain sizes are shown in Figure 3.7 and Figure 3.8 for drainage and imbibition, respectively. As we can see, in each figure, the curves have a similar shape and range for domains bigger than 400 µm in size. This is in good agreement with the REV size we obtained based on porosity and permeability results (Figure 3.4 and Figure 3.5).

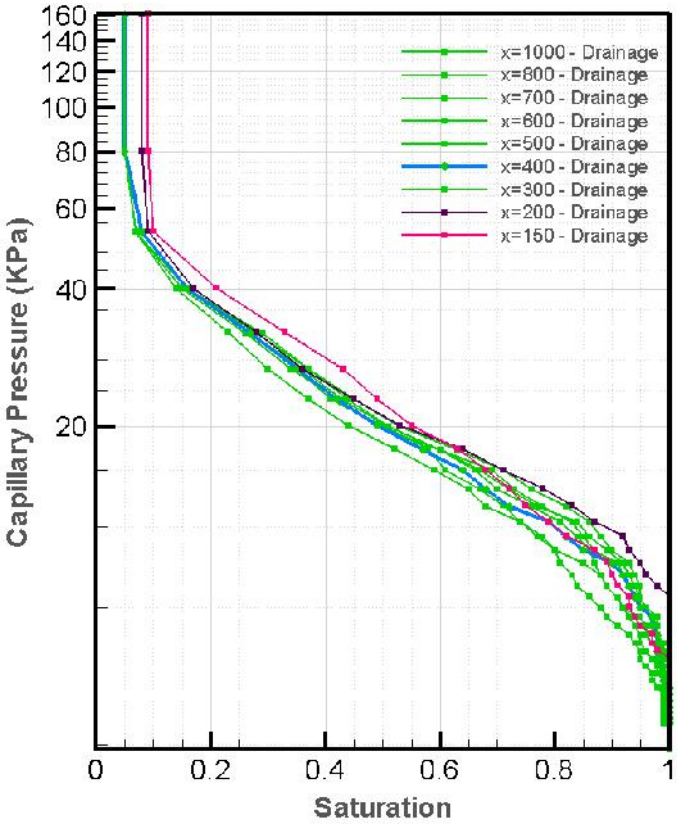

Figure 3.7 Drainage curves for selected domain sizes

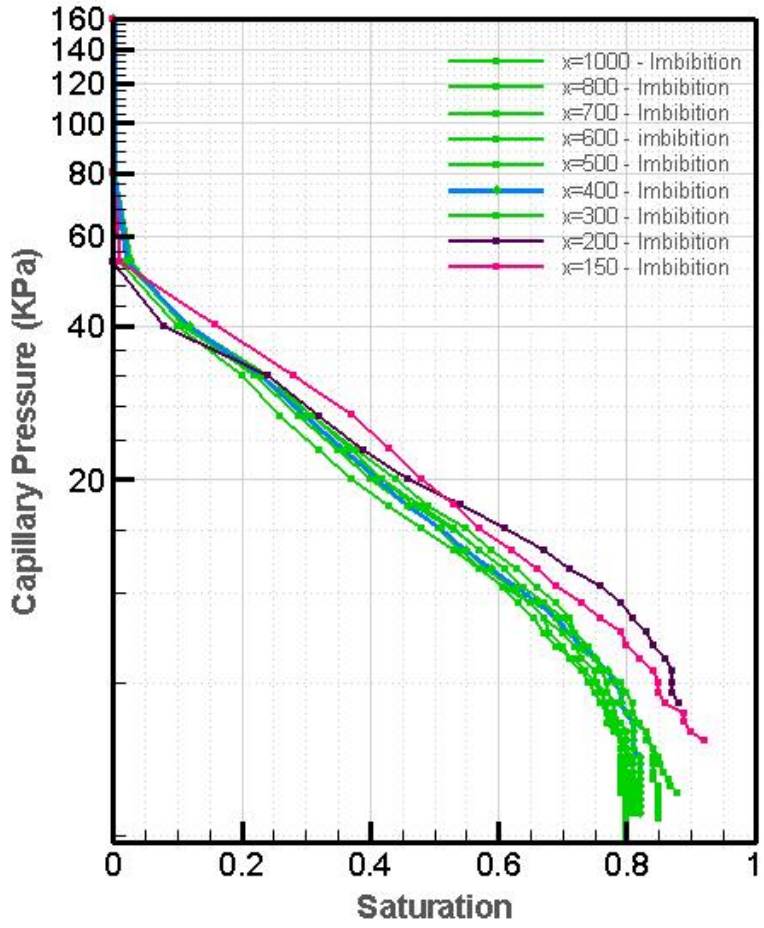

Figure 3.8 Imbibition curves for selected domain sizes

We fitted the van Genuchten (van Genuchten 1980) empirical equation to our simulated capillary pressure-saturation curves.

$$S_e(P_c) = [1 + (\alpha P_c)^n]^{-m} \quad 3\text{-}5$$

$$S_e = \frac{S_w - S_{ti}}{1 - S_{ti} - S_r} \quad 3\text{-}6$$

where S_e, S_r, S_{ii} , and S_w are effective saturation, air residual saturation, irreversible wetting phase saturation, and wetting phase saturation, respectively, P_c is the capillary pressure, α and n are empirical parameters reflecting the average pore size and width of the pore-size distribution, respectively. Commonly, we assume *m=1-1/n*. Fitting parameters based on primary imbibition diagrams for different domain sizes are shown in Figure 3.9.

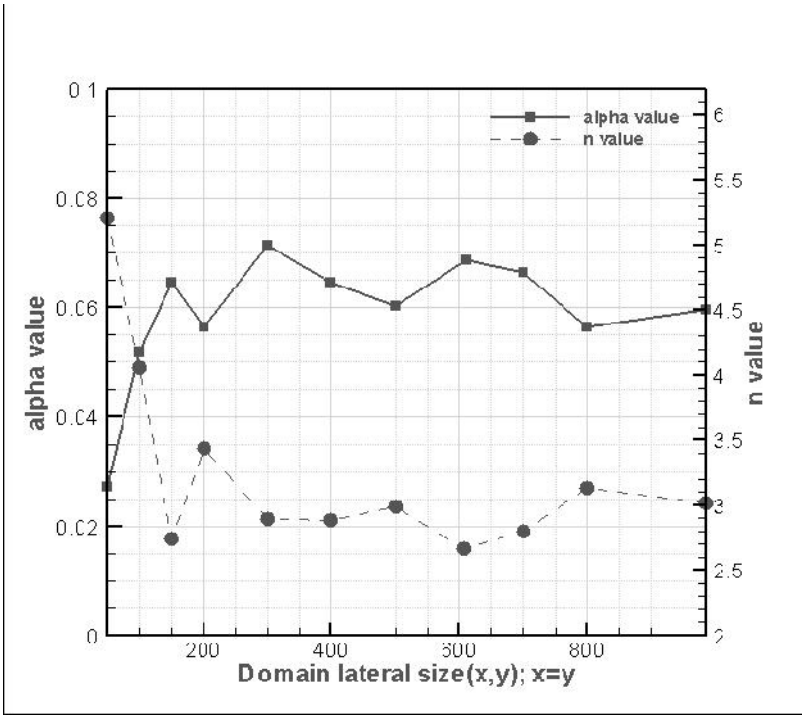

Figure 3.9 van Genuchten parameters (α and n values) for different domain sizes

We can see that a minimum averaging domain size of 200 x 200 x 150 μm^3 is sufficient for the capillary pressure-saturation curve. Thus, an REV size of 400 x 400 x 150μm^3 can be used for all properties. The parameter values for the selected REV size are given in Table 3-2.

Table 3-2 Values of the van Genuchten parameters of the Pc-S curve

	n	***α* (kPa^{-1})**	***S_r***	***S_{ir}***
Primary Imbibition	2.8	0.06	0.83	0.00
Primary Drainage	5.00	0.731	0.00	0.082

3.3.3 Directional independence of Pc- S curves

For the determination of capillary pressure- saturation curves, a non-wetting phase reservoir was assigned to one side of the domain and a wetting phase reservoir was fixed to another side. This meant that the invasion of the domain by a phase was forced to be in a given direction. The question was raised whether the selection of domain sides for wetting and non-wetting phase reservoirs had an effect on the resulting capillary pressure curve. Figure 3.10a shows wetting and non-wetting phase reservoir connection sides and Figure 3.10b shows the resulting P_c-S curves. It is evident that all curves coincide for the most part. There are some differences at high saturation, but these are negligible for all practical cases. This result is commensurate with the fact that capillary pressure and saturation are scalar quantities and their relationship should be independent of direction.

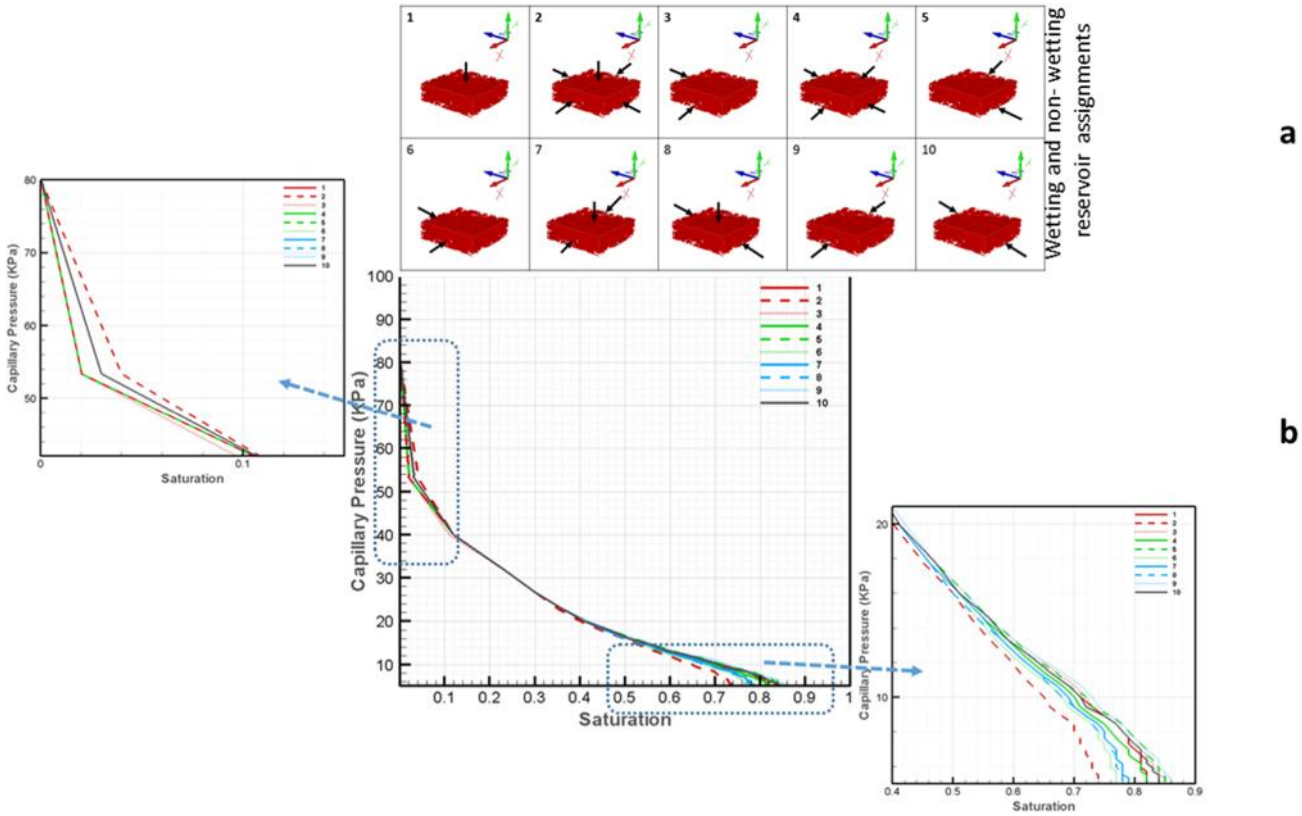

Figure 3.10 Wetting and non-wetting phase connection side effect on capillary pressure- Saturation curves; a) Wetting phase connection-side configuration. b) Pc-S curves

3.3.4 Effect of deformation of layer on P_c-S curves

Deformation of paper is a relevant process in printing. Due to the compressibility of fibrous layer and possible pressing effect during printing, the pore space of paper may change in shape and size. To determine whether deformation may change macroscopic hydraulic properties of the layer, capillary pressure-saturation imbibition curves were obtained for different compression percentages (5, 15, 30, and 50%). Results are shown in Figure 3.11. The effect of compression on pore space was simulated. A comparison of 50% reduces the layer thickness to half its original size. As compression decreases the size of the pores, it increases the entry capillary pressure value (as expected based on equation 3-1). Compression less than 30% had a negligible effect on capillary pressure-saturation curve.

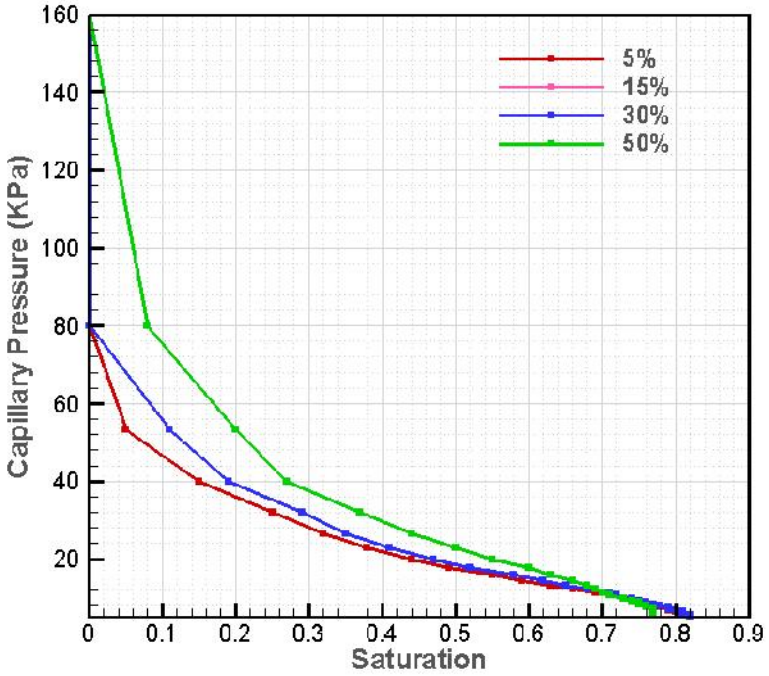

Figure 3.11 Effect of paper deformation on primary imbibition curve. Four different compression values are plotted with different colors (The curves of 15% and 30% are overlaping)

3.3.5 Visualization of flow in fibrous layer

Water penetration into the paper fibrous layer is different from water movement into a granular porous material. In case of granular materials, water moves into the pores and wets the surface of pores simultaneously. But in a fibrous

layer made of cellulose fibers, in addition to water movement inside pores which are made between fibers, individual fibers also have a rule in movement of water. The fibers are known to be made of bundle of fibrils. A bundle of fibrils is made of individual fibrils with a dimeter of about 2 nm. Figure 3.12a shows a SEM image of one single fiber, in which few fibril bundles are visible. The cellulose material of the fibril is known to be strongly hydrophilic (see e.g. (Hirn and Schennach 2015)). So, the empty spaces between fibrils inside a bundle (about a few nanometers) are expected to imbibe water strongly. In addition, SEM images show that the fiber surface has sub-micron roughness (Figure 3.12b), forming micro channels that can have a high capillary action.

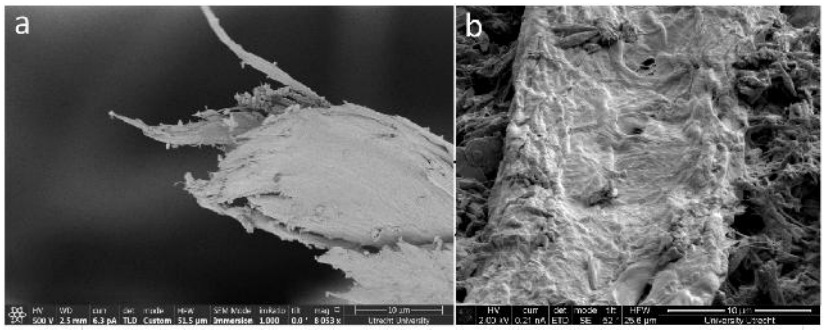

Figure 3.12 Visualization of individual fibers using electron microscopy: a. bundle of fibrils, b. surface of individual fiber

Indeed, confocal laser scanning microscopy of water movement in the fibrous layer provides a sequence of images, during time (interval 3s), showing how water moves inside the layer. In Figure 3.13, fibers are imaged in green color and water (containing fluorescent particles) is shown in red. The right hand side of the fibrous layer is connected to water reservoir. Based on the results, water first wets the surface of fibers and perhaps fills its internal pores before filling the pores between fibers. We see in Figure 3.13 that two wetting fronts develop; a very irregular zigzag front where water invades individual fibers and a relatively regular front moving behind and filling the pores.

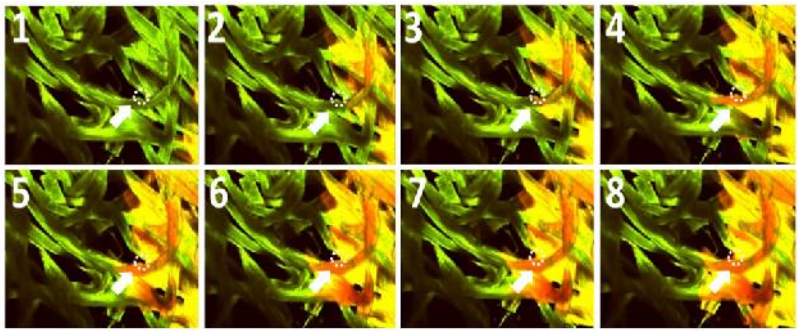

Figure 3.13 Snapshots of water movement into a fibrous layer images of penetration of water injected into a fibrous layer are shown obtained using a confocal laser microscope (Nikon A1+). Numbers represent time steps; green and red colors represent dry and wet fibers, respectively; yellow colour shows intermediate saturation

Comparing liquid flow in granular material and fibrous layer, in first case, liquid fills pores and follows their connectivity. In addition, wetting the pore surface and imbibition of the pore occurs at the same time. Nevertheless, in case of fibrous layer, liquid wets surface of fibers and moves on surface of fibers; fingering-like front. A liquid front behind the fingering front moves and fills the pores between fibers.

Cellulose fibers absorb water and swell. Consequently, the diameter of fibers increases. In turn, this causes deformation of the layer. In Figure 3.14, a swollen single fiber is shown. The fiber diameter before wetting was 26.74 µm. When water arrived to the selected area of fiber, it caused swelling and fiber diameter reached 32.87 µm in 50 seconds. Then, after drying for 280 seconds, the diameter decreased to a value of 27.96 µm. This shows that the change in fiber diameter is not completely reversible.

Figure 3.14 Swelling of a single cellulose fiber

3.4 Conclusion

In this work, pore-scale imaging and modeling of fluid flow in a fibrous layer were performed to determine hydraulic parameters of the layer. Imaging of the layer was done by µCT and then, by means of image analysis methods, 3D reconstruction of the layer was extracted. By comparison of porosity and permeability values as well as P_c-S curves for various domain sizes, the REV size of the layer was found to be 400 x 400 x 150 (μm^3), with the layer thickness being 150 µm. The porosity and mean pore size values for the REV were found to be 50% and 12 µm, respectively. Checking the percolation path for the layer in three different directions, we found that bigger pores connection exists in z direction (the thickness direction) but it has shorter normalized path length in y direction. No directional dependence for P_c-s curves were found.

In order to check the impact of layer deformation (compression during printing) on P_c-S curve, four different compression values were chosen and checked. That was concluded that compression less than 30%, doesn't has any significant effect on P_c-S curves.

Finally, dynamic visualization of water flow in fibrous layer showed that water moves along and into the fiber first and then fills the pore between them. Swelling of individual fibers was measured and was found to be partially irreversible.

3.5 References

Aronsson, M., Henningsson, O. & Sävborg, Ö. Slice-based digial volume assembly of a small paper sample. Nord. Pulp Pap. Res. J. 17, 29–33 (2001).

Samuelsen, E. J., Houen, P., Gregersen, Ø. W. & Helle, T. Three-dimensional imaging of paper by use of synchrotron x-ray microtomography. J. Pulp Pap. Sci. 27, 50–53 (2001).

Rolland du Roscoat, S., Decain, M., Geindreau, C., Thibault, X. & Bloch, J.-F. Microstructural Analysis of Paper Using Synchrotron X-ray Microtomography: Numerical Estimation of the Permeability and Effective Thermal Conductivity. Appita J. J. Tech. Assoc. Aust. New Zeal. Pulp Pap. Ind. 61, 286 (2008).

Holmstad. Comparison of 3D structural characteristics of high and low resolution X-ray microtomographic images of paper. Nord. Pulp Pap. Res. J. 20, 283–288 (2005).

Axelsson, M. Image analysis for volumetric characterisation of microstructure. 2009, (2009).

Axelsson, M. & Svensson, S. 3D pore structure characterisation of paper. Pattern Anal. Appl. 13, 159–172 (2010).

Delerue, J. F., Perrier, E., Yu, Z. Y. & Velde, B. New algorithms in 3D image analysis and their application to the measurement of a spatialized pore size distribution in soils. Phys. Chem. Earth, Part A Solid Earth Geod. 24, 639–644 (1999).

Huang, S., Goel, A., Ramaswamy, S., Ramarao, B. & Choi, D. Transverse and in-plane pore structure characterization of paper. Appita journal 55, 230–234 (2002).

Ramaswamy, S. et al. The 3D structure of paper and its relationship to moisture transport in liquid and vapor forms. in 12th Fundamental Research Symposium, Oxford 1289–1311 (2001).

Kanit, T., Forest, S., Galliet, I., Mounoury, V. & Jeulin, D. Determination of the size of the representative volume element for random composites: statistical and numerical approach. Int. J. Solids Struct. 40, 3647–3679 (2003).

Lindsay, J. D. The anisotropic permeability of paper: theory, measurements, and analytical tools. (1988).

Zhu, S., Pelton, R. H. & Collver, K. Mechanistic modelling of fluid permeation through compressible fiber beds. Chem. Eng. Sci. 50, 3557–3572 (1995).

Das, S. & Ramarao, B. V. Inversion of lime mud and papermaking pulp filtration data to determine compressibility and permeability relationships. Sep. Purif. Technol. 28, 149–160 (2002).

Wei, H. & Ramarao, B. V. Characterization of pulp slurries using a novel drainage tester. in Tappi Engineering Conference 517–524 (1996).

Ingmanson, W. L., Andrews, B. D. & Johnson, R. C. Internal Pressure Distributions in Compressible Mats under Fluid Stress. TAPPI J. 42, 840–849 (1959).

Zhao, H. et al. Studying cellulose fiber structure by SEM, XRD, NMR and acid hydrolysis. Carbohydr. Polym. 68, 235–241 (2007).

Hirn, U. & Schennach, R. Comprehensive analysis of individual pulp fiber bonds quantifies the mechanisms of fiber bonding in paper. Sci. Rep. 5, 10503 (2015).

Hilpert, Markus, Miller & T., C. Pore-morphology-based simulation of drainage in totally wetting porous media. Adv. Water Resour. 24, 243–255 (2001).

Schulz, V. P., Wargo, E. A. & Kumbur, E. C. Pore-morphology-based simulation of drainage in porous media featuring a locally variable contact angle. Transp. Porous Media 107, 13–25 (2014).

Aslannejad, H. et al. Characterizing the hydraulic properties of paper coating layer using FIB-SEM tomography and 3D pore-scale modeling. Chem. Eng. Sci. 160, 275–280 (2017).

Cheng et al. PleatLab. A pleat scale simulation environment for filtration simulation. (2013).

Dodson, C. T. J. & Sampson, W. W. The effect of paper formation and grammage on its pore size distribution. J. pulp Pap. Sci. 22, J165–J169 (1996).

van Genuchten, M. A closed-form equation for predicting the hydraulic conductivity of unsaturated soils. Soil Sci. Soc. Am. J. 44.5, 892–898. (1980).

Characterization of the interface between coating and fibrous layers of paper

Abstract

Coated paper is an example of a multi-layer porous medium, involving a coating layer along the two surfaces of the paper and a fibrous layer in the interior of the paper. The interface between these two media needs to be characterized in order to develop relevant modeling tools. After careful cutting of the paper, a cross-section was imaged using focused-ion beam scanning electron microscopy (FIB-SEM). The resulting image was analyzed to characterize the coating layer and its transition to the fibrous layer. Such image analysis showed that the coating layer thickness is highly variable, with a significant fraction of it being thinner than a minimum thickness required to keep ink from invading into the fibrous layer. The overall structure of the coating and fibrous layers observed in this analysis provides insights into how the system should be modeled, with the resulting conclusion pointing to a specific kind of multi-scale modeling approach.

Published as: H Aslannejad, SM Hassanizadeh. Characterization of the interface between coating and fibrous layers of paper. *Transport in Porous Media (2018), 1573-1634*

4.1 Introduction

Cellulose-based papers are the main substrate for the printing industry as well as the main component of a new generation of 'biodegradable' medical diagnostic devices.

Similar considerations apply to microfluidic kits for diagnostic devices (cf., López-Marzo and Merkoçi, 2016), where movement of water into and between cellulose fibers is largely controlled by the hydrophilic property of the fibers. In inkjet printers, a cartridge delivers tiny droplets of ink (pico-liter in size) on the paper surface. As soon as a pico-liter size droplet of ink reaches the paper, it starts penetrating into the porous substrate.

Uncoated paper is an anisotropic porous medium, which consists of bundles of fibers crossing over each other in a planar orientation. The fibrous medium is commonly impregnated by granular mineral materials as filler. Observations have shown that penetrating liquid in a fibrous layer first follows the direction of fibers and wets them. Then, the pore space between fibers is filled up with the liquid (Aslannejad and Hassanizadeh, 2017) .

In order to reduce the ink penetration into the fibrous layer and produce a high print quality, coated papers are often used. The added coating material is normally an isotropic granular medium, which has pores in the range of only a few hundred nano-meters. The small pores produce suitable conditions for sucking in the droplet from the surface of paper in a relatively uniform penetration and spreading pattern. A uniform final pattern is desirable from the point of view of print quality.

Paper surface roughness and application of the coating layer on different basesheets have been studied previously. Gane et al. (Gane et al. 1991) used optical imaging techniques to study the effect of fiber furnish on the coating structure, roughness and coverage of the paper. They reported that the aqueous coating color caused a relaxation in surface profile of the thermomechanical pulp basesheet and yielded an uneven coating distribution and rough uncalendered coated paper. The ground wood basesheet retained stability in its surface profile during the coating process, although the basesheet itself is a rough basesheet. In case of using pressurized ground wood basesheet, a smooth coated sheet resulted with a relatively uniform distribution of the coating layer.

In another work, Gane and Hooper (Gane and Hooper 1989) used coating thickness analysis and frequency transform procedures to study basesheet surface

profile change during paper coating application. They showed that the relaxation of the basesheet depends on the type of coating pigments, their size distribution, their rheology and dewatering interaction between the coating and basesheet. They also concluded that dewatering characteristics were determined by base absorbency, pigment particle packing, and suspension of the fluid viscosity.

The print quality is partly determined by the spatial variation of paper properties and ink density. If they have irregularities, it leads to non-uniform ink absorbency across the surface of the paper, which is referred to as mottle in printing. Gane (Gane 1989) used the Walsh transform spectrum to identify the main reason for mottle in a printed sample. He established that the binder migration (i.e., the redistribution of binder by penetrating ink) is the main cause of mottle. He showed that binder migration depends on coating distribution and variations in the base sheet absorbency.

Lamminmäki et al. (Lamminmäki et al. 2011) tried to clarify the effect of ionic charge distribution in the coating layer on dye fixation properties. They chose surface inert precipitated inorganic silica and modified calcium carbonate as model coating structure. Non-ionic polyvinyl alcohol (PVOH) and anionic polymer were added as binder. Then, the surface was treated by applying a cationic polymer. The ab/adsorption of the colorant part of ink was evaluated using UV-VIS spectroscopy. They showed that addition of PVOH and anionically dispersed coating increased colorant fixation. In addition, cationic additive application slowed down the ink imbibition into paper. Altogether, this resulted in less bleeding and improved water fastness properties.

In high speed inkjet printing process, the pore network of the coating layer plays an important role in ink uptake. Lamminmäki et al. (Lamminmäki et al. 2011), (Lamminmäki et al. 2012) studied the possibility of lowering the thickness of the coating layer and reducing bleeding, which is when the ink spreads during setting. They showed that at the early stage of ink arrival on the surface of coated paper, capillary flow is dominant. Nevertheless, just four milliseconds after application of ink, permeability plays a more important role. Moreover, once the coating layer becomes too thin, then the pigment type and binder amount in the coating layer were found to have no influence on results.

In the case of coated paper, we should characterize not only the two different thin porous layers – the coating layer and the fibrous layer - but also the interface between them. In the case of the fibrous layer, some studies were done using X-ray microtomography imaging techniques to extract the paper's three-dimensional (3D)

pore space (du Roscoat et al., 2005; Rolland du Roscoat et al., 2008). The extracted domain has been used in direct simulations using Lattice Boltzmann methods (Hyväluoma et al., 2007; Ramaswamy et al., 2004; Rosenholm, 2015; Järnström et al., 2010). In some simpler approaches, the fibrous layer has been considered as an array of similar structure units representing the real pore space (Salmas et al., 2001; Washburn, 1921; Schoelkopf et al., 2002).

Ghassemzadeh and Sahimi (2004a) reported a method to determine the size distribution and connectivity of fibrous layers of paper using two-dimensional (2D) cross-sectional SEM images. They used the results to conduct pore-network simulations of fluid flow into paper during coating (Ghassemzadeh and Sahimi 2004a).

In another work, Ghassemzadeh and Sahimi (Ghassemzadeh and Sahimi 2004b) developed a statistical approach to characterize paper structure using the distribution of radius and length of pores between fibers. Based on extracted data, the paper layer was represented by a 3D network of interconnected channels. Then, they used the network to determine the effective permeability tensor of paper.

Ridgway et al. (Ridgway et al. 2002) and (Kettle et al. 2010) studied the effect of pore network structure on dynamic imbibition into paper. They used the Bosanquet equation in a 3D network simulator (called Pore-Cor). In their work, film flow along the fibers was not considered. They concluded that over a short time interval, smaller pores were filled faster than larger pores, which is not in agreement with Washburn equation. In addition, they found that the aspect ratio of a pore, defined as the ratio of length to radius, plays an important role in the filling rate of the pore.

In an earlier work, using X-ray microtomography, the 3D structure of a fibrous layer was extracted and reconstructed (Aslannejad and Hassanizadeh 2017). Then, a Pore-Morphology method was used to obtain the pore-size distribution, and curves of capillary pressure and relative permeability, as functions of fluid saturation. Recently, Focused Ion Beam Scanning Electron Microscopy (FIB-SEM) imaging techniques were used to acquire and reconstruct the 3D pore network of the coating layer (Aslannejad et al. 2017a). The extracted network was used for pore-network modeling and determination of hydraulic properties of the coating layer. Pore size distribution of the coating and fibrous layers were determined. Using the Pore Morphology method, capillary pressure - saturation curves of the two layers were also determined. Graphs of pore-size distribution and capillary pressure-saturation curves are shown in Figure 4.1. As expected, capillary pressure-saturation

curves show much higher capillary pressure values for the coating layer. This is related to much smaller mean pore size of the coating layer (Figure 4.1a). To the best of our knowledge, an imaging of the transition from coating layer to the fibrous layer in a coated paper has not been done up to now. Therefore, here we are focusing on not the coating and fibrous layer but on the transition area from the coating to the fibrous layer.

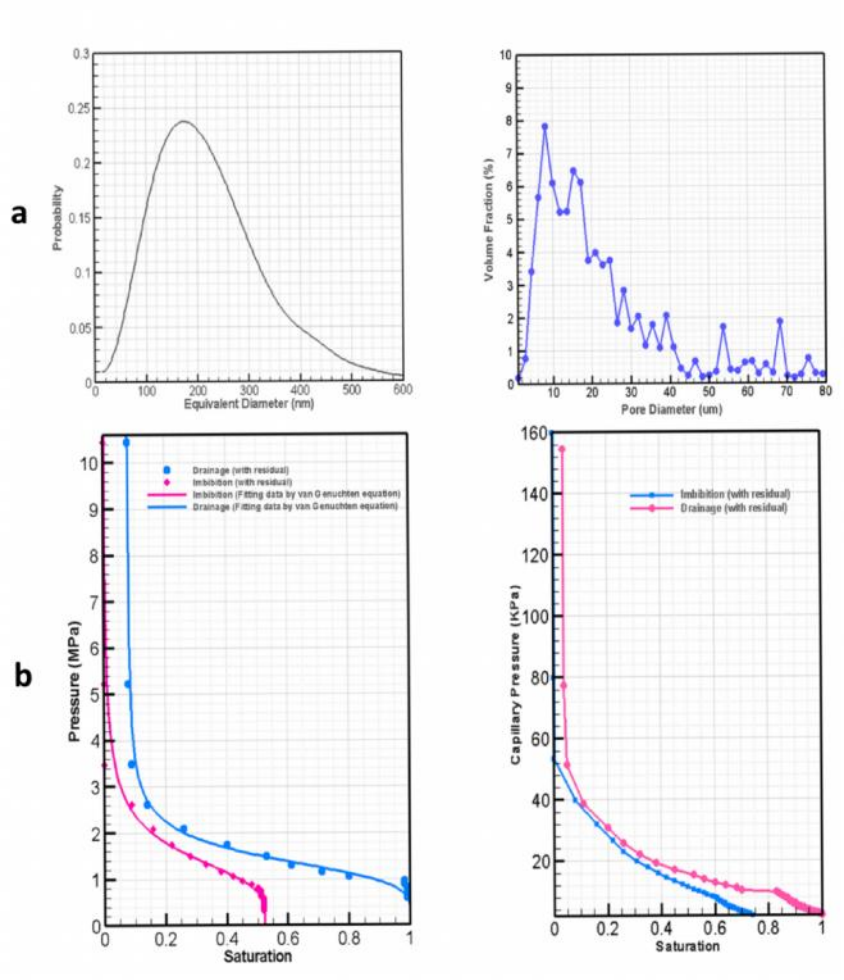

Figure 4.1 a) Pore size distribution of the coating and fibrous layers, and b) Capillary-pressure - saturation curve of the coating and fibrous layers (Aslannejad et al. 2017a), (Aslannejad and Hassanizadeh 2017)

In the case of multi-layer porous media, like the coating layer – fibrous layer system, there is always a contact interface between the two layers. Depending on the details of the spatial structure of this interface, it might be modeled as a uniform planar surface of discontinuity in material properties, a zero-thickness interface with its own properties, or as a finite-thickness transition zone between the layers.

In this paper, we focus on understanding the characteristics of the interface between the coating layer and the fibrous layer in a coated paper system and its effect on ink absorption into the coated paper. We first present a brief overview of the pore space and properties of coating and fibrous layers. Then we provide information about the interface between the two layers. We have obtained this information with the aid of imaging techniques and image analysis. This includes measurement of the coating layer thickness as a function of location along the interface. From that analysis, we generated a coating thickness histogram for a relatively large cross section of the coated paper. Based on this information, we discuss whether the coating layer and the interface with basesheet can be simulated by traditional macroscale modelling approaches. We also provide suggestions for including the effect of variation of the coating layer thickness in computational models. Finally, we have estimated the minimum thickness of coating layer required in order to ensure that water does not reach the fibrous layer. Identifying this minimum layer thickness is a novel contribution to the understanding of the role of coating layer in print quality.

4.2 Material and Methods

4.2.1 Paper sample

In this work, we studied samples of a coated paper (Magno gloss, Sappi, Germany), which is primarily an offset printing grade and is not usually used in inkjet printing. However, as we are interested in studying the coating-basepaper interface and liquid transfer through it, we have used it to illustrate our characterization method and analysis approach. Our results and approach can be used to study papers that are optimized for inkjet printing. The paper cross-sectional view is shown in Figure 4.2. As seen in the figure, the coated paper has a base layer made of cellulose fibers covered (on both sides) with coating layer consisting of a pre-coat and a topcoat, these are clearly delineated by particle size. In addition, the space between the pigment particles in the pre-coat is largely filled by soluble binder, whereas the topcoat contains particulate binder. This is typical of double coated gloss offset papers. The coating layer is mainly (88% mass fraction) made of compressed $CaCO_3$ powder with an average thickness of 15 µm, porosity of 34%, and mean pore size of 180 nm. The amount of binder present in the layer is about 8% by mass, or 20% by volume. This is a significant volume and will affect the connectivity of the coating layer pore structure (Aslannejad et al. 2017a).

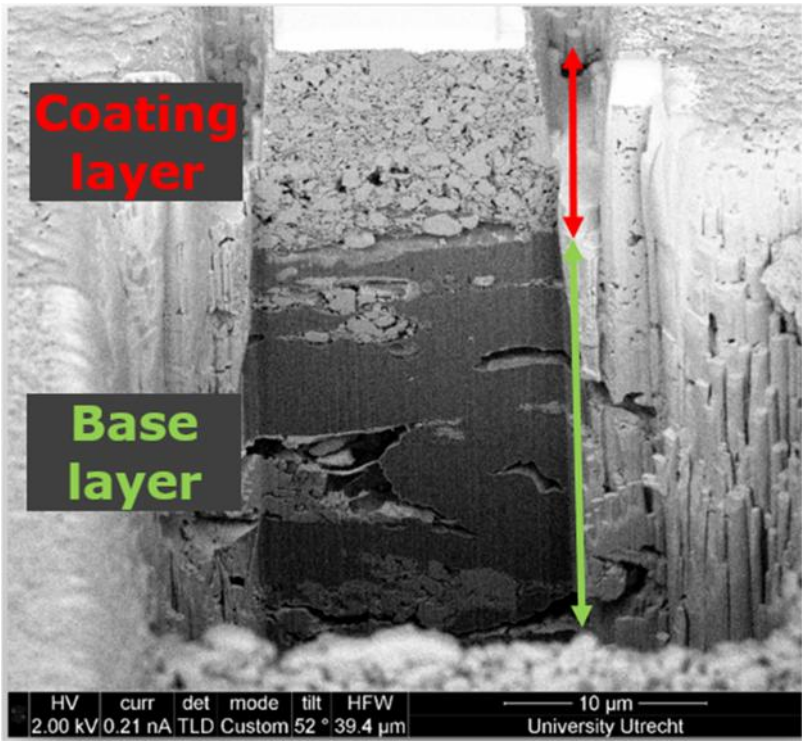

Figure 4.2 Cross-sectional view of the coated paper showing the coating layers and part of the fibrous layer

In order to compare the coated and uncoated papers, samples of an uncoated printing paper, Ziegler Z-Plot 650 (Ziegler papier AG, Germany), were analyzed. The paper consisted of a single layer with an average thickness of 150 µm, made of filler-free cellulose-based fibers. This paper has a porosity of 50% and mean pore size of 12 µm (Aslannejad and Hassanizadeh 2017). It should be mentioned that in fibrous layers, normally there are two directions, machine and perpendicular directions. Most of the fibers lie in the plane of these two sheet directions, with the majority aligned in the machine direction. This is also the case in the samples analyzed. Table 4-1 shows detailed information about the samples used in this study.

Table 4-1 Coating layer, coated paper and uncoated paper properties

	Thickness (µm)	Porosity	Mean pore size	Permeability * (mDarcy)	Grammage (g/m^2)	Ref.
Coating layer	15	34%	180 nm	0.1	-	**
Coated paper	85	-	-	-	115	***
Uncoated paper	150	50%	12 µm	5500	90	****

* in thickness direction
** (Aslannejad et al. 2017a)
***(https://www.sappi.com/magno)
**** (Aslannejad and Hassanizadeh, 2017)

4.2.2 Imaging

The imaging of coated paper was done using a Nova Nanolab 600 Focused Ion Beam Scanning Electron Microscope (FIB-SEM) (FEI Company, Eindhoven, Netherlands). Typical imaging conditions were 2 kV and 0.21 nA. The FIB acceleration voltage was 30 kV for all processes (e.g., deposition, rough cutting, polishing); the current density was varied according to the required process. For more details, readers are referred to Aslannejad et al. (2017).

Note that the FIB-SEM could not be used for imaging the full thickness of fibrous layer. The maximum practical domain size to be imaged by FIB-SEM is a cube of 20 x 15 x 15 μm^3 (the cube in Figure 4.3). As shown in Figure 4.3, the imaged domain contained not only coating material but also some fibers of the fibrous layer.

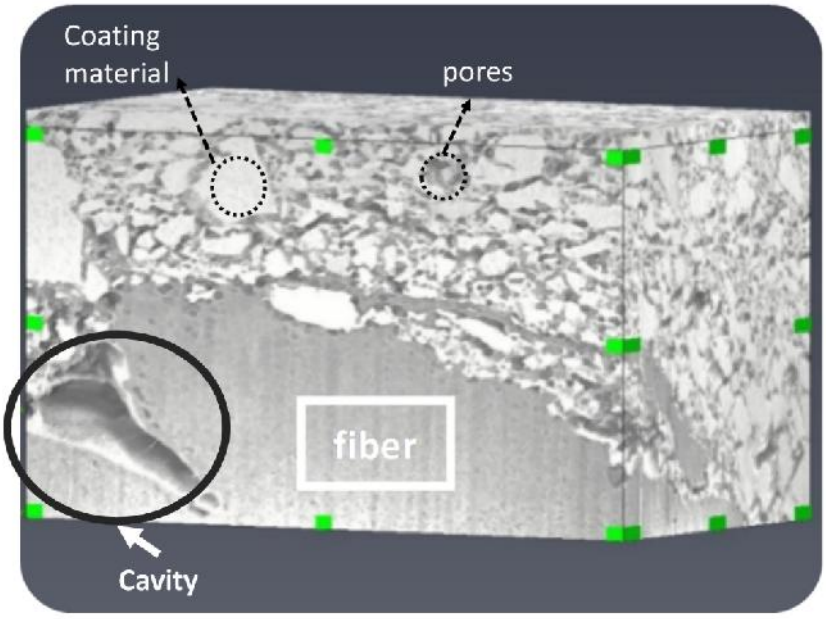

Figure 4.3 3D domain of coated paper showing coating layer as well as the connection to the fibrous layer (Observation domain has dimensions of 20*15*15 μm^3)

4.2.3 Image analysis

From the acquired images and using Avizo software (Fire edition, FEI, Oregon, US), we reconstructed the paper pore space. First, a non-local means filter was applied to remove the imaging noise. Then, alignment and thresholding modules

with appropriate adjustments were applied to extract binary three-dimensional (3D) structure of the solid phase. In the extracted images shown Figure 4.3, coating material, fibers and pores can be distinguished.

4.2.4 Determination of coating layer thickness along paper cross section

In order to study thickness of the coating layer along the coated-paper cross section, the paper sample was cut using a microtome (Clamp-able Manual Microtome MT.5503). This resulted in a sharp cross section of sample without mixing layers of paper or damaging any fiber. Then, the cut edge was imaged using FIB-SEM. In total, 20 cross sectional locations were imaged, each about 200 µm long. Then, the images were put together to obtain a relatively long cross sectional view of coated paper, about 4 mm long. Figure 4.4 shows the resulting cross-sectional view of the coated paper.

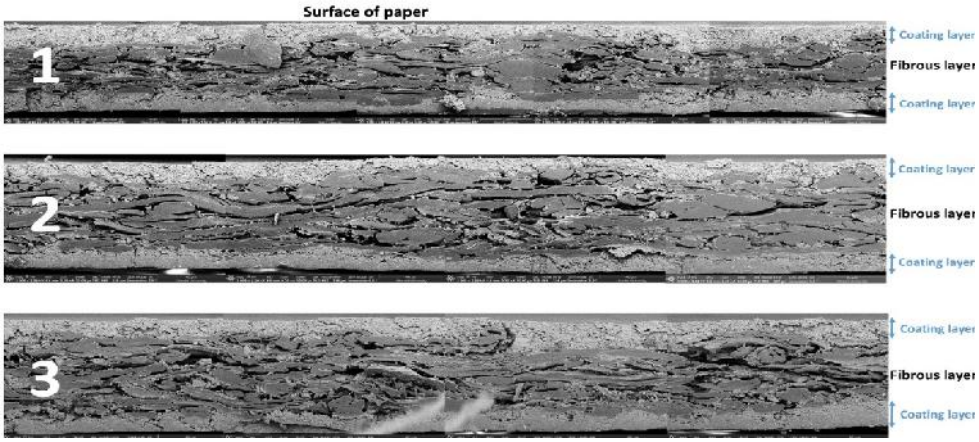

Figure 4.4 Cross section of a piece of coated paper 4 mm long, obtained by SEM imaging

4.2.5 Print quality

To study the role of the coating layer and its required minimum thickness for keeping the ink inside it and preventing it from reaching the fibrous layer, two different printing qualities were considered: 600 and 1 200 DPI (dots per inch). In inkjet printing, each printed character on the paper is made of several ink droplets. The spacing of droplets forming a character is usually given as DPI. In the case of 600 DPI, droplets of ink with diameter of about 10 µm are jetted onto the paper with center-to-center distance of about 18 µm (Lamminmäki et al. 2009).

In the case of 1 200 DPI, droplets are usually jetted closer to each other, which results in higher print resolution. For instance, droplets of ink with diameter of 10 μm are jetted with spacing of 9 μm. Figure 4.5 shows a schematic representation of 600 and 1 200 DPI print qualities. As seen in the figure, the droplets usually have small overlap in the case of 1 200 DPI.

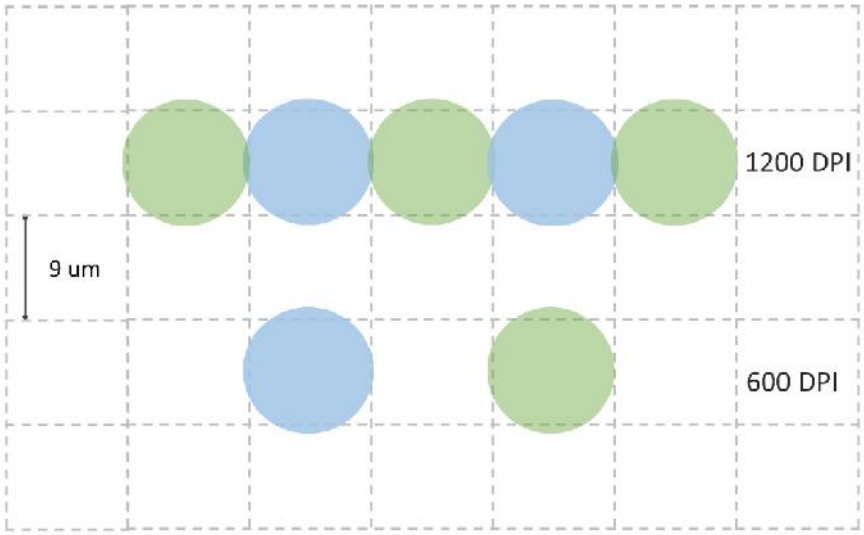

Figure 4.5 Schematic representation of droplet spacing jetted on paper for the cases of 600 and 1200 DPI print qualities

In order to understand the consequences of water-based ink reaching the base layer (fibrous layer), water movement into the fibrous base layer needs to be studied (as e.g., in Aslannejad and Hassanizadeh, 2017). Fibers are highly hydrophilic and as soon as water reaches any of them, water starts to creep on their surfaces and penetrates them. This is shown in Figure 3.13, where snapshots of images of penetration of water injected into a fibrous layer are shown. Water was introduced from the right side and images were obtained using a confocal laser microscope (Nikon A1^{+}). We see that saturation has gone up in fibers (dark orange color) ahead of the main front (yellow color).

For a better print quality, all fibers should be sufficiently covered with the coating layer; otherwise ink may come into contact with fibers and get transported into the fibrous layer. The main detrimental effect of ink penetrating the fibrous layer is that the film flow along the fiber surface leads to wicking and a spider-leg like effect on the print. The swelling of fibers is another important effect, which may

change the thickness of paper; this could potentially cause tray blockage during the printing process. Since the fibrous layer is made of elongated fibers, its surface commonly has a relatively significant roughness. The roughness has a major effect on the thickness and quality of the coating layer. As seen in Figure 4.4, tiny particles of the coating material cover the fibrous layer and form a relatively smooth coating layer. Rougher fibrous layers need larger coating layer thickness to cover all fibers.

Although the permeability value of the coating layer is low (Aslannejad et al. 2017a) and the droplet stays for a while on the paper surface and evaporation plays a role, the coating layer should have enough thickness to keep all the remaining ink liquid within the layer. The required minimum thickness of coating layer for absorbing the liquid part of ink depends on the volume of ink in the droplet: a larger volume needs more thickness to handle the liquid part. For example, if we ignore evaporation, in the case of 600 DPI printing, where an ink droplet has a diameter of 10 μm, the coating layer should have a thickness of 18 μm. In making this rough estimate, we have assumed that the droplet has a spherical shape and invades the coating layer (with porosity of 34%) cylindrically. The assumption that the liquid penetrates cylindrically was made only in order to make a rough estimate. We know from previous works that the liquid absorbs via a preferred pathway and many of the coating layer pores remain unfilled prior to the liquid reaching the base paper (see e.g. Ridgway et al. (Ridgway and Gane 2002), Schoelkopf et al. (Schoelkopf et al., 2002b) and Aslannejad et al. (Aslannejad et al., 2018).

4.3 Results and discussion

In this section, the results of the image analysis are presented. This includes the spatial distribution of the coating layer thickness, its associated spatial correlation structure, and the frequency of occurrence of coating thicknesses below the estimated minimum required thickness. We refer to locations with thickness below the minimum amount as "weak points". In addition to the spatial analysis, we also discuss an approach for modeling all layers of the coated paper.

4.3.1 Distribution of paper coating layer thickness and weak points

The cross-sectional images were analyzed to identify the thickness of the coating layer along the entire length of the cross section. This provides thickness as a function of location. That function is plotted in Figure 4.6a, with a summary histogram of the data plotted in Figure 4.6b. These data show a maximum thickness of 30 µm and a minimum thickness of one micrometer, with a distribution weighted toward the lower thickness values. The data show that most of the thickness values fall below the estimated target value of 18 µm. This indicates that the paper fails to satisfy the requirements of coating thickness to produce high quality printing results for a 10-µm-diameter droplet. However, we must note that this failure was expected for the paper type studied in this work, as it was designed for offset printing and not inkjet printing technology.

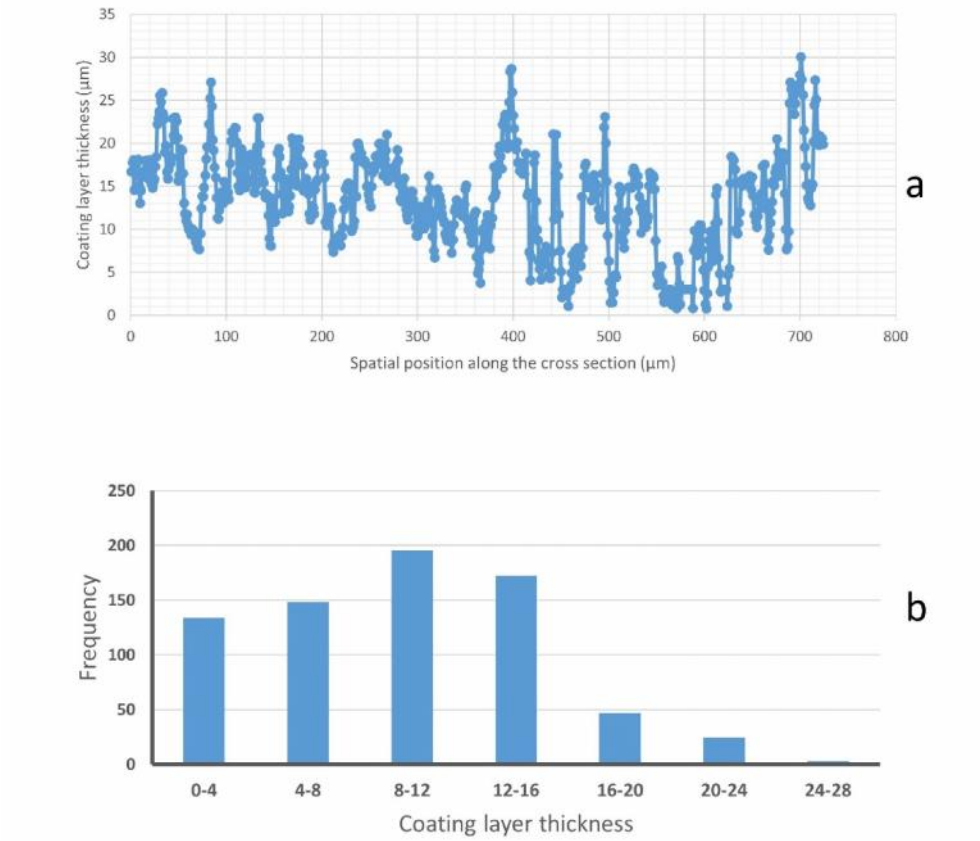

Figure 4.6 a) The coating layer thickness as a function of (one-dimensional) spatial location and b) Coating layer thickness histogram

In order to estimate the spatial correlation structure of the thickness function, a semi-variogram was calculated, with the results shown in Figure 4.7. The variance is 40 µm while the correlation length is around 200 µm. This shows that the thickness has significant spatial variability and there is some level of spatial structure in the variability of the thickness function. The correlation length of 200 µm could well relate to the floc site of fibers due to the sheet formation. The correlation length, as described by Gane et al. (Patrick A. Gane et al. 1996), is a primary property of a base sheet when designing a suitable coating strategy for both coverage and print uniformity. In addition to that, all of these might be useful parameters in building models to analyze fluid flow in such complex structures.

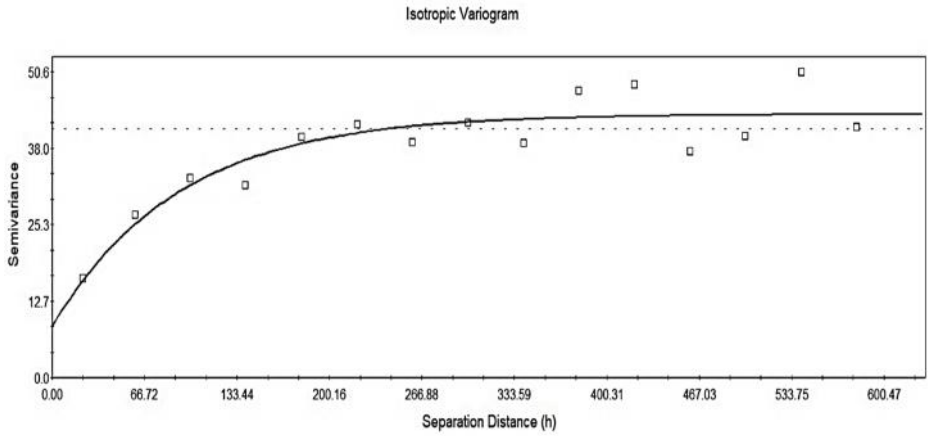

Figure 4.7 Semivariance diagram showing correlation length

4.3.2 Modeling of ink imbibition into coated paper

There are two main modeling approaches for modeling ink imbibition into a layer of coating material. One is the traditional three-dimensional macro-scale (or continuum) model of unsaturated flow. The other one is pore-scale modeling, including direct simulation or pore-network modeling methods.

For macro-scale models to be applicable, it is commonly stated that one should be able to identify a Representative Elementary Volume (REV), over which average quantities can be defined. An REV is required to contain a large number of pores in each direction. In addition, its size must be much smaller than dimensions of the domain that is to be modelled. In the case of (coated) paper, the two criteria are mutually excluding; if the REV is to be much larger than the pore size, it cannot be much smaller than the layer thickness. This is even more so in the case of coated paper studied here.

As explained in section 4.2.1, the coating layer consists of a pre-coat and a topcoat, whose average thicknesses are 10 and 2 µm, respectively. Thus, even though the mean particle sizes is 100 nm, it is not feasible to consider the coating layer as a three-dimensional continuum, as the basic criteria for the definition of average macroscopic quantities cannot be satisfied.

In addition to that, there are places where the coating thickness is very small. This may happen if the coating penetrates into the basepaper and/or is shunted away from high points, leaving fibers wholly uncoated. Then, as explained earlier, as soon as liquid reaches any fiber, it will be absorbed and the fiber will start to swell. Therefore, in modelling the coated paper, it seems necessary to model individual

fibers embedded in the coating layer. This, however, will not be straightforward in the framework of a macro-scale modeling. Alternatively, a full pore-scale description, resolving pores in both the coating layer and the fibrous layer, could be pursued. The swelling behavior of the fibers is important, so special attention needs to be paid to the detailed topology, geometry and structure of the fibers. For example, as fibers have a micro-porosity; this probably leads to a kind of dual-porosity approach. Overall, with this level of detail and the complex spatial structure of the coating layer and the fibers, this is a major modeling challenge and represents an important and interesting area for further research.

4.4 Conclusion

The thickness of the coating layer of a sample of coated paper was analyzed by precisely cutting the sample and then imaging the resulting cross section using FIB-SEM technologies. Subsequent analysis of the images provided a detailed quantification of the spatial structure of the coating layer. The thickness of the coating layer is highly variable, with a significant fraction (80%) showing a thickness below the estimated minimum thickness required to prevent ink from reaching the fibrous layer. Analysis of the variability and spatial structure of the thickness showed a variance of 40 μm and a correlation length of 200 μm. This is a primary property of a coated paper when designing a suitable coating strategy for both coverage and print uniformity.

This kind of analysis provides detailed insights into the effectiveness of the coating layer, and can form the basis of detailed modeling studies for this kind of layered system. Because the coating layer is made of two thin layers, each containing limited pores in the cross-sectional direction, a continuum-scale simulation does not seem appropriate for the coating layer. Similarly, the complex nature of the fibrous layer also fails to satisfy criteria for continuum equations. In both the coating and fibrous layers, enough REVs along the thickness, which is needed for the applicability of continuum-scale modelling, cannot be identified. However, a pore-scale model should be able to include details of the fluid flow through the coating layer of paper and to couple that with the fibrous layer below. The discrete nature of the fibers and their importance in the definition of the overall geometry of the system suggests that these fibers, and the pore spaces between them and within them, need to be modeled discretely. Because swelling of fibers when contacted with the invading wetting fluid is an important consideration, the micro-porous fibers themselves need proper resolution, leading to a multi-scale model. This will be a significant and very interesting modeling challenge.

This approach of detailed imaging with associated image analysis can also be useful for other layered systems, where it can also be used to guide in the development of appropriate modeling tools. Based on layer thicknesses, their REV sizes, and their connection (with or without overlap), a proper modeling approach can be identified, based on appropriate measures that come directly from the image analysis.

4.5 References

Alam, P., Byholm, T., Kniivilä, J., Sinervo, L., Toivakka, M.: Calculating the permeability of model paper coating structures comprising incongruent particle shapes and sizes. (2009)

Alam, P., Toivakka, M., Backfolk, K., Sirviö, P.: Impact spreading and absorption of Newtonian droplets on topographically irregular porous materials. Chem. Eng. Sci. 62, 3142–3158 (2007). doi:10.1016/j.ces.2007.03.018

Anderson, D.M., Linville, A.: Temperature Fluctuations Accompanying Water Movement through Porous Media Published by : American Association for the Advancement of Science. Am. Assoc. Adv. Sci. 131, 1370–1371 (1960)

Anderson, D.M., Linville, A.: Temperature Fluctuations at a Wetting Front: I. Characteristic Temperature-Time Curves1. Soil Sci. Soc. Am. J. 26, 14 (1962). doi:10.2136/sssaj1962.03615995002600010005x

Anderson, D.M., Linville, A., Sposito, G.: Temperature Fluctuations at a Wetting Front: III. Apparent Activation Energies for Water Movement in the Liquid and Vapor Phases1. Soil Sci. Soc. Am. J. 27, 610 (1963)(a). doi:10.2136/sssaj1963.03615995002700060014x

Anderson, D.M., Sposito, G., Linville, A.: Temperature Fluctuations at a Wetting Front: II. The Effect of Initial Water Content of the Medium on the Magnitude of the Temperature Fluctuations1. Soil Sci. Soc. Am. J. 27, 367 (1963)(b). doi:10.2136/sssaj1963.03615995002700040005x

Aronsson, M., Henningsson, O., Sävborg, Ö.: Slice-based digial volume assembly of a small paper sample. Nord. Pulp Pap. Res. J. 17, 29–33 (2001). doi:10.3183/NPPRJ-2002-17-01-p029-033

Aslannejad, H., Hassanizadeh, S.M.: Study of Hydraulic Properties of Uncoated Paper: Image Analysis and Pore-Scale Modeling. Transp. Porous Media. (2017). doi:10.1007/s11242-017-0909-x

Aslannejad, H., Hassanizadeh, S.M., Raoof, A., de Winter, D.A.M., Tomozeiu, N., van Genuchten, M.T.: Characterizing the hydraulic properties of paper coating layer using FIB-SEM tomography and 3D pore-scale modeling. Chem. Eng. Sci. 160, 275–280 (2017)(a). doi:10.1016/j.ces.2016.11.021

Aslannejad, H., Terzis, A., Hassanizadeh, S.M., Weigand, B.: Occurrence of temperature spikes at a wetting front during spontaneous imbibition. Sci. Rep. 7, 7268 (2017)(b). doi:10.1038/s41598-017-07528-7

Axelsson, M.: Image analysis for volumetric characterisation of microstructure. (2009)

Axelsson, M., Svensson, S.: 3D pore structure characterisation of paper. Pattern Anal. Appl. 13, 159–172 (2010). doi:10.1007/s10044-009-0146-1

Bangham, D.H., Razouk, R.I.: Adsorption and the wettability of solid surfaces. Trans. Faraday Soc. 33, 1459 (1937). doi:10.1039/tf9373301459

Bedram, A., Moosavi, A.: Breakup of droplets in micro and nanofluidic T-junctions. J. Appl. Fluid Mech. 6, 81–86 (2013). doi:10.4028/www.scientific.net/AMM.110-116.3673

Blumer, M.: Thermometric Monitor for Chromatographic Streams. Anal. Chem. 32, 772–776 (1960)

Bosanquet, C.H.: LV. On the flow of liquids into capillary tubes. Philos. Mag. Ser. 6. 45, 525–531 (1923). doi:10.1080/14786442308634144

Carsel, R.F., Parrish, R.S.: Developing joint probability distributions of soil water retention characteristics. Water Resour. Res. 24, 755–769 (1988)

Cheng, Kirsch, L., Wiegmann, R., Gervais, A., Bardin-Monnier, P.-C., N. Thomas, D.: PleatLab. A pleat scale simulation environment for filtration simulation. (2013)

Claxton, G.: Detector for liquid-solid chromatography. J. Chromatogr. A. 2, 136–139 (1959). doi:10.1016/S0021-9673(01)86273-7

Dalton, Preston, J.., Heard, J.., Allen, P.., Elton, G.., Husband, N..: Investigation into the distribution of ink components throughout printed coated paper. Colloids Surfaces A Physicochem. Eng. Asp. 205, 199–213 (2002). doi:10.1016/S0927-7757(02)00021-3

Das, S., Ramarao, B.V.: Inversion of lime mud and papermaking pulp filtration data to determine compressibility and permeability relationships. Sep. Purif. Technol. 28, 149–160 (2002). doi:10.1016/S1383-5866(02)00047-3

de Gans, B.-J., Duineveld, P.C., Schubert, U.S.: Inkjet Printing of Polymers: State of the Art and Future Developments. Adv. Mater. 16, 203–213 (2004). doi:10.1002/adma.200300385

Delerue, J.F., Perrier, E., Yu, Z.Y., Velde, B.: New algorithms in 3D image analysis and their application to the measurement of a spatialized pore size distribution in soils. Phys. Chem. Earth, Part A Solid Earth Geod. 24, 639–644 (1999). doi:10.1016/S1464-1895(99)00093-9

Desie, G., Deroover, G., De Voeght, F., Soucemarianadin, A.: Printing of dye and pigment-based aqueous inks onto porous substrates. J. Imaging Sci. Technol. 48, 389–397 (2004)

Do-Quang, M., Carlson, A., Amberg, G.: The impact of ink-jet droplets on a paper-like structure. Fluid Dyn. Mater. Process. 7, 389–402 (2011). doi:10.3970/fdmp.2011.007.389

Dodson, C.T.J., Sampson, W.W.: The effect of paper formation and grammage on its pore size distribution. J. pulp Pap. Sci. 22, J165–J169 (1996)

Fathi, H., Raoof, A., Mansouri, S.H.: Insights into the role of wettability in cathode catalyst layer of proton exchange membrane fuel cell; pore scale immiscible flow and transport processes. J. Power Sources. 349, 57–67 (2017). doi:10.1016/j.jpowsour.2017.03.012

Gambaryan-Roisman, T.: Liquids on porous layers: wetting, imbibition and transport processes. Curr. Opin. Colloid Interface Sci. 19, 320–335 (2014). doi:10.1016/j.cocis.2014.09.001

Gane, P., Hooper, J.: An evaluation of interactions between coating color and basepaper by coating profile analysis. Fundamentals of Papermaking. In: Trans. 9th Fundamental Reasearch Symposium, Ed. Baker and Punton, Mech. Eng. Publ., London, UK. pp. 871–893 (1989)

Gane, P.A.C.: Mottle and the influence of coating and binder migration. Pap. Technol. Ind. 30, 34–41 (1989)

Gane, P.A.C., Hooper, J.J., Baumeister, M.: The influence of furnish content on formation and basesheet profile stability during coating. Tappi J. 74, 193–201 (1991)

Gane, P.A.C., Salo, M., Kettle, J.P., Ridgway, C.J.: Comparison of Young-Laplace pore size and microscopic void area distributions in topologically similar structures: a new method for characterising connectivity in pigmented coatings. J. Mater. Sci. 44, 422–432 (2008). doi:10.1007/s10853-008-3134-8

van Genuchten, M.: A closed-form equation for predicting the hydraulic conductivity of unsaturated soils. Soil Sci. Soc. Am. J. 44.5, 892–898. (1980)

Ghanbarian-Alavijeh, B., Liaghat, A., Huang, G.-H., van Genuchten, M.T.: Estimation of the van Genuchten soil water retention properties from soil textural data. Pedosphere. 20, 456–465 (2010)

Ghassemzadeh, J., Sahimi, M.: Pore network simulation of fluid imbibition into paper during coating—III: modelling of the two-phase flow. Chem. Eng. Sci. 59, 2281–2296 (2004)(a). doi:10.1016/j.ces.2004.01.058

Ghassemzadeh, J., Sahimi, M.: Pore network simulation of fluid imbibition into paper during coating: II. Characterization of paper's morphology and computation of its effective permeability tensor. Chem. Eng. Sci. 59, 2265–2280 (2004)(b). doi:10.1016/j.ces.2004.01.057

Girard, F., Attané, P., Morin, V.: A new analytical model for impact and spreading of one drop: Application to inkjet printing. Tappi J. 5, 24–32 (2006)

Gronfors, J.: Use of fillers in paper and paperboard grades, (2010)

Hassanizadeh, S.M., Gray, W.G.: Mechanics and thermodynamics of multiphase flow in porous media including interface boundaries. Adv. Water Resour. 13, 169–186 (1990)

Hassanizadeh, S.M., Gray, W.G.: Thermodynamic basis of capillary pressure in porous media. Water Resour. Res. 29, 3389–3405 (1993). doi:10.1029/93WR01495

Heard, P.J., Preston, J.S., Parsons, D.J., Cox, J., Allen, G.C.: Visualisation of the distribution of ink components in printed coated paper using focused ion beam techniques. Colloids Surfaces A Physicochem. Eng. Asp. 244, 67–71 (2004). doi:10.1016/j.colsurfa.2004.05.012

Hilpert, Markus, Miller, T., C.: Pore-morphology-based simulation of drainage in totally wetting porous media. Adv. Water Resour. 24, 243–255 (2001). doi:10.1016/S0309-1708(00)00056-7

Hird, K.F.: Offset lithographic technology. Goodheart-Willcox Co, Tinley Park, Illinois (2000)

Hirn, U., Schennach, R.: Comprehensive analysis of individual pulp fiber bonds quantifies the mechanisms of fiber bonding in paper. Sci. Rep. 5, 10503 (2015)

Hodgson, K.T., Berg, J.C.: Dynamic Wettability Properties of Single Wood Pulp Fibers and Their Relationship to Absorbency. Wood Fiber Sci. 20, 3–17 (2007)

Holmstad: Comparison of 3D structural characteristics of high and low resolution X-ray microtomographic images of paper. Nord. Pulp Pap. Res. J. 20, 283–288 (2005). doi:10.3183/NPPRJ-2005-20-03-p283-288

Huang, S., Goel, A., Ramaswamy, S., Ramarao, B., Choi, D.: Transverse and in-plane pore structure characterization of paper, (2002)

Hyväluoma, J., Koponen, A., Raiskinmäki, P., Timonen, J.: Droplets on inclined rough surfaces. Eur. Phys. J. E. 23, 289–293 (2007). doi:10.1140/epje/i2007-10190-7

Hyväluoma, J., Raiskinmäki, P., Jäsberg, A., Koponen, A., Kataja, M., Timonen, J.: Simulation of liquid penetration in paper. Phys. Rev. E. 73, 036705 (2006). doi:10.1103/PhysRevE.73.036705

Ingmanson, W.L., Andrews, B.D., Johnson, R.C.: Internal Pressure Distributions in Compressible Mats under Fluid Stress. TAPPI J. 42, 840–849 (1959)

Järnström, J., Väisänen, M., Lehto, R., Jäsberg, A., Timonen, J., Peltonen, J.: Effect of latex on surface structure and wetting of pigment coatings. Colloids Surfaces A

Physicochem. Eng. Asp. 353, 104–116 (2010). doi:10.1016/j.colsurfa.2009.11.001

Kanit, T., Forest, S., Galliet, I., Mounoury, V., Jeulin, D.: Determination of the size of the representative volume element for random composites: statistical and numerical approach. Int. J. Solids Struct. 40, 3647–3679 (2003). doi:10.1016/S0020-7683(03)00143-4

Karwacki, L., de Winter, D.A., Aramburo, L.R., Lebbink, M.N., Post, J.A., Drury, M.R., Weckhuysen, B.M.: Architecture-Dependent Distribution of Mesopores in Steamed Zeolite Crystals as Visualized by FIB-SEM Tomography. Angew. Chemie Int. Ed. 50, 1294–1298 (2011)

Kettle, J., Lamminmäki, T., Gane, P.: A review of modified surfaces for high speed inkjet coating. Surf. Coatings Technol. 204, 2103–2109 (2010). doi:10.1016/j.surfcoat.2009.10.035

Kuijpers, C.J., van Stiphout, T.A.P., Huinink, H.P., Tomozeiu, N., Erich, S.J.., Adan, O.C.G.: Quantitative measurements of capillary absorption in thin porous media by the Automatic Scanning Absorptometer. Chem. Eng. Sci. 178, 70–81 (2018). doi:10.1016/J.CES.2017.12.024

Lamminmäki, T., Kettle, J., Rautkoski, H., Kokko, A., Gane, P.: Limitations of Current Formulations when Decreasing the Coating Layer Thickness of Papers for Inkjet Printing. Ind. Eng. Chem. Res. 50, 7251–7263 (2011). doi:10.1021/ie102114s

Lamminmaki, T., Kettle, J.P., Puukko, P., Gane, P.A.C., Ridgway, C.: Inkjet print quality: the role of polyvinyl alcohol in speciality CaCO3 coatings. J. Pulp Pap. Sci. 35, 137–147 (2009)

Lamminmäki, T.T., Kettle, J.P., Gane, P.A.C.: Absorption and adsorption of dye-based inkjet inks by coating layer components and the implications for print quality. Colloids Surfaces A Physicochem. Eng. Asp. 380, 79–88 (2011). doi:10.1016/j.colsurfa.2011.02.015

Lamminmäki, T.T., Kettle, J.P., Puukko, P.J.T., Ridgway, C.J., Gane, P.A.C.: Short timescale inkjet ink component diffusion: an active part of the absorption mechanism into inkjet coatings. J. Colloid Interface Sci. 365, 222–235 (2012). doi:10.1016/j.jcis.2011.08.045

Le, H.P.: Progress and trends in ink-jet printing technology. J. Imaging Sci. Technol. 42, 49–62 (1998)

Lee, H.K., Joyce, M.K., Fleming, P.D., Cameron, J.H.: Production of a single coated glossy inkjet paper using conventional coating and calendering methods, https://wmich.pure.elsevier.com/en/publications/production-of-a-single-coated-glossy-inkjet-paper-using-conventio-3, (2002)

Leij, F.J., Russell, W.B., Lesch, S.M.: Closed-form expressions for water retention and conductivity data. Ground Water. 35, 848–858 (1997)

Lindsay, J.D.: The anisotropic permeability of paper: theory, measurements, and analytical tools. (1988)

Liu, G., Fu, S., Lu, Z., Zhang, M., Ridgway, C., Gane, P.: Contrasting liquid imbibition into uncoated versus pigment coated paper enables a description of imbibition into new-generation surface-filled paper. Eur. Phys. J. E. 40, 111 (2017). doi:10.1140/epje/i2017-11600-y

López-Marzo, A.M., Merkoçi, A.: Paper-based sensors and assays: A success of the engineering design and the convergence of knowledge areas, http://xlink.rsc.org/?DOI=C6LC00737F, (2016)

Luckner, L., van Genuchten, M.T., Nielsen, D.R.: A consistent set of parametric models for the two-phase flow of immiscible fluids in the subsurface. Water Resour. Res. 25, 2187–2193 (1989). doi:10.1029/WR025i010p02187

Malla, Devisetti: Novel kaolin pigment for high solids ink jet coating. Pap. Technol. 46, 17–27 (2005)

Matilainen, K., Hämäläinen, T., Savolainen, A., Sipiläinen-Malm, T., Peltonen, J., Erho, T., Smolander, M.: Performance and penetration of laccase and ABTS inks on various printing substrates. Colloids Surfaces B Biointerfaces. 90, 119–128 (2012). doi:10.1016/j.colsurfb.2011.10.015

Modaressi, H., Garnier, G.: Mechanism of wetting and absorption of water droplets on sized paper: Effects of chemical and physical heterogeneity. Langmuir. 18, 642–649 (2002). doi:10.1021/la0104931

Oce: Specificaties Océ VarioPrint i300 - Canon Nederland, https://www.canon.nl/business-printers-and-faxes/cut-sheet-colour-printers/varioprint-i300/specifications/

Oostrom, M., Dane, J.H., Lenhard, R.J.: Fluid Contents. J.H. Dane and G.C. Topp; Soil Science Society of America , Madison, WI, United States(US). (2002)

Palakurthi, N.K., Konangi, S., Ghia, U., Comer, K.: Micro-scale simulation of unidirectional capillary transport of wetting liquid through 3D fibrous porous media: Estimation of effective pore radii. Int. J. Multiph. Flow. 77, 48–57 (2015). doi:10.1016/j.ijmultiphaseflow.2015.07.010

Patrick A. Gane, †, John P. Kettle, ‡, G. Peter Matthews, * and, Ridgway, C.J.: Void Space Structure of Compressible Polymer Spheres and Consolidated Calcium Carbonate Paper-Coating Formulations. (1996). doi:10.1021/IE950413M

Perrier, E. R.; Prakash, O.M.: Heat and vapor movement during infiltration into dry soils. Soil Sci. 124, 73–73 (1976)

Podsiadlo, P., Choi, S.-Y., Shim, B., Lee, J., Cuddihy, M., Kotov, N.A.: Molecularly Engineered Nanocomposites: Layer-by-Layer Assembly of Cellulose Nanocrystals. Biomacromolecules. 6, 2914–2918 (2005). doi:10.1021/bm050333u

Prunty, L.: Thermal Transients in Closed , Unsaturated Soil Systems. Therm. Transient. 1–4 (2002)

Prunty, L., Bell, J.: Soil Temperature Change over Time during Infiltration. Soil Sci. Soc. Am. J. 69, 766 (2005). doi:10.2136/sssaj2004.0219

Ramaswamy, S., Gupta, M., Goel, A., Aaltosalmi, U., Kataja, M., Koponen, A., Ramarao, B..: The 3D structure of fabric and its relationship to liquid and vapor transport. Colloids Surfaces A Physicochem. Eng. Asp. 241, 323–333 (2004). doi:10.1016/j.colsurfa.2004.04.023

Ramaswamy, S., Huang, S., Goel, A., Cooper, A., Choi, D., Bandyopadhyay, A., Ramarao, B. V: The 3D structure of paper and its relationship to moisture transport in liquid and vapor forms. In: 12th Fundamental Research Symposium, Oxford. pp. 1289–1311 (2001)

Ridgway, C.J., Gane, P.A.C.: Controlling the absorption dynamic of water-based ink into porous pigmented coating structures to enhance print performance. Nord. Pulp Pap. Res. J. 17, 119–129 (2002)

Ridgway, C.J., Gane, P.A.C., Schoelkopf, J.: Effect of capillary element aspect ratio on the dynamic imbibition within porous networks. J. Colloid Interface Sci. 252, 373–382 (2002). doi:10.1006/jcis.2002.8468

Rolland du Roscoat, S., Decain, M., Geindreau, C., Thibault, X., Bloch, J.-F.: Microstructural Analysis of Paper Using Synchrotron X-ray Microtomography: Numerical Estimation of the Permeability and Effective Thermal Conductivity. Appita J. J. Tech. Assoc. Aust. New Zeal. Pulp Pap. Ind. 61, 286 (2008)

du Roscoat, S.R., Bloch, J.F., Thibault, X.: Characterization of the 3D paper structure with X-ray synchrotron radiation microtomography. In: The 13th FRC Symposium, Robinson College, Cambridge. pp. 901–920 (2005)

Rosenholm, J.B.: Liquid spreading on solid surfaces and penetration into porous matrices: Coated and uncoated papers. Adv. Colloid Interface Sci. 220, 8–53 (2015). doi:10.1016/j.cis.2015.01.009

Salmas, C.E., Stathopoulos, V.N., Pomonis, P.J., Rahiala, H., Rosenholm, J.B., Androutsopoulos, G.P.: An investigation of the physical structure of MCM-41 novel mesoporous materials using a corrugated pore structure model. Appl. Catal. A Gen. 216, 23–39 (2001). doi:10.1016/S0926-860X(01)00520-8

Samuelsen, E.J., Houen, P., Gregersen, Ø.W., Helle, T.: Three-dimensional imaging of paper by use of synchrotron x-ray microtomography. J. Pulp Pap. Sci. 27, 50–53 (2001)

Sappi: The Paper Making Process, https://www.youtube.com/redirect?redir_token=VEjJPq2aJlcjBgVBNfN_Rc4CZfl8MTU0MDIxMjEyMkAxNTQwMTI1NzIy&event=video_description&v=E4C3X26dxbM&q=http%3A%2F%2Fwww.na.sappi.com%2Feducation%2Flifecycle

Schoelkopf, J., Gane, P.A.., Ridgway, C.J., Matthews, G.P.: Practical observation of deviation from Lucas–Washburn scaling in porous media. Colloids Surfaces A Physicochem. Eng. Asp. 206, 445–454 (2002). doi:10.1016/S0927-7757(02)00066-3

Schoelkopf, J., Gane, P.A.C., Ridgway, C.J., Matthews, G.P.: Influence of inertia on liquid absorption into paper coating structures. Nord. Pulp Pap. Res. J. 15, 422–430 (2000)

Schulz, V.P., Wargo, E.A., Kumbur, E.C.: Pore-morphology-based simulation of drainage in porous media featuring a locally variable contact angle. Transp. Porous Media. 107, 13–25 (2014). doi:10.1007/s11242-014-0422-4

Singh, M., Haverinen, H.M., Dhagat, P., Jabbour, G.E.: Inkjet Printing-Process and Its Applications. Adv. Mater. 22, 673–685 (2010). doi:10.1002/adma.200901141

Song, Y., Davy, C.A., Bertier, P., Troadec, D.: Understanding fluid transport through claystones from their 3D nanoscopic pore network. Microporous Mesoporous Mater. 228, 64–85 (2016). doi:10.1016/j.micromeso.2016.03.023

Suffield, S., Jokar, A.: Modeling the Flow of a Liquid Droplet Diffusing Into Various Porous Media for Inkjet Printing Applications. In: Volume 10: Heat Transfer, Fluid Flows, and Thermal Systems, Parts A, B, and C. pp. 1013–1022. ASME (2008)

Tåg, C.-M., Järn, M., Granqvist, B., Järnström, J., Peltonen, J., Rosenholm, J.B.: Influence of surface structure on wetting of coated offset papers. Holzforschung. 61, 516–522 (2007). doi:10.1515/HF.2007.073

Terzis, A., Roumeli, E., Weishaupt, K., Brack, S., Aslannejad, H., Groß, J., Hassanizadeh, S.M., Helmig, R., Weigand, B.: Heat release at the wetting front during capillary filling of cellulosic micro-substrates. J. Colloid Interface Sci. 504, 751–757 (2017). doi:10.1016/j.jcis.2017.06.027

Vikman, K., Vuorinen, T.: Water fastness of ink jet prints on modified conventional coatings. 48, 138–147 (2004)

Washburn, E.W.: The Dynamics of Capillary Flow. Phys. Rev. 17, 273–283 (1921). doi:10.1103/PhysRev.17.273

Wei, H., Ramarao, B. V: Characterization of pulp slurries using a novel drainage tester. In: Tappi Engineering Conference. pp. 517–524 (1996)

Weller, H.G.: A new approach to VOF-based interface capturing methods for incompressible and compressible flow. OpenCFD Ltd., Rep. TR/HGW/04. (2008)

Xu, L., Zhang, W.W., Nagel, S.R.: Drop splashing on a dry smooth surface. Phys. Rev. Lett. 94, 184505 (2005). doi:10.1103/PhysRevLett.94.184505

Yarin, A.L.: DROP IMPACT DYNAMICS: Splashing, Spreading, Receding, Bouncing…. Annu. Rev. Fluid Mech. 38, 159–192 (2006). doi:10.1146/annurev.fluid.38.050304.092144

Zhao, H., Kwak, J.H., Conrad Zhang, Z., Brown, H.M., Arey, B.W., Holladay, J.E.: Studying cellulose fiber structure by SEM, XRD, NMR and acid hydrolysis. Carbohydr. Polym. 68, 235–241 (2007). doi:10.1016/j.carbpol.2006.12.013

Zhu, S., Pelton, R.H., Collver, K.: Mechanistic modelling of fluid permeation through compressible fiber beds. Chem. Eng. Sci. 50, 3557–3572 (1995). doi:10.1016/0009-2509(95)00205-J

Zoladek-Nowak, J., Milczarek, J.J., Fija-Kirejczyk, I.M., Zoldek, J., Jurkowski, Z.: Transient Thermal Phenomena during Spontaneous Water Migration in Zeolite Beds. ACTA Phys. Pol. 122, 415–418 (2012)

Product information sheet Magno TM gloss Coated fine paper available in sheets and reels for offset printing Technical specifications Print recommendations Dot area Mill certifications. 2016 (2016)

Movement of a liquid droplet within a fibrous layer: direct pore-scale modeling and experimental observations

Abstract

In this study, the spreading of a liquid droplet on the surface of a fibrous paper and its penetration into the paper is studied. The spreading of the droplet was visualized using confocal microscopy and the penetration depth was quantified using Automatic Scanning Absorptiometry (ASA) measurements. The three-dimensional structure of the paper was obtained through micro-tomography imaging with a resolution of 0.9 µm. The obtained images were used to reconstruct the pore space, which was in turn used in direct numerical simulations of penetration of a droplet into paper. Simulations were performed using open source code OpenFOAM, which solves equations of two-phase flow (in our case air and water) in pores based on the Volume of Fluid Method. Simulation results showed a good agreement with the experimental observations. In particular, the dimensions of spreading area of a droplet and the depth of penetration were simulated reasonably well. Then, we used the model to investigate effects of changes in various liquid properties on spreading and penetration of a droplet liquid. We made calculations for three different values of contact angle (*CA*): 0°, 60°, and 120°. We found the largest penetration depth for *CA*=0. For *CA*=60 and *CA*=120, we found that the liquid droplet moved sideways from the jetted location, which is not favorable in inkjet printing. We also made simulations with larger values for viscosity and density, based on properties of an ink-based liquid used in inkjet printing. The results have shown a slower spreading and penetration compared with water. The model

Published as: H. Aslannejad, H. Fathi, S.M. Hassanizadeh, A. Raoof, N. Tomozeiu, Movement of a liquid droplet within a fibrous layer: Direct pore-scale modeling and experimental observations, Chemical Engineering Science, Volume 191, 2018, Pages 78-86, DOI: https://doi.org/10.1016/j.ces.2018.06.054

can be used to study effects of changes in either ink physical properties or paper layer microstructure on final spreading/penetration extent.

5.1 Introduction

Cellulose fibers are renewable natural materials, which are encountered in many industrial applications, such as paper and printing, packaging, and paper-based diagnostic devices. Their main features important to these applications are light weight, mechanical strength, and low cost (Podsiadlo et al. 2005).

In the majority of applications, a fibrous layer comes into contact with some liquid (mainly water-based liquid). Because cellulose fibers are hydrophilic, liquid will move rapidly along and into fibers. This can cause unwanted spreading of ink in paper, for example in case of inkjet printing (Figure 5.1), or swelling of fibers, which can be a problem in the case of packaging application.

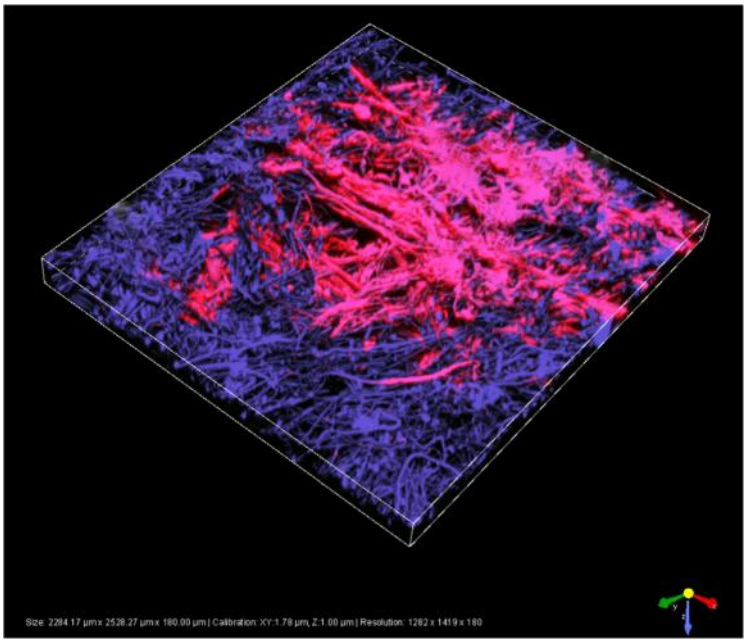

Figure 5.1 Water spreading in a fibrous layer; fibers are shown in blue and water in pink. The image was obtained using confocal microscopy

Generally, a fibrous layer can be considered as a porous medium, although liquid flow in the layer is different from traditional porous media. Usually, a liquid moves into pores of a porous network and, based on connectivity of pores, invades some of them. However, in the case of a fibrous layer, water moves first on the surface of fibers and/or into them, and then later on fills the pores between fibers (Aslannejad and Hassanizadeh 2017). Schoelkopf et al. (Schoelkopf et al. 2000)

stated that under a condition of constant wettability and surface energy, pore diameter and geometry are the controlling factors. Therefore, contradictory to Lucas-Washburn equation which predicts the large pores to be filled faster than small pores, liquid droplet in a paper layer proceeds by filling finer pores together with inertial retardation of larger pores and then, later, viscosity-controlled absorption dynamics becomes prominent. Liu et al. (Liu et al. 2017) also considered the difference between coated and uncoated paper from droplet wicking point of view and they conclude that, in case of uncoated paper, the wicking behavior follows neither viscosity-controlled model of Lucas-Washburn nor inertia-included model of Bosanquet. Modarresi and Garnier (Modaressi and Garnier 2002) also reported such a flow behavior in a partially hydrophobized fibrous layer. They did an experiment and reported that the droplet first imbibed into the fibrous layer forming a pattern in the layer and then when it reached steady state, it was absorbed into the fibers.

In case of inkjet printing, there are two types of paper: plain and coated. Plain papers, made of cellulose fibers, may absorb too much ink. In order to limit ink uptake by plain paper, often a thin layer of coating material is applied on the surface of fibrous layer. However, due to their overall low cost, uncoated papers are more commonly used in inkjet printers. Then, various measures are taken to reduce the uptake of ink and its spreading into the fibrous layer. These relate to the modification of the properties of ink and/or fibers. Effects of such measures have been studied in recent decades. Yarin (Yarin 2006) studied normal impact of a droplet on dry paper surface and characterized effects of surface roughness, surface texture, and wettability. Modification of liquid properties by adding a polymer mixture was also studied. Xu (Xu et al. 2005) reported that by controlling the pressure artificially generated in a gas atmosphere (helium, air, krypton, and SF) during droplet impact on the solid surface, they could control splash of droplet.

Alam et al. (Alam et al. 2007) studied the kinetic-energy-driven phase of spreading of a liquid on the irregular surface of a porous material using the Volume of Fluid method (VOF). They performed computations and showed that the spreading width is inversely correlated with the depth of penetration. They studied different surface roughness types: flat, randomly located monodisperse hemispheres, and pyramidal structures. Analysis of various roughness parameters and their impact on spreading were done in their work.

Hyväluoma et al. (Hyväluoma et al. 2006) studied penetration of a liquid in paperboard using a Lattice Boltzmann method. They used reconstructed pore space

of a sample imaged by micro tomography. Capillary-driven flow into the domain was simulated and compared with well-known Lucas-Washburn equation results. They concluded that there is a need to study and determine advancing of the liquid front into the paper. They also concluded that water penetration occurs along fibers and much faster in the planar direction than in the perpendicular.

Do-Quang et al. (Do-Quang et al. 2011) investigated numerically the impact of ink onto the surface of a paper-like structure; they used a model structure as a fibrous web. They simulated multi-phase flow of air and liquid and they determined the penetration pattern of the droplet in the structure. They also studied the impact of change in wettability on penetration.

To the best of our knowledge, there have been little to no direct comparisons made of spreading of a liquid on a fibrous layer and the degree of its penetration with numerical simulations. In addition, studies involving a liquid with ink-like properties comparable to ink have been limited.

In this study, we focus on not only spreading of a droplet on a paper surface, but also its penetration into the fibrous layer. The fibrous layer pore and fiber structure were reconstructed using high-resolution micro-tomography images. The resulting digitized layer was then used as input in two-phase simulations of penetration of a droplet into the fibrous layer. Simulation results were then compared with experimental results from confocal microscopy and automatic scanning absorptiometry ASA measurements. The effect of wettability change was studied by specifying different values for contact angles. In addition, the effects of change in fluid properties (density, viscosity and surface tension) on resulting penetration/spreading are reported. The results of this study will contribute to a better understanding of the flow in printing paper. By optimizing properties of the liquid and paper, a cheaper production of high quality prints can be made possible. Moreover, results of this research are relevant to the general understanding of interaction of complex fluids with complicated porous structures.

5.2 Material and Methods

5.2.1 Paper and liquids

A Ziegler uncoated paper sample (Ziegler paper, Switzerland) was used in this study. Figure 5.2 shows an SEM image of the cross section and surface of the paper sample. The fibrous layer of paper is an anisotropic medium, where the fibers are aligned with the majority in one direction. In the terminology used in paper fabrication, the major alignment direction is termed the machine direction, and the alignment reflects the flow orientation in the papermaking process. The planar direction perpendicular to this machine running direction is termed the cross-machine direction. The sample had a thickness of 150 µm with mean pore size of 10 µm (Aslannejad and Hassanizadeh 2017). The porosity of the layer was about 50% and the fiber diameters lay in the range 10-25 µm. In a previous study (Aslannejad and Hassanizadeh 2017), we determined a permeability value of about 5 Darcy. All paper samples were kept under standard laboratory conditions before imaging and ink pattern visualization.

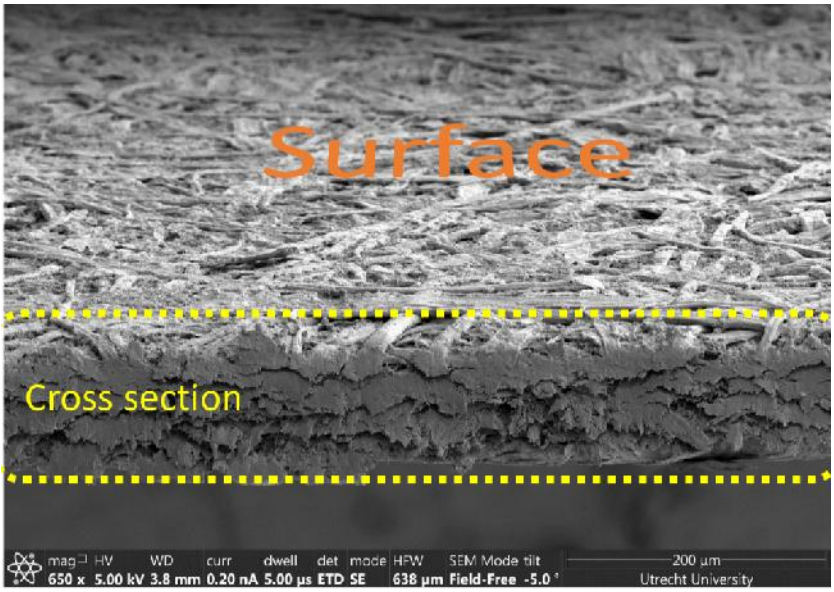

Figure 5.2 Three-dimensional SEM image of cross section and surface of a Ziegler paper sample

In experimental observations, water with a very low concentration of fluorescent salt (1 g/l) was used. The salt was added in order to improve tracking and monitoring of water under the confocal microscope. Properties of salt-water were used in simulations of experiments. For a typical inkjet printer, the ink consists of 2-5 weight% dye or pigment, 2-5% surfactants, 30% humectant (ethylene glycol), and 65% water (Lee et al. 2002). In addition to the simulation of our experiments, we also performed numerical modelling of the penetration of an ink-like liquid, having the same properties (namely, viscosity, density, and surface tension) as ink. We did not consider presence of pigments in our simulations.

5.2.2 Microstructure imaging and reconstruction

An accurate reconstruction of the pore space, with a sufficient resolution, is essential for pore-scale modeling. In order to reconstruct the 3D domain of a fibrous paper sample, imaging was done using micro-computational tomography (µCT), Zeiss Xradia Versa 520, with a resolution of 0.9 µm. The pores of a domain of 1000 x 1000 x 150 μm^3 were then seprated using watershed segmentation (Aslannejad and Hassanizadeh 2017). Figure 5.3 shows part of the reconstructed fibrous layer with a dimension of 400 × 400 × 150 μm^3.

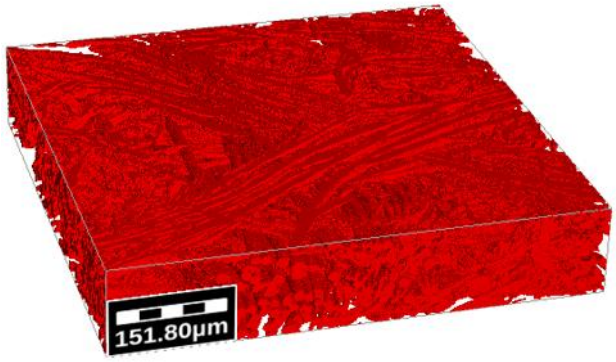

Figure 5.3 Reconstructed fibrous layer with dimensions of 400 x 400 x 150 μm^3

5.2.3 Droplet dispenser and confocal microscopy setup

In order to produce a very small ink droplet (comparable with inkjet printer droplets size), a micro droplet dispenser (Microdrop Technologies GmbH, Germany) was mounted next to the microscope objective. The dispenser was able to produce a small droplet with a volume of 180 pL. It was mounted at an angle of 45°

to the microscope objective, in order to make it possible shooting the droplet to a location on the paper within the field of view of the confocal microscope (Nikon A1+). Figure 5.4 shows the droplet dispenser-microscope setup.

Confocal microscopy was used to visualize the liquid distribution in the paper substrate. For visualization, two Argon laser wavelengths were used: 457 nm and 488 nm. Doing so, water and the fibrous layer were clearly distinguishable; fibers and water could be seen in blue and green colors, respectively.

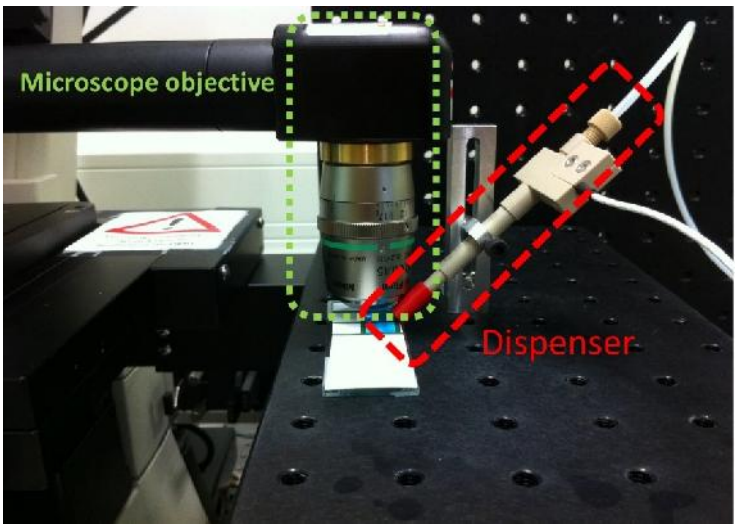

Figure 5.4 Droplet dispenser and microscope setup

5.2.4 ASA measurement setup

The Automatic Scanning Absorptiometry (ASA) is an instrument for quantifying uptake of a liquid by paper within a certain time. The ASA instrument we have used (Kumagai Riki Kogyo (KM 500win)) is shown in Figure 5.5. The main part of ASA is a horizontal rotary disk (turntable) with eccentric. A piece of paper is placed on the disk and the liquid is delivered onto the paper surface via a nozzle. The nozzle is mounted on an extended arm having a fixed length from a rotation mounting at one end. The mounting has a fixed distance from the axial sample rotation point, like a disk record player. The liquid is delivered from a glass capillary, and the Transferred Liquid Volume (TLV) is monitored within the capillary, and the resultant liquid track on the porous material forms a spiral that can be characterized by its radius and pitch (the distance between the two consecutive radii at the same polar angle).

In a typical analysis of ASA measurements, the penetration depth is estimated from TLV, the nozzle width and length and assuming all pores are filled by the absorbed liquid (Kuijpers et al. 2018). In our experiment, we determined the penetration depth for a given TLV using SEM and observing the cross section of paper.

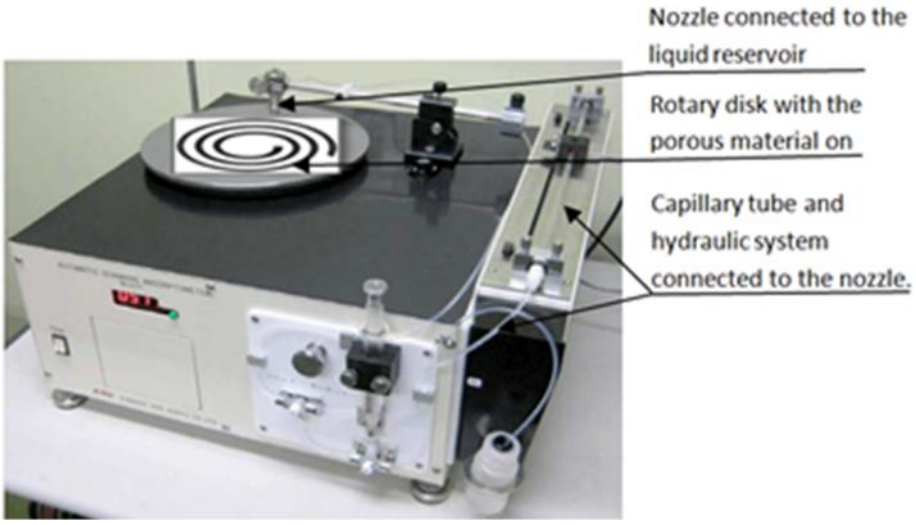

Figure 5.5 ASA measurement setup

5.2.5 Two-phase flow modeling

The spreading of a liquid droplet on the paper surface and its penetration into the fibrous layer was modeled as simultaneous movement of the two phases in interface contact (air and water) in the pore space. Two-phase flow simulations were performed using open source software, OpenFOAM (The OpenFOAM Foundation, 2017. http://www.openfoam.org/ (accessed 22 October 2017)), which solves an extended form of the Navier-Stokes equations. Palakurthi et al. (Palakurthi et al. 2015) verified the solution of OpenFOAM for liquid penetration in virtual fibrous media. They checked the results against Lucas–Washburn kinetics at the micro-scale, being limited to a parallel bundle of capillaries only, and found them acceptable apart from the very initial stages dominated by inertial forces.

Several studies have employed the Volume of Fluid (VOF method to simulate two-phase flow at the micro- and nanoscale (Fathi et al. 2017). Ability of the VOF method to model micro- and nanoscale processes was shown by Bedram and Moosavi (Bedram and Moosavi 2013). In this method, continuity and momentum balance equations were solved in order to obtain the liquid phase volume

fraction in each numerical cell, such that $F_v = \alpha V_{cell}$, where F_v is the volume of liquid phase in a cell with volume V_{cell}. The value of α varies between zero and one. The movement of air-liquid interfaces is simulated by solving a transport equation for α as:

$$\frac{\partial}{\partial} + \nabla(U\ ) + \nabla.(\alpha(-\alpha)U_r) = 0 \qquad 5\text{-}1$$

in which U_r is the velocity of the interface and defines as:

$$U_{\mathrm{r}} = c_{\mathrm{r}}|U|\frac{\nabla\alpha}{|\nabla\alpha|} \qquad 5\text{-}2$$

The last term of equation 5-1 is non-zero only in cells where an interface exists and α is between zero and one. This term represents a numerical compression term as suggested by Weller (Weller 2008) in order to minimize the smearing of the interface. The parameter c_r in Equation 5-2 controls the compression of the interface. Following Weller, the value of c_r was taken to be the range $1 \leq c_r \leq 4$ in order to maintain a sharp interface. The physical properties of the "equivalent liquid" in a numerical cell were calculated as averages of properties of the two phase weighted with the volume fraction α. For example, the fluid density at any point within the domain is given by:

$$\rho = \alpha\rho_{\mathrm{w}} + (1-\alpha)\rho_{\alpha} \qquad 5\text{-}3$$

where ρ_w and ρ_a are the densities of water and air, respectively. The viscosity, μ, is calculated in a similar way. For boundary conditions, we assumed the surface of fibers as solid surfaces with a contact angle of 15° and symmetry condition were applied for the boundaries.

5.3 Results and discussion

5.3.1 Experimental results

In order to consider heterogeneity of the fibrous layer and its effect on results, four-different locations on the paper surface were chosen. At each location, a liquid droplet of 180 pL was placed on fibrous layer. The final distributions of water on paper surface, imaged using confocal microscopy, are shown in Figure 5.6; fibers are seen in blue color and ink-like liquid in green color. The extent of spreading was measured in two directions, i.e. in the machine direction and cross-machine direction.

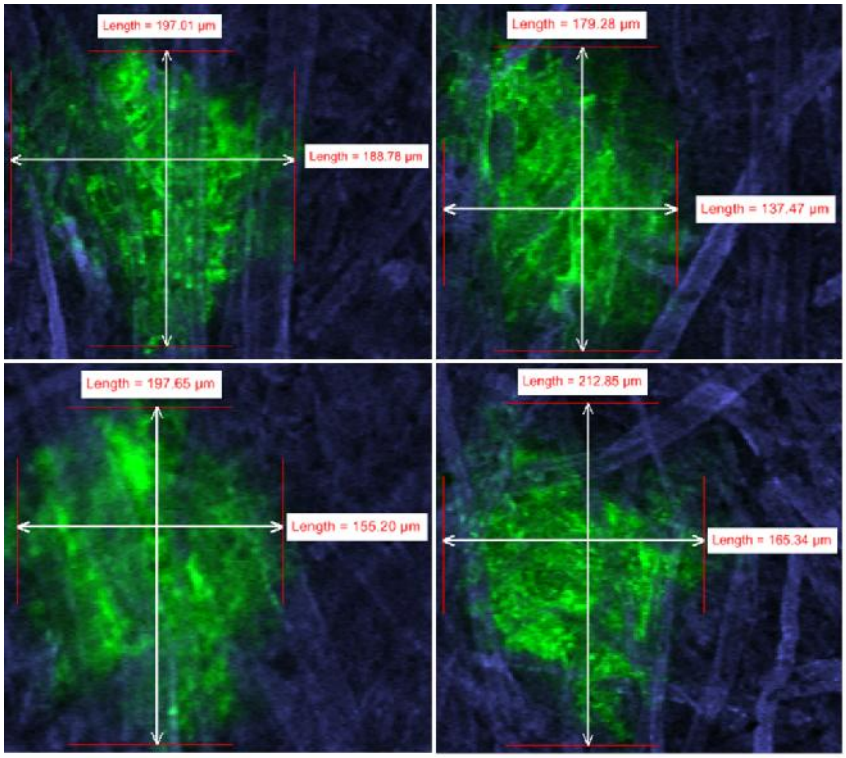

Figure 5.6 Final states of liquid spread on paper at four different locations; imaging was done using confocal microscopy. Fibers are in blue and ink is seen in green

The penetration depth was found to be smaller than the spreading extent in planar directions. This is to be expected as the fibers lie mainly in the plane of paper since most fibers are laid down oriented in machine direction. Along the machine

direction, the ink spread was in the range of 180- 210 µm, while in the perpendicular direction it spread around 140-190 µm.

During the experiment, it was observed that as soon as droplet arrives on surface of layer, it starts to spread on fibers and then evaporation occurs immediately. Although swelling was expected, but due to very small amount of water and relatively fast evaporation at the end of spreading, no change in fiber size was recorded. In the other words, for a single droplet of 180 pL, no fiber swelling was observed, consequently, that can be assumed that in case of single droplet, water intake of fibers is negligible.

The penetration depth for a 200 pL of liquid was determined to be 50 µm, using ASA measurements as explained earlier. Since the major axes of fibers are in the plane of the sheet, the spreading length is larger than the vertical penetration depth.

5.3.2 Simulation results

Since the sheet is so thin, the traditional penetration model is used, i.e. that of direct porosity-filling, in contrast to the wicking and spread function employing the software modelling based on volume of fluid. For the simulation of experiments, a spherical droplet with diameter of 75 µm was placed on the fibrous layer (Figure 5.7) at four different locations. The reconstructed pore geometry was used as the modelling domain. This had a size of 400 x 400 x 150 μm^3. The grid size of the computational domain was assigned small enough to ensure the grid independency of the results.

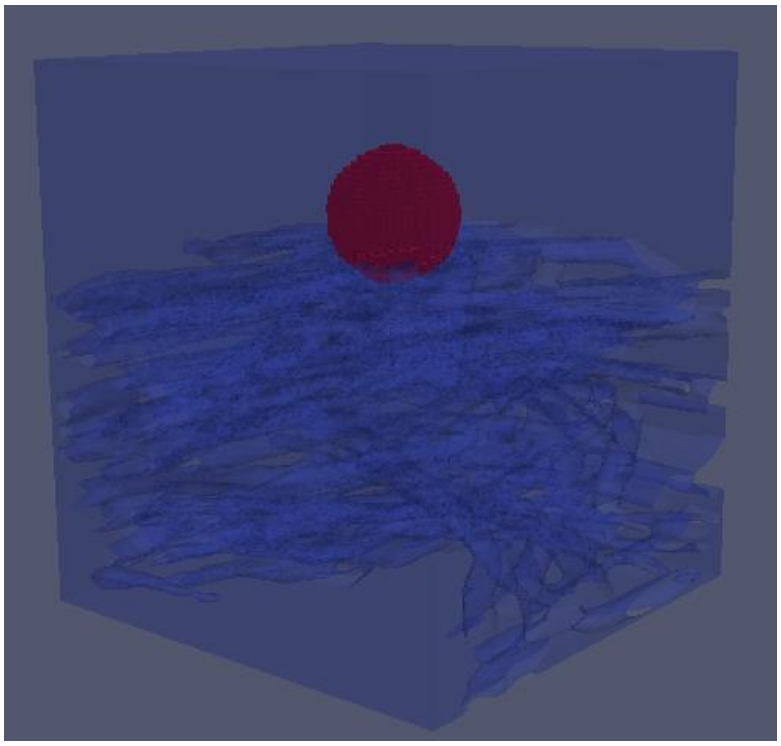

Figure 5.7 Initial condition: droplet (in red color) on fibrous layer (in blue color)

The final spreading area of water on paper at four locations are shown qualitatively in Figure 5.8. In order to compare modeling and experimental results, Figure 5.9 shows spreading extents of a droplet in machine and perpendicular directions for modeling and experimental results. It can be observed that the spreading extends along the machine and the perpendicular directions are in the same range as those measured from the experimental results: 150-250 µm. The penetration depth in modeling cases was resulted to be 50 µm on average, which is also in good agreement with the ASA measurement results.

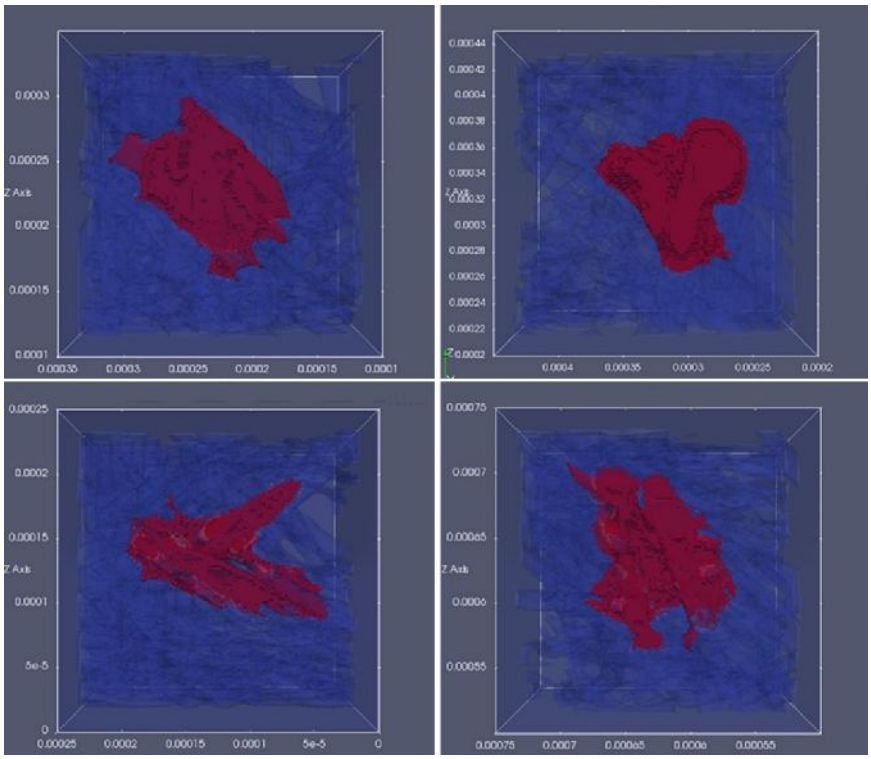

Figure 5.8 Modeling results of water spreading in fibrous layer of paper at four different locations (spreading in *x*- *z*, here the axis *y* is along the tickness of layer)

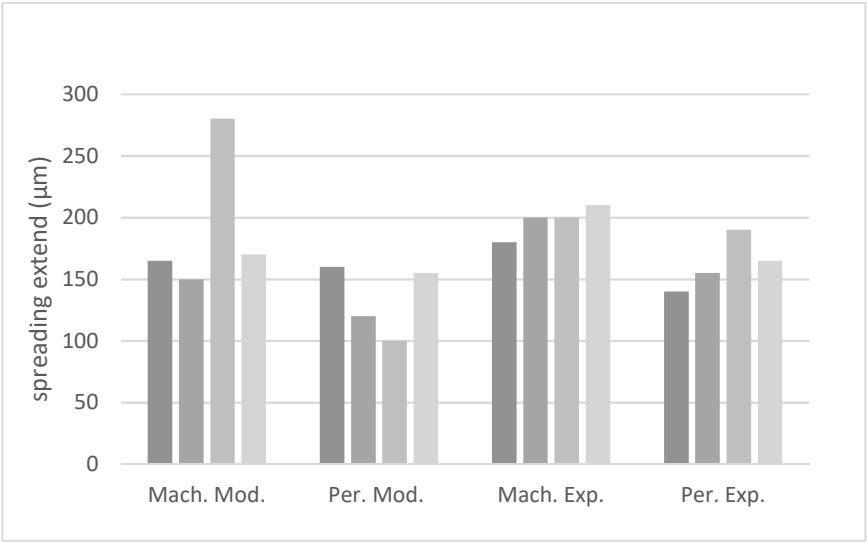

Figure 5.9 Ink spreading extent in machine and perpendicular directions based on modeling and experimental results. (In *x* axis, Mach. and Per. are Machine and

Perpendicular to machine directions respectively. Mod. and Exp. Stand for modeling and experimental results respectively.)

5.3.3 Water and ink-like liquid

Simulations were also performed for a liquid with properties similar to those of ink-like liquid and results were compared with those of water. Table 5-1 shows physical properties of ink-like liquid, which have been used in this study. Figure 5.10 shows the distribution of the liquid phase within the fibrous layer for the case of water (5.10a) and ink-like liquid (5.10b). The extent of lateral spreading in both cases is approximately the same, but water penetrated deeper than ink-like case. Higher viscosity and lower surface tension of ink-like liquid cause less penetration depth in paper. It may be concluded that ink-like liquid, which has a higher viscosity and density, has a slower imbibition rate, as expected. The amount of water in a rectangular parallelepiped section of the domain (shown in Figure 5.11) was determined and plotted over time (shown in Figure 5.12). It is clear that water reaches certain depth of paper much faster than the ink-based liquid.

Table 5-1 Water and ink-based liquid properties

	Kinematic Viscosity (m^2/s)	Density (kg/m^3)	Surface tension (N/m)
Water	1e-6	1000	0.0707
Ink-based liquid	2e-6	2050	0.03571

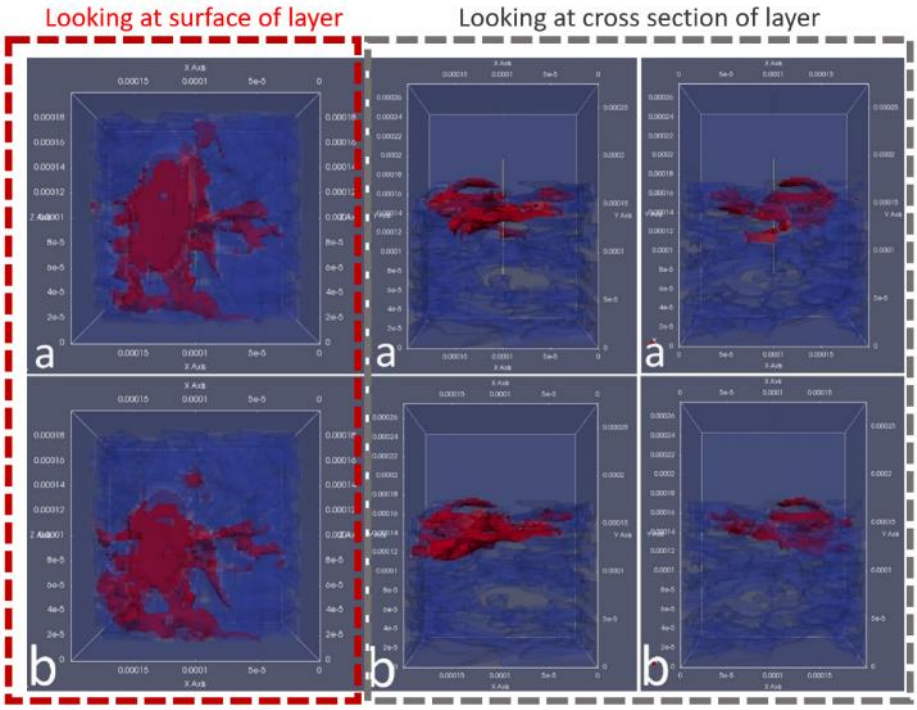

Figure 5.10 Simulations results of spreading and penetration in two different cross sections; a) water and b) ink-like liquid

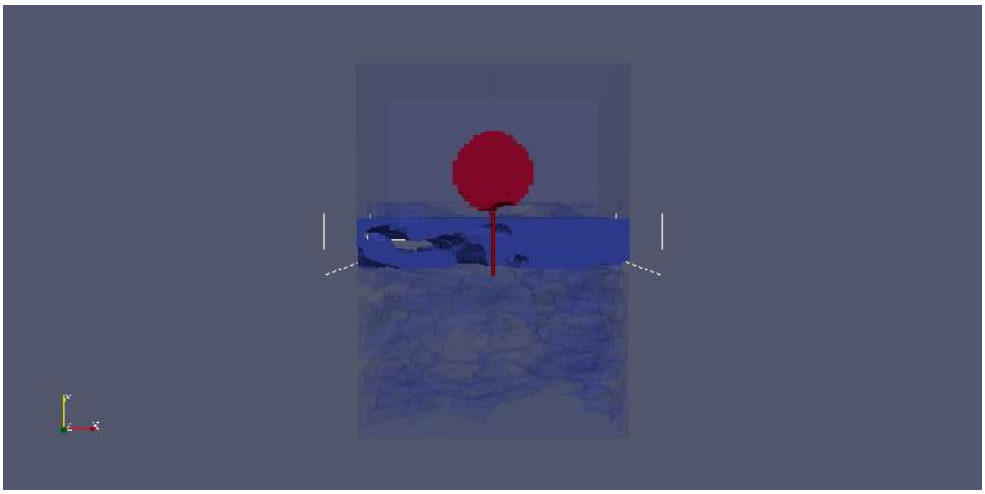

Figure 5.11 Cropped domain to determine imbibition rate inside it

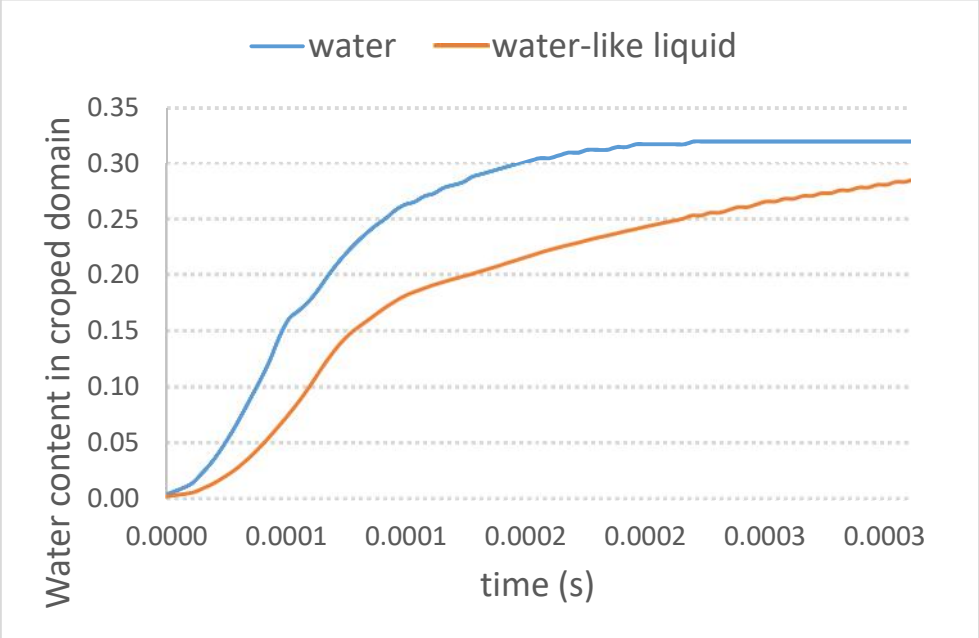

Figure 5.12 Water content increase in cropped section of domain during time; for two cases, water and ink-like liquid

5.3.4 Contact angle effect

The hydrophilicity of surfaces, which affects the spreading and penetration depth, depends on the contact angle on fibers and surface tension. While values of surface tension of water and ink-based liquid are known, to the best of our knowledge, the contact angle of an air-water meniscus on cellulose fiber surfaces is not measured yet. We did not vary the value of surface tension as its value is multiplied by cosine of contact angle. Therefore, we performed several simulations for three different contact angles of 0, 60°, and 120°. Contact angle of zero may correspond better to the case of water and fibers, which are primarily hydrophilic (Aslannejad et al. 2017b). However, in the paper fabrication, fibers are treated to decrease their hydrophilicity. Therefore, usually larger contact angles, around 60°, may have to be considered. Figure 5.13 shows the results of simulations for contact angle values of 0, 60°, and 120°. In case of contact angle of zero, we got the largest spreading and penetration depth. Increasing the hydrophobicity of the fiber surfaces, i.e. the contact angle of 60° caused less spreading and penetration depth. However, as shown in Figure 5.13, the droplet moved slightly to the side (here towards the right side) before penetrating the layer. The direction of move is because of pore geometry but the contact angle is facilitating the movement. This caused movement of penetration location compared to the zero contact angle case. Therefore, this means that during printing, the ink may settle at a somewhat random location, resulting in a decrease of the print quality. In the case of contact angle of 120°, this was even more marked; the case; the droplet moved out of the domain and moved about 100 µm away from the anticipated penetration location.

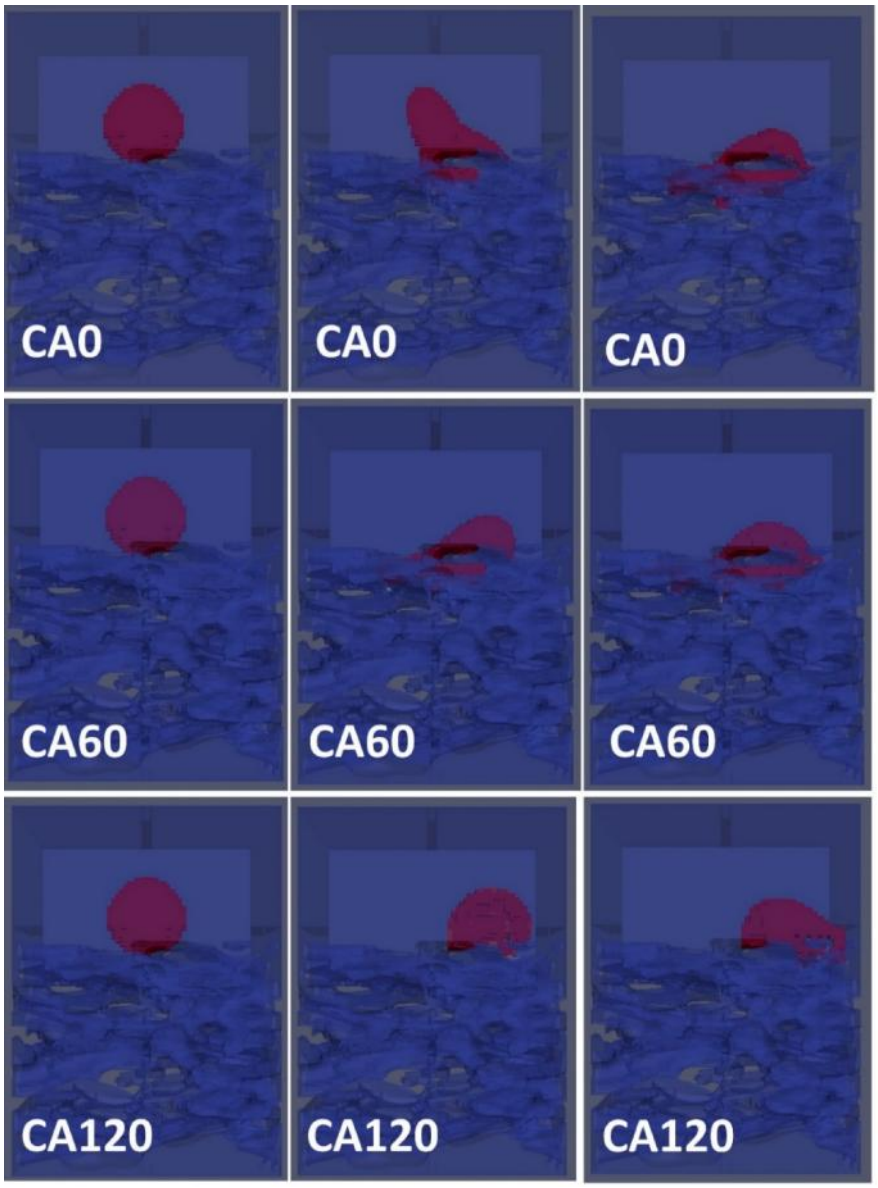

Figure 5.13 Contact angle effect on water spreading/ penetration in fibrous layer; a, b, and c are 0, 60°, and 120° respectively

The effects of contact angle on the penetration depth and spreading area are presented in Table 5-2. The resulting spreading/penetration lengths are in the range of values measured in experiments (the contact angle was not measured in the experiment). Penetration of water deeper into the fibrous layer may cause

deformation, which is undesirable for printing. In addition, when droplet moves to sides, away from jetted location, it can cause a lower print quality. Thus, it is better to have a smaller contact angle and prevent droplet movement on fibers, and one may treat the surface so that the contact angle falls in an optimum range between 0-60°.

Table 5-2 The effect of contact angle on penetration depth and spreading area

Contact angle	Penetration depth (μm)	Spreading area (μm^2)	Position
0	50	190 x 150	-
60	30	180 x 120	Slight droplet move to the sides
120	Not Available	Not Available	Dramatic droplet move to the sides

5.4 Conclusion

We have combined experimental and numerical studies to investigate the role of various factors on the fate of a liquid droplet deposited on an uncoated paper. The 3D structure of an uncoated paper was imaged using micro computational tomography and reconstructed to obtain a digital domain for use in numerical simulations. The spreading of a water droplet was monitored using confocal microscopy and penetration depth of water was determined based on measurements by an Automatic Scanning Absorptiometry (ASA) instrument. Simulations were performed using Volume of Fluid method. We found acceptable agreement between results of numerical simulations and experimental measurements. This provided confidence in our modelling method.

The developed model was then used to study the effect of several factors on the movement of the droplet; these were contact angle, density, viscosity, and surface tension. Simulations were performed for three different values of contact angle: 0, 60◦, and 120◦. Contact angle of zero showed the largest penetration depth compared to CA60 and CA120. In the case of CA60 , the liquid moved horizontally away from the jetted location. This was even more marked in the case CA120. Such behavior is not desirable in printing as it can cause blurring and low quality print.

Modeling results showed that increasing the density and viscosity, all by a factor two, had insignificant effect on spreading and penetration extent. However, it took a given volume of the heavier liquid much longer to penetrate. Slower penetration means that the there is more time for the liquid to evaporate near the surface of the paper. We can postulate, therefore, that this behaviour of an ink liquid phase could be positive in that pigments and/or dye in a complete ink could be better retained near the surface.

5.5 References

Alam, P., Byholm, T., Kniivilä, J., Sinervo, L., Toivakka, M.: Calculating the permeability of model paper coating structures comprising incongruent particle shapes and sizes. (2009)

Alam, P., Toivakka, M., Backfolk, K., Sirviö, P.: Impact spreading and absorption of Newtonian droplets on topographically irregular porous materials. Chem. Eng. Sci. 62, 3142–3158 (2007). doi:10.1016/j.ces.2007.03.018

Anderson, D.M., Linville, A.: Temperature Fluctuations Accompanying Water Movement through Porous Media Published by : American Association for the Advancement of Science. Am. Assoc. Adv. Sci. 131, 1370–1371 (1960)

Anderson, D.M., Linville, A.: Temperature Fluctuations at a Wetting Front: I. Characteristic Temperature-Time Curves1. Soil Sci. Soc. Am. J. 26, 14 (1962). doi:10.2136/sssaj1962.03615995002600010005x

Anderson, D.M., Linville, A., Sposito, G.: Temperature Fluctuations at a Wetting Front: III. Apparent Activation Energies for Water Movement in the Liquid and Vapor Phases1. Soil Sci. Soc. Am. J. 27, 610 (1963)(a). doi:10.2136/sssaj1963.03615995002700060014x

Anderson, D.M., Sposito, G., Linville, A.: Temperature Fluctuations at a Wetting Front: II. The Effect of Initial Water Content of the Medium on the Magnitude of the Temperature Fluctuations1. Soil Sci. Soc. Am. J. 27, 367 (1963)(b). doi:10.2136/sssaj1963.03615995002700040005x

Aronsson, M., Henningsson, O., Sävborg, Ö.: Slice-based digial volume assembly of a small paper sample. Nord. Pulp Pap. Res. J. 17, 29–33 (2001). doi:10.3183/NPPRJ-2002-17-01-p029-033

Aslannejad, H., Hassanizadeh, S.M.: Study of Hydraulic Properties of Uncoated Paper: Image Analysis and Pore-Scale Modeling. Transp. Porous Media. (2017). doi:10.1007/s11242-017-0909-x

Aslannejad, H., Hassanizadeh, S.M., Raoof, A., de Winter, D.A.M., Tomozeiu, N., van Genuchten, M.T.: Characterizing the hydraulic properties of paper coating layer using FIB-SEM tomography and 3D pore-scale modeling. Chem. Eng. Sci. 160, 275–280 (2017)(a). doi:10.1016/j.ces.2016.11.021

Aslannejad, H., Terzis, A., Hassanizadeh, S.M., Weigand, B.: Occurrence of temperature spikes at a wetting front during spontaneous imbibition. Sci. Rep. 7, 7268 (2017)(b). doi:10.1038/s41598-017-07528-7

Axelsson, M.: Image analysis for volumetric characterisation of microstructure. (2009)

Axelsson, M., Svensson, S.: 3D pore structure characterisation of paper. Pattern Anal. Appl. 13, 159–172 (2010). doi:10.1007/s10044-009-0146-1

Bangham, D.H., Razouk, R.I.: Adsorption and the wettability of solid surfaces. Trans. Faraday Soc. 33, 1459 (1937). doi:10.1039/tf9373301459

Bedram, A., Moosavi, A.: Breakup of droplets in micro and nanofluidic T-junctions. J. Appl. Fluid Mech. 6, 81–86 (2013). doi:10.4028/www.scientific.net/AMM.110-116.3673

Blumer, M.: Thermometric Monitor for Chromatographic Streams. Anal. Chem. 32, 772–776 (1960)

Bosanquet, C.H.: LV. On the flow of liquids into capillary tubes. Philos. Mag. Ser. 6. 45, 525–531 (1923). doi:10.1080/14786442308634144

Carsel, R.F., Parrish, R.S.: Developing joint probability distributions of soil water retention characteristics. Water Resour. Res. 24, 755–769 (1988)

Cheng, Kirsch, L., Wiegmann, R., Gervais, A., Bardin-Monnier, P.-C., N. Thomas, D.: PleatLab. A pleat scale simulation environment for filtration simulation. (2013)

Claxton, G.: Detector for liquid-solid chromatography. J. Chromatogr. A. 2, 136–139 (1959). doi:10.1016/S0021-9673(01)86273-7

Dalton, Preston, J.., Heard, J.., Allen, P.., Elton, G.., Husband, N..: Investigation into the distribution of ink components throughout printed coated paper. Colloids Surfaces A Physicochem. Eng. Asp. 205, 199–213 (2002). doi:10.1016/S0927-7757(02)00021-3

Das, S., Ramarao, B.V.: Inversion of lime mud and papermaking pulp filtration data to determine compressibility and permeability relationships. Sep. Purif. Technol. 28, 149–160 (2002). doi:10.1016/S1383-5866(02)00047-3

de Gans, B.-J., Duineveld, P.C., Schubert, U.S.: Inkjet Printing of Polymers: State of the Art and Future Developments. Adv. Mater. 16, 203–213 (2004). doi:10.1002/adma.200300385

Delerue, J.F., Perrier, E., Yu, Z.Y., Velde, B.: New algorithms in 3D image analysis and their application to the measurement of a spatialized pore size distribution in soils. Phys. Chem. Earth, Part A Solid Earth Geod. 24, 639–644 (1999). doi:10.1016/S1464-1895(99)00093-9

Desie, G., Deroover, G., De Voeght, F., Soucemarianadin, A.: Printing of dye and pigment-based aqueous inks onto porous substrates. J. Imaging Sci. Technol. 48, 389–397 (2004)

Do-Quang, M., Carlson, A., Amberg, G.: The impact of ink-jet droplets on a paper-like structure. Fluid Dyn. Mater. Process. 7, 389–402 (2011). doi:10.3970/fdmp.2011.007.389

Dodson, C.T.J., Sampson, W.W.: The effect of paper formation and grammage on its pore size distribution. J. pulp Pap. Sci. 22, J165–J169 (1996)

Fathi, H., Raoof, A., Mansouri, S.H.: Insights into the role of wettability in cathode catalyst layer of proton exchange membrane fuel cell; pore scale immiscible flow and transport processes. J. Power Sources. 349, 57–67 (2017). doi:10.1016/j.jpowsour.2017.03.012

Gambaryan-Roisman, T.: Liquids on porous layers: wetting, imbibition and transport processes. Curr. Opin. Colloid Interface Sci. 19, 320–335 (2014). doi:10.1016/j.cocis.2014.09.001

Gane, P., Hooper, J.: An evaluation of interactions between coating color and basepaper by coating profile analysis. Fundamentals of Papermaking. In: Trans. 9th Fundamental Reasearch Symposium, Ed. Baker and Punton, Mech. Eng. Publ., London, UK. pp. 871–893 (1989)

Gane, P.A.C.: Mottle and the influence of coating and binder migration. Pap. Technol. Ind. 30, 34–41 (1989)

Gane, P.A.C., Hooper, J.J., Baumeister, M.: The influence of furnish content on formation and basesheet profile stability during coating. Tappi J. 74, 193–201 (1991)

Gane, P.A.C., Salo, M., Kettle, J.P., Ridgway, C.J.: Comparison of Young-Laplace pore size and microscopic void area distributions in topologically similar structures: a new method for characterising connectivity in pigmented coatings. J. Mater. Sci. 44, 422–432 (2008). doi:10.1007/s10853-008-3134-8

van Genuchten, M.: A closed-form equation for predicting the hydraulic conductivity of unsaturated soils. Soil Sci. Soc. Am. J. 44.5, 892–898. (1980)

Ghanbarian-Alavijeh, B., Liaghat, A., Huang, G.-H., van Genuchten, M.T.: Estimation of the van Genuchten soil water retention properties from soil textural data. Pedosphere. 20, 456–465 (2010)

Ghassemzadeh, J., Sahimi, M.: Pore network simulation of fluid imbibition into paper during coating—III: modelling of the two-phase flow. Chem. Eng. Sci. 59, 2281–2296 (2004)(a). doi:10.1016/j.ces.2004.01.058

Ghassemzadeh, J., Sahimi, M.: Pore network simulation of fluid imbibition into paper during coating: II. Characterization of paper's morphology and computation of its effective permeability tensor. Chem. Eng. Sci. 59, 2265–2280 (2004)(b). doi:10.1016/j.ces.2004.01.057

Girard, F., Attané, P., Morin, V.: A new analytical model for impact and spreading of one drop: Application to inkjet printing. Tappi J. 5, 24–32 (2006)

Gronfors, J.: Use of fillers in paper and paperboard grades, (2010)

Hassanizadeh, S.M., Gray, W.G.: Mechanics and thermodynamics of multiphase flow in porous media including interface boundaries. Adv. Water Resour. 13, 169–186 (1990)

Hassanizadeh, S.M., Gray, W.G.: Thermodynamic basis of capillary pressure in porous media. Water Resour. Res. 29, 3389–3405 (1993). doi:10.1029/93WR01495

Heard, P.J., Preston, J.S., Parsons, D.J., Cox, J., Allen, G.C.: Visualisation of the distribution of ink components in printed coated paper using focused ion beam techniques. Colloids Surfaces A Physicochem. Eng. Asp. 244, 67–71 (2004). doi:10.1016/j.colsurfa.2004.05.012

Hilpert, Markus, Miller, T., C.: Pore-morphology-based simulation of drainage in totally wetting porous media. Adv. Water Resour. 24, 243–255 (2001). doi:10.1016/S0309-1708(00)00056-7

Hird, K.F.: Offset lithographic technology. Goodheart-Willcox Co, Tinley Park, Illinois (2000)

Hirn, U., Schennach, R.: Comprehensive analysis of individual pulp fiber bonds quantifies the mechanisms of fiber bonding in paper. Sci. Rep. 5, 10503 (2015)

Hodgson, K.T., Berg, J.C.: Dynamic Wettability Properties of Single Wood Pulp Fibers and Their Relationship to Absorbency. Wood Fiber Sci. 20, 3–17 (2007)

Holmstad: Comparison of 3D structural characteristics of high and low resolution X-ray microtomographic images of paper. Nord. Pulp Pap. Res. J. 20, 283–288 (2005). doi:10.3183/NPPRJ-2005-20-03-p283-288

Huang, S., Goel, A., Ramaswamy, S., Ramarao, B., Choi, D.: Transverse and in-plane pore structure characterization of paper, (2002)

Hyväluoma, J., Koponen, A., Raiskinmäki, P., Timonen, J.: Droplets on inclined rough surfaces. Eur. Phys. J. E. 23, 289–293 (2007). doi:10.1140/epje/i2007-10190-7

Hyväluoma, J., Raiskinmäki, P., Jäsberg, A., Koponen, A., Kataja, M., Timonen, J.: Simulation of liquid penetration in paper. Phys. Rev. E. 73, 036705 (2006). doi:10.1103/PhysRevE.73.036705

Ingmanson, W.L., Andrews, B.D., Johnson, R.C.: Internal Pressure Distributions in Compressible Mats under Fluid Stress. TAPPI J. 42, 840–849 (1959)

Järnström, J., Väisänen, M., Lehto, R., Jäsberg, A., Timonen, J., Peltonen, J.: Effect of latex on surface structure and wetting of pigment coatings. Colloids Surfaces A

Physicochem. Eng. Asp. 353, 104–116 (2010). doi:10.1016/j.colsurfa.2009.11.001

Kanit, T., Forest, S., Galliet, I., Mounoury, V., Jeulin, D.: Determination of the size of the representative volume element for random composites: statistical and numerical approach. Int. J. Solids Struct. 40, 3647–3679 (2003). doi:10.1016/S0020-7683(03)00143-4

Karwacki, L., de Winter, D.A., Aramburo, L.R., Lebbink, M.N., Post, J.A., Drury, M.R., Weckhuysen, B.M.: Architecture-Dependent Distribution of Mesopores in Steamed Zeolite Crystals as Visualized by FIB-SEM Tomography. Angew. Chemie Int. Ed. 50, 1294–1298 (2011)

Kettle, J., Lamminmäki, T., Gane, P.: A review of modified surfaces for high speed inkjet coating. Surf. Coatings Technol. 204, 2103–2109 (2010). doi:10.1016/j.surfcoat.2009.10.035

Kuijpers, C.J., van Stiphout, T.A.P., Huinink, H.P., Tomozeiu, N., Erich, S.J.., Adan, O.C.G.: Quantitative measurements of capillary absorption in thin porous media by the Automatic Scanning Absorptometer. Chem. Eng. Sci. 178, 70–81 (2018). doi:10.1016/J.CES.2017.12.024

Lamminmäki, T., Kettle, J., Rautkoski, H., Kokko, A., Gane, P.: Limitations of Current Formulations when Decreasing the Coating Layer Thickness of Papers for Inkjet Printing. Ind. Eng. Chem. Res. 50, 7251–7263 (2011). doi:10.1021/ie102114s

Lamminmaki, T., Kettle, J.P., Puukko, P., Gane, P.A.C., Ridgway, C.: Inkjet print quality: the role of polyvinyl alcohol in speciality CaCO3 coatings. J. Pulp Pap. Sci. 35, 137–147 (2009)

Lamminmäki, T.T., Kettle, J.P., Gane, P.A.C.: Absorption and adsorption of dye-based inkjet inks by coating layer components and the implications for print quality. Colloids Surfaces A Physicochem. Eng. Asp. 380, 79–88 (2011). doi:10.1016/j.colsurfa.2011.02.015

Lamminmäki, T.T., Kettle, J.P., Puukko, P.J.T., Ridgway, C.J., Gane, P.A.C.: Short timescale inkjet ink component diffusion: an active part of the absorption mechanism into inkjet coatings. J. Colloid Interface Sci. 365, 222–235 (2012). doi:10.1016/j.jcis.2011.08.045

Le, H.P.: Progress and trends in ink-jet printing technology. J. Imaging Sci. Technol. 42, 49–62 (1998)

Lee, H.K., Joyce, M.K., Fleming, P.D., Cameron, J.H.: Production of a single coated glossy inkjet paper using conventional coating and calendering methods, https://wmich.pure.elsevier.com/en/publications/production-of-a-single-coated-glossy-inkjet-paper-using-conventio-3, (2002)

Leij, F.J., Russell, W.B., Lesch, S.M.: Closed-form expressions for water retention and conductivity data. Ground Water. 35, 848–858 (1997)

Lindsay, J.D.: The anisotropic permeability of paper: theory, measurements, and analytical tools. (1988)

Liu, G., Fu, S., Lu, Z., Zhang, M., Ridgway, C., Gane, P.: Contrasting liquid imbibition into uncoated versus pigment coated paper enables a description of imbibition into new-generation surface-filled paper. Eur. Phys. J. E. 40, 111 (2017). doi:10.1140/epje/i2017-11600-y

López-Marzo, A.M., Merkoçi, A.: Paper-based sensors and assays: A success of the engineering design and the convergence of knowledge areas, http://xlink.rsc.org/?DOI=C6LC00737F, (2016)

Luckner, L., van Genuchten, M.T., Nielsen, D.R.: A consistent set of parametric models for the two-phase flow of immiscible fluids in the subsurface. Water Resour. Res. 25, 2187–2193 (1989). doi:10.1029/WR025i010p02187

Malla, Devisetti: Novel kaolin pigment for high solids ink jet coating. Pap. Technol. 46, 17–27 (2005)

Matilainen, K., Hämäläinen, T., Savolainen, A., Sipiläinen-Malm, T., Peltonen, J., Erho, T., Smolander, M.: Performance and penetration of laccase and ABTS inks on various printing substrates. Colloids Surfaces B Biointerfaces. 90, 119–128 (2012). doi:10.1016/j.colsurfb.2011.10.015

Modaressi, H., Garnier, G.: Mechanism of wetting and absorption of water droplets on sized paper: Effects of chemical and physical heterogeneity. Langmuir. 18, 642–649 (2002). doi:10.1021/la0104931

Oce: Specificaties Océ VarioPrint i300 - Canon Nederland, https://www.canon.nl/business-printers-and-faxes/cut-sheet-colour-printers/varioprint-i300/specifications/

Oostrom, M., Dane, J.H., Lenhard, R.J.: Fluid Contents. J.H. Dane and G.C. Topp; Soil Science Society of America , Madison, WI, United States(US). (2002)

Palakurthi, N.K., Konangi, S., Ghia, U., Comer, K.: Micro-scale simulation of unidirectional capillary transport of wetting liquid through 3D fibrous porous media: Estimation of effective pore radii. Int. J. Multiph. Flow. 77, 48–57 (2015). doi:10.1016/j.ijmultiphaseflow.2015.07.010

Patrick A. Gane, †, John P. Kettle, ‡, G. Peter Matthews, * and, Ridgway, C.J.: Void Space Structure of Compressible Polymer Spheres and Consolidated Calcium Carbonate Paper-Coating Formulations. (1996). doi:10.1021/IE950413M

Perrier, E. R.; Prakash, O.M.: Heat and vapor movement during infiltration into dry soils. Soil Sci. 124, 73–73 (1976)

Podsiadlo, P., Choi, S.-Y., Shim, B., Lee, J., Cuddihy, M., Kotov, N.A.: Molecularly Engineered Nanocomposites: Layer-by-Layer Assembly of Cellulose Nanocrystals. Biomacromolecules. 6, 2914–2918 (2005). doi:10.1021/bm050333u

Prunty, L.: Thermal Transients in Closed , Unsaturated Soil Systems. Therm. Transient. 1–4 (2002)

Prunty, L., Bell, J.: Soil Temperature Change over Time during Infiltration. Soil Sci. Soc. Am. J. 69, 766 (2005). doi:10.2136/sssaj2004.0219

Ramaswamy, S., Gupta, M., Goel, A., Aaltosalmi, U., Kataja, M., Koponen, A., Ramarao, B..: The 3D structure of fabric and its relationship to liquid and vapor transport. Colloids Surfaces A Physicochem. Eng. Asp. 241, 323–333 (2004). doi:10.1016/j.colsurfa.2004.04.023

Ramaswamy, S., Huang, S., Goel, A., Cooper, A., Choi, D., Bandyopadhyay, A., Ramarao, B. V: The 3D structure of paper and its relationship to moisture transport in liquid and vapor forms. In: 12th Fundamental Research Symposium, Oxford. pp. 1289–1311 (2001)

Ridgway, C.J., Gane, P.A.C.: Controlling the absorption dynamic of water-based ink into porous pigmented coating structures to enhance print performance. Nord. Pulp Pap. Res. J. 17, 119–129 (2002)

Ridgway, C.J., Gane, P.A.C., Schoelkopf, J.: Effect of capillary element aspect ratio on the dynamic imbibition within porous networks. J. Colloid Interface Sci. 252, 373–382 (2002). doi:10.1006/jcis.2002.8468

Rolland du Roscoat, S., Decain, M., Geindreau, C., Thibault, X., Bloch, J.-F.: Microstructural Analysis of Paper Using Synchrotron X-ray Microtomography: Numerical Estimation of the Permeability and Effective Thermal Conductivity. Appita J. J. Tech. Assoc. Aust. New Zeal. Pulp Pap. Ind. 61, 286 (2008)

du Roscoat, S.R., Bloch, J.F., Thibault, X.: Characterization of the 3D paper structure with X-ray synchrotron radiation microtomography. In: The 13th FRC Symposium, Robinson College, Cambridge. pp. 901–920 (2005)

Rosenholm, J.B.: Liquid spreading on solid surfaces and penetration into porous matrices: Coated and uncoated papers. Adv. Colloid Interface Sci. 220, 8–53 (2015). doi:10.1016/j.cis.2015.01.009

Salmas, C.E., Stathopoulos, V.N., Pomonis, P.J., Rahiala, H., Rosenholm, J.B., Androutsopoulos, G.P.: An investigation of the physical structure of MCM-41 novel mesoporous materials using a corrugated pore structure model. Appl. Catal. A Gen. 216, 23–39 (2001). doi:10.1016/S0926-860X(01)00520-8

Samuelsen, E.J., Houen, P., Gregersen, Ø.W., Helle, T.: Three-dimensional imaging of paper by use of synchrotron x-ray microtomography. J. Pulp Pap. Sci. 27, 50–53 (2001)

Sappi: The Paper Making Process, https://www.youtube.com/redirect?redir_token=VEjJPq2aJlcjBgVBNfN_Rc4CZfl8MTU0MDIxMjEyMkAxNTQwMTI1NzIy&event=video_description&v=E4C3X26dxbM&q=http%3A%2F%2Fwww.na.sappi.com%2Feducation%2Flifecycle

Schoelkopf, J., Gane, P.A.., Ridgway, C.J., Matthews, G.P.: Practical observation of deviation from Lucas–Washburn scaling in porous media. Colloids Surfaces A Physicochem. Eng. Asp. 206, 445–454 (2002). doi:10.1016/S0927-7757(02)00066-3

Schoelkopf, J., Gane, P.A.C., Ridgway, C.J., Matthews, G.P.: Influence of inertia on liquid absorption into paper coating structures. Nord. Pulp Pap. Res. J. 15, 422–430 (2000)

Schulz, V.P., Wargo, E.A., Kumbur, E.C.: Pore-morphology-based simulation of drainage in porous media featuring a locally variable contact angle. Transp. Porous Media. 107, 13–25 (2014). doi:10.1007/s11242-014-0422-4

Singh, M., Haverinen, H.M., Dhagat, P., Jabbour, G.E.: Inkjet Printing-Process and Its Applications. Adv. Mater. 22, 673–685 (2010). doi:10.1002/adma.200901141

Song, Y., Davy, C.A., Bertier, P., Troadec, D.: Understanding fluid transport through claystones from their 3D nanoscopic pore network. Microporous Mesoporous Mater. 228, 64–85 (2016). doi:10.1016/j.micromeso.2016.03.023

Suffield, S., Jokar, A.: Modeling the Flow of a Liquid Droplet Diffusing Into Various Porous Media for Inkjet Printing Applications. In: Volume 10: Heat Transfer, Fluid Flows, and Thermal Systems, Parts A, B, and C. pp. 1013–1022. ASME (2008)

Tåg, C.-M., Järn, M., Granqvist, B., Järnström, J., Peltonen, J., Rosenholm, J.B.: Influence of surface structure on wetting of coated offset papers. Holzforschung. 61, 516–522 (2007). doi:10.1515/HF.2007.073

Terzis, A., Roumeli, E., Weishaupt, K., Brack, S., Aslannejad, H., Groß, J., Hassanizadeh, S.M., Helmig, R., Weigand, B.: Heat release at the wetting front during capillary filling of cellulosic micro-substrates. J. Colloid Interface Sci. 504, 751–757 (2017). doi:10.1016/j.jcis.2017.06.027

Vikman, K., Vuorinen, T.: Water fastness of ink jet prints on modified conventional coatings. 48, 138–147 (2004)

Washburn, E.W.: The Dynamics of Capillary Flow. Phys. Rev. 17, 273–283 (1921). doi:10.1103/PhysRev.17.273

Wei, H., Ramarao, B. V: Characterization of pulp slurries using a novel drainage tester. In: Tappi Engineering Conference. pp. 517–524 (1996)

Weller, H.G.: A new approach to VOF-based interface capturing methods for incompressible and compressible flow. OpenCFD Ltd., Rep. TR/HGW/04. (2008)

Xu, L., Zhang, W.W., Nagel, S.R.: Drop splashing on a dry smooth surface. Phys. Rev. Lett. 94, 184505 (2005). doi:10.1103/PhysRevLett.94.184505

Yarin, A.L.: DROP IMPACT DYNAMICS: Splashing, Spreading, Receding, Bouncing…. Annu. Rev. Fluid Mech. 38, 159–192 (2006). doi:10.1146/annurev.fluid.38.050304.092144

Zhao, H., Kwak, J.H., Conrad Zhang, Z., Brown, H.M., Arey, B.W., Holladay, J.E.: Studying cellulose fiber structure by SEM, XRD, NMR and acid hydrolysis. Carbohydr. Polym. 68, 235–241 (2007). doi:10.1016/j.carbpol.2006.12.013

Zhu, S., Pelton, R.H., Collver, K.: Mechanistic modelling of fluid permeation through compressible fiber beds. Chem. Eng. Sci. 50, 3557–3572 (1995). doi:10.1016/0009-2509(95)00205-J

Zoladek-Nowak, J., Milczarek, J.J., Fija-Kirejczyk, I.M., Zoldek, J., Jurkowski, Z.: Transient Thermal Phenomena during Spontaneous Water Migration in Zeolite Beds. ACTA Phys. Pol. 122, 415–418 (2012)

Product information sheet Magno ™ gloss Coated fine paper available in sheets and reels for offset printing Technical specifications Print recommendations Dot area Mill certifications. 2016 (2016)

Occurrence of temperature spikes at a wetting front during spontaneous imbibition

Abstract

It is reported that temperature rises at wetting front during water infiltration into soil. The temperature goes back to the background value after passage of the water front. Different explanations have been provided for the source of energy causing the temperature spike. Some have contributed it to heat of condensation released due to condensation of vapor on "dry" solid surface. Some others stated that the heat of wetting or heat of adsorption is responsible for the temperature rise. In this research, we revisited this issue. First, we provide a comprehensive review about occurrence of temperature spike at a wetting front. Then, we report about experiments we performed on the rise of water in dry paper. Using infrared and optical imaging techniques, we could monitor temperature changes in time and space. For all samples maximum temperature rise occurred at the wetting front. The magnitude of temperature spike depended on paper material, thickness, and liquid composition. It was larger for cellulose-fiber-based paper than for plastic-based paper (non-woven product made of synthetic fibers). For a given paper type, thicker samples showed a larger temperature spike. Adding salt to the water caused reduction of temperature spike. It was concluded that replacement of air-solid interface with water-solid interface releases energy, which causes temperature rise.

Published as: Occurrence of temperature spikes at a wetting front during spontaneous imbibition. Hamed Aslannejad, Alexandros Terzis, S Majid Hassanizadeh, Bernhard Weigand. Scientific reports 7 (Article number: 7268). https://doi.org/10.1038/s41598-017-07528-7

6.1 Introduction

Spontaneous imbibition of water is an important process in many natural and industrial porous media. It is observed that water rushes into a relatively dry hydrophilic porous solid despite resistance from viscous drag and even against gravity. Only if the resident phase (e.g. air in the case of unsaturated soil) is put under high pressure, the wetting of the porous medium can be halted. One may pose the questions why spontaneous imbibition occurs and/or which driving force is it that can overcome gravitational and viscous forces. The usual answer is: capillary forces, induced by interfacial tension. In two-phase flow in porous media, there exist indeed three interfaces: two fluid-solid interfaces and one fluid-fluid interface, each with their own interfacial tension.

Commonly a given solid has (a larger) affinity for one of the fluids, called the wetting phase. The other fluid is called the non-wetting phase. The interfacial tension of the non-wetting fluid-solid interface is always larger than that of the wetting fluid-solid interface. Given the fact that the interfacial tension is directly related to the interfacial energy per unit area, we can state that a porous solid filled by the non-wetting phase has a higher energy than when it is filled with the wetting phase, under isothermal conditions. That is why the solid phase would spontaneously imbibe the wetting fluid; the solid-fluids system goes to a lower energy state. The spontaneous imbibition would be stronger, the larger the affinity of the solid phase for a given fluid. This is clearly reflected in the definition of capillary pressure on both microscale and macroscale. For a capillary tube, the microscale capillary pressure p^c is given by the Young-Laplace equation:

$$p^c = \frac{2}{r}\gamma^w \cos\theta \qquad 6\text{-}1$$

where r is the tube radius, θ is the contact angle, and γ^w is the interfacial tension between the wetting and non-wetting fluid phases. This equation can be combined with Young's equation (equilibrium balance of forces for a contact line) to obtain:

$$p^c = \frac{2}{r}(\gamma^n - \gamma^w) \qquad 6\text{-}2$$

where γ^n and γ^w are the solid-nonwetting phase and solid-wetting phase interfacial tensions, respectively. Clearly, the larger the difference between these two interfacial tensions (i.e., the larger the affinity of the solid for the wetting phase), the larger the capillary pressure. A similar link can be established between macroscale capillary pressure and interfacial surface energies. According to Hassanizadeh and Gray(Hassanizadeh and Gray 1993),(Hassanizadeh and Gray 1990), the macroscale capillary pressure, P^c, can be defined as:

$$P^c = -\frac{1}{\varepsilon}\left(\frac{\partial F^w}{\partial S^w} + \frac{\partial F^n}{\partial S^w} + \frac{\partial F^w}{\partial S^w}\right) \qquad 6\text{-}3$$

where F^α is the macroscale specific free energy of α -interface (i.e., the total free energy of all α -interfaces within an averaging volume per total area of those interfaces), ε is porosity, and S^w is the saturation of wetting phase. Here, the changes of free energies of bulk phases are neglected. Obviously, for P^c to be positive, there must be a net decrease of the energy of all interfaces when the saturation of the wetting phase increases. This is the basis of spontaneous imbibition.

This reasoning suggests that during spontaneous imbibition, energy should be released. As we have a closed system, the released energy should result in a (temporary) rise of temperature. This was shown to be indeed the case as early as 1960 (Anderson and Linville 1960). Anderson and Linville (1960) observed a temperature spike at a front where a non-wetting phase was displaced by a wetting phase. The rise was of limited duration as the amount of released energy is limited and the fluid arriving behind the front dissipates the generated heat. Early explanation of the observed temperature spike was based on the heat of condensation of vapor on soil grains (Anderson and Linville 1960). It was only later that it was shown that the energy needed for the observed temperature rise is much more than the heat of vapor condensation.

In this paper, first, we provide a detailed review of the literature on the occurrence of a temperature spike at a front where a wetting phase displaces a non-wetting phase. Next, various paper types used in our study and the experimental setup are described. Results are presented and their significance and how they correspond to the results of other authors are discussed.

Although in this work we used water as wetting phase and paper samples as porous medium, however the idea of temperature rise during imbibition of a liquid

in a porous material can be used in various areas. The liquid could be in a wide range of solutions, water, blood, urine and the porous material could be paper, soil, a pack of particles. The idea of temperature rise can be used in broad applications; for instance, in case of diagnostic medical kit, a certain temperature rise could be assigned to a concentration or existence of certain component in the liquid.

6.2 Review of experiments on temperature spikes in porous media

To the best of our knowledge, Claxton (Claxton 1959) was the first one to report the increase of temperature of a porous medium upon the arrival of a front. He filled a capillary tube with silica gel saturated with an organic liquid (e.g. iso-octane, butylene and/or benzene) and then the resident liquid was displaced by iso-propyl alcohol. The temperature change was measured by a thermocouple installed near the bottom of the column. The temperature value was not reported as it was a qualitative experiment. But, a clear rise and fall of temperature was shown by the thermocouple (see Figure 6.1). Claxton attributed the temperature rise to the preferential adsorption of the displacing liquid on the solid surface. He stated that this "… *is accompanied by the evolution of heat due to a decrease in free energy of the system. This heat is called the heat of adsorption*."

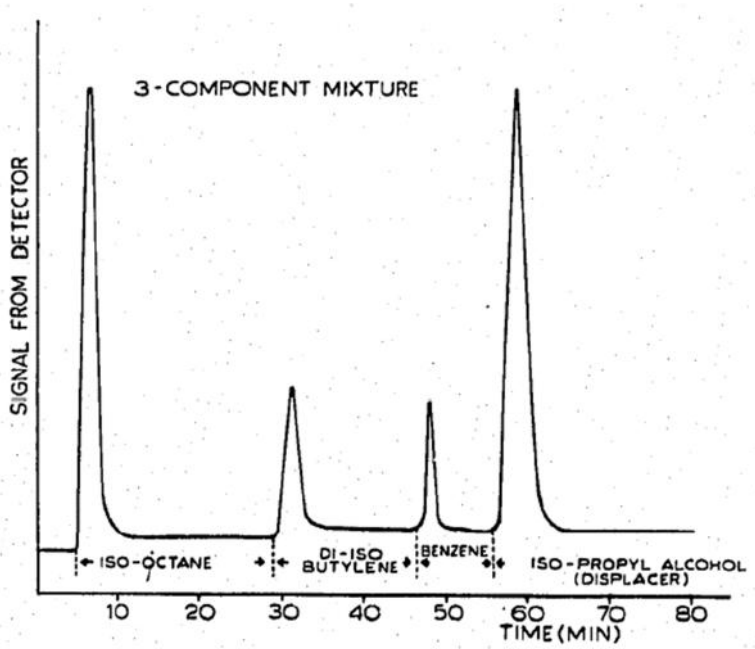

Figure 6.1 Signal from a thermocouple as a function of time. The temperature spike occurs as the resident liquid is replaced by iso-propyl alcohol (Claxton 1959)

Almost simultaneously, a similar concept was developed by Blumer (Blumer 1960), for use in finding and recording changes in the composition of liquids in liquid-solid chromatographic columns. He measured the change of temperature using a thermistor embedded in a column of silica gel. The column was

initially filled by n-heptane, which was then displaced by a mixture of pentane and benzene (3 to 2). After the breakthrough of pentane-benzene mixture, it was replaced by a benzene-acetone mixture. The arrivals of the two fronts were accompanied by temperature rises of about 3 ºC and 11 ºC, respectively. The temperature returned to the initial value after the front passage (see Figure 6.2). Bulmer also attributed such temperature rise to the heat of adsorption.

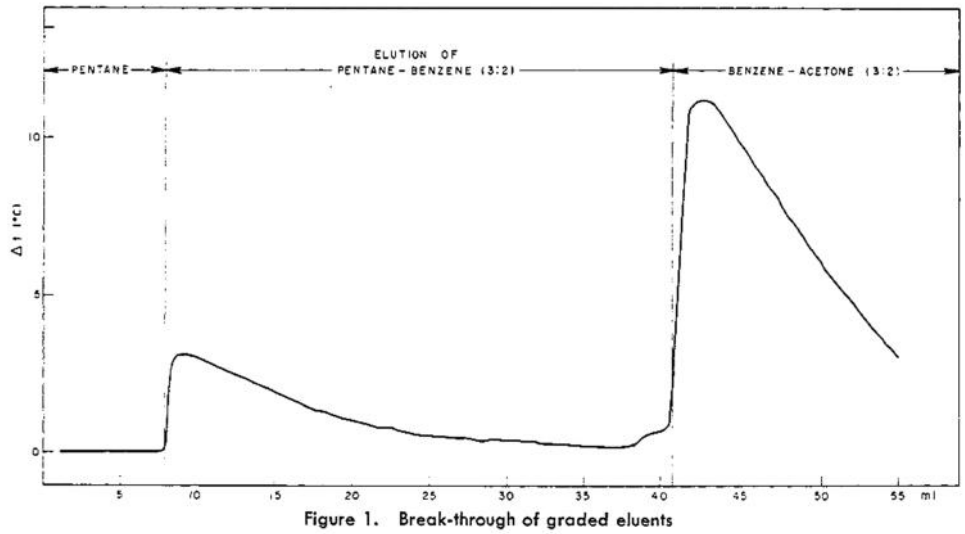

Figure 1. Break-through of graded eluents

Figure 6.2 The sharp rise of temperature at the arrival of a liquid front for which the solid phase has a higher affinity, compared to the resident liquid (Blumer 1960)

Anderson and Linville (Anderson and Linville 1962) were the first to perform similar experiments but with water infiltrating into a dry soil sample. They used kaolinite, glass beads, or bentonite as the soil. The porous sample was packed in a vertical plastic cylinder (1.5 cm inside diameter and 6 cm long). At the time of filling of the cylinder, two thermistors were embedded in the sample, one at 5 mm and the other 10 mm from the sample top. Deionized water under a 5-mm falling head was introduced at the top of the sample and allowed to percolate downward. The temperature of the water, sample, and sample holder was brought to 30°C at the beginning of the experiment in a thermostated chamber which was maintained at constant temperature.

They found an increase of temperature at a given location as the water content increased, followed by a temperature decrease (see Figure 6.3). They measured a temperature rise of about 0.1 ºC for glass beads, 4 ºC for kaolinite and about 9 ºC for bentonite.

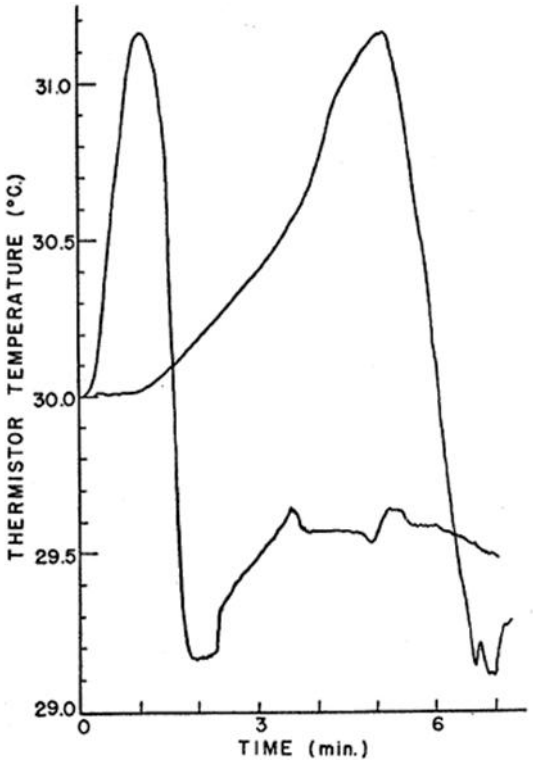

Figure 6.3 Temperature spikes in dry kaolinite as the water front arrives at two different positions along a soil sample (Anderson and Linville 1960)

Anderson and Linville (Anderson and Linville 1960) hypothesized that the temperature increase was due to the condensation of vapor on dry solid surface ahead of the front arrival. The released heat was assumed to be the heat of condensation of vapor. The drop in the temperature below its original value was attributed to the cooling of the system due to the evaporation of water at the wetting front.

Similar experiments were performed by Anderson and Linville (Anderson et al. 1963b) on more soil types (bentonite, kaolinite, Pima clay, Palo Verde loam, and glass beads) and with different values of initial moisture content. They tried three different types of temperature-sensitive devices: thermistor encased by a tiny glass bead, thermistor positioned in the tip of a hypodermic needle, and thermocouple. They found that the fastest response, and the closest approach to identity with a particle of the various porous media used in their experiments, was obtained with thermistors encased by tiny glass bead. They used glass beads of radius 0.546 mm. This means they were measuring local pore-scale temperature and

not the average soil temperature. The ambient temperature of the apparatus was kept at 30 °C by means of a thermostated air bath. For all soil types, Anderson and Linville (1962) (Anderson and Linville 1962) found temperature spikes, similar to the results shown in Figure 6.4. The curves all have the same characteristics. In all cases, there was a gradual rise in temperature with time elapsed after the water was introduced, followed by a rather abrupt decline in temperature after which the temperature gradually stabilized. However, contrary to the results of Anderson and Linville (1960) (Anderson and Linville 1960), this time the temperature did not drop below the original temperature of the medium. In fact, in most cases, it became stable at a level higher than the initial temperature. Anderson and Linville (1962) (Anderson and Linville 1962) stated that this "*may be explained by the fact that the wetting process is exothermic and that due to the evolution of the remaining heat of immersion and to thermal conduction, the wetting front need not necessarily be cooler than the initial temperature of both water and medium*".

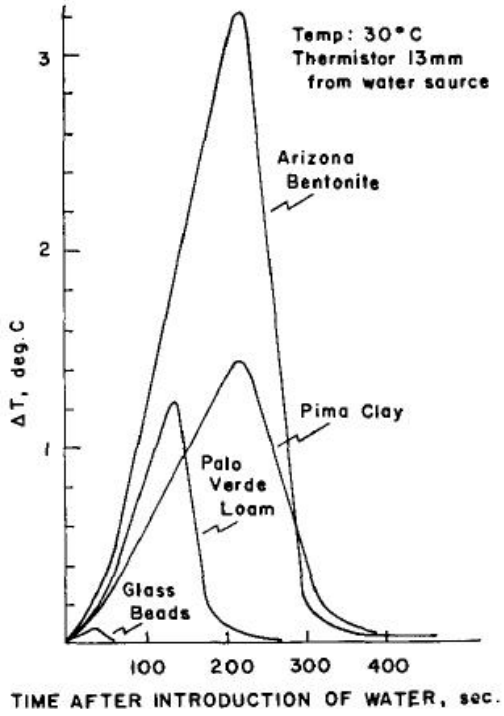

Figure 6.4 Temperature spikes observed for different types of porous medium (from Anderson and Linville, 1962) (Anderson and Linville 1962).

The difference in the magnitude of the temperature spike for different materials was attributed to the difference in their specific surface and affinity for water. It is indeed a fact that bentonite has a much larger specific surface and exchange capacity than glass bead. Consequently, it has a much higher heat of adsorption. The initial water content of the sample was found to affect the magnitude of the temperature spike; it was significantly smaller for higher initial moisture content as seen in Figure 6.5 (Anderson et al. 1963a).

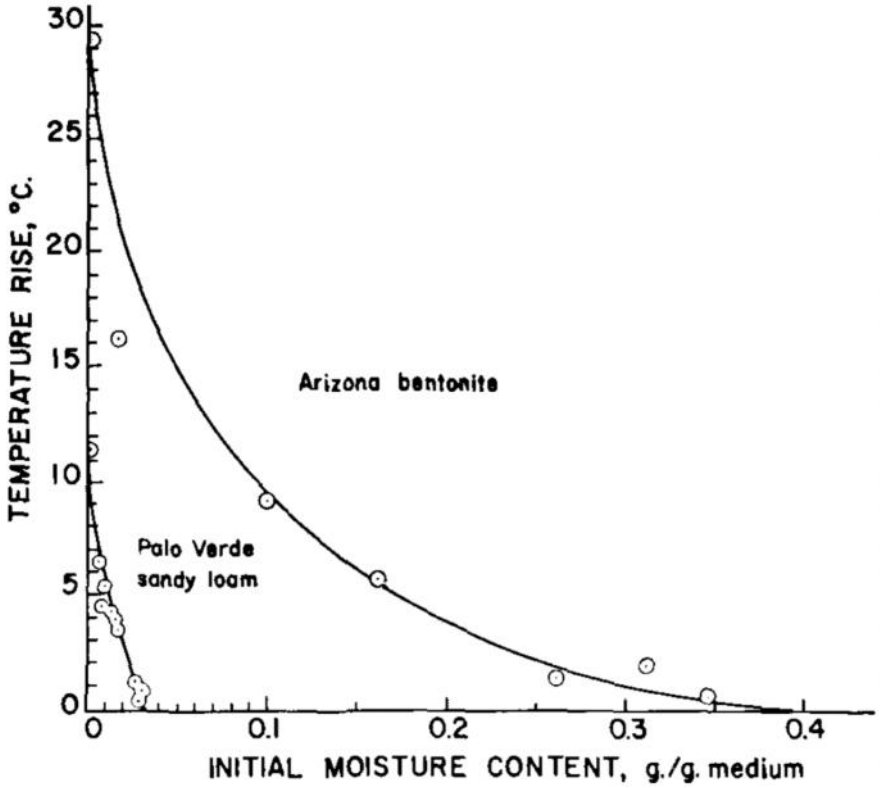

Figure 6.5 The magnitude of the temperature spike as a function of initial water content for two different soils (Anderson et al. 1963b)

Anderson and Linville (1962) (Anderson and Linville 1962) reiterated the hypothesis that the temperature rise is due to the condensation of vapor moving ahead of the water front. They associated the onset of temperature rise with the arrival of a vapor front at the thermistor site and the moment of sharp temperature drop with the arrival of the liquid front. In order to confirm this hypothesis, they performed two additional experiments. In one experiment, a 0.1 N solution of NaCl replaced the distilled water as the infiltrating liquid and compacted kaolinite was

used as the porous medium. Their measurements showed that the water content at thermistor site increased during the initial temperature rise, but the chloride ion was not present at the thermistor site. So, this must have been due to condensation of vapor phase. The time that the temperature began to drop sharply coincided with the arrival of the chloride ion, which was in the water phase. In the second set of experiments, an air gap about 4 mm wide was made halfway between the thermistors and the water source by excavating a channel in the porous medium. The plastic specimen holder was coated with silicone grease making it water repellent so that the liquid front would not cross the air gap under the small hydraulic head they employed. The resulting temperature-time curves for Arizona bentonite are shown in Figure 6.6. A temperature rise similar to the one shown in Figure 6.4 above was found, but there was no drop in the temperature anymore. Anderson and Linville (1963) (Anderson et al. 1963a) concluded that the rise of temperature must have been due to the condensation of water vapor that had crossed the gap. Measurement of moisture content of the medium across the gap showed a significant increase. They could confirm that the liquid water did not cross the air gap by visual inspection after the data were recorded.

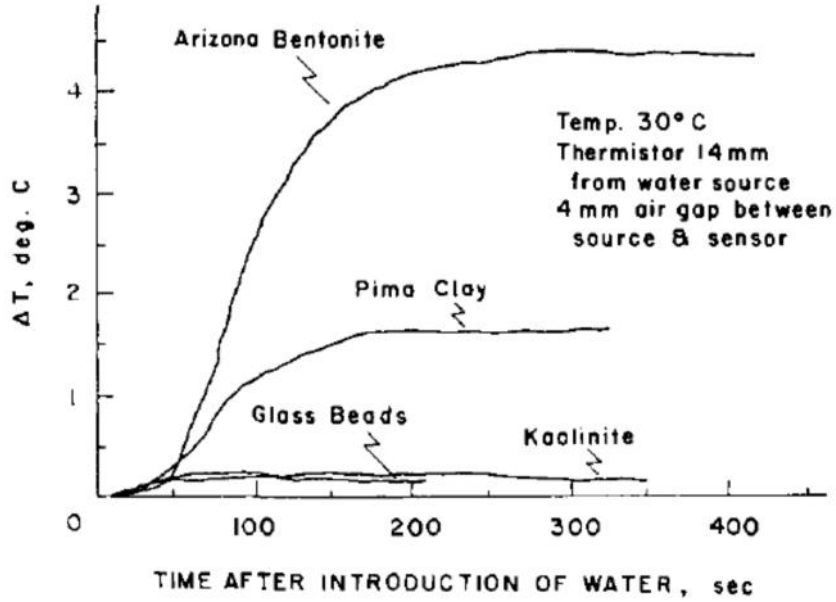

Figure 6.6 Rise of temperature in a region of soil separated from the water source by an air gap about 4 mm wide. That region was accessible to the vapor only and

not to the liquid water (from Anderson and Linville, 1962) (Anderson and Linville 1962).

In experiments by Anderson and coworkers, water flow was downward. So, the flow was not only due to spontaneous imbibition but it was also gravity driven. Horizontal water infiltration experiments, with water flow due to spontaneous imbibition only, were performed by Perrier and Prakash (1976) (Perrier, E. R.; Prakash 1976). In addition, they measured not only temperature but also air humidity in the soil. They prepared two columns, both filled with Flanagan silt loam; air dried for one column and oven dried for the other column. Typical results are shown in Figure 6.7. As with earlier experiments, the temperature rose as the water approached a given position, and decreased after the passage of the front. But, contrary to experiments of Anderson and coworkers, it stayed above the original temperature of the column. In addition, the magnitude of the spike became smaller with increasing distance along the column.

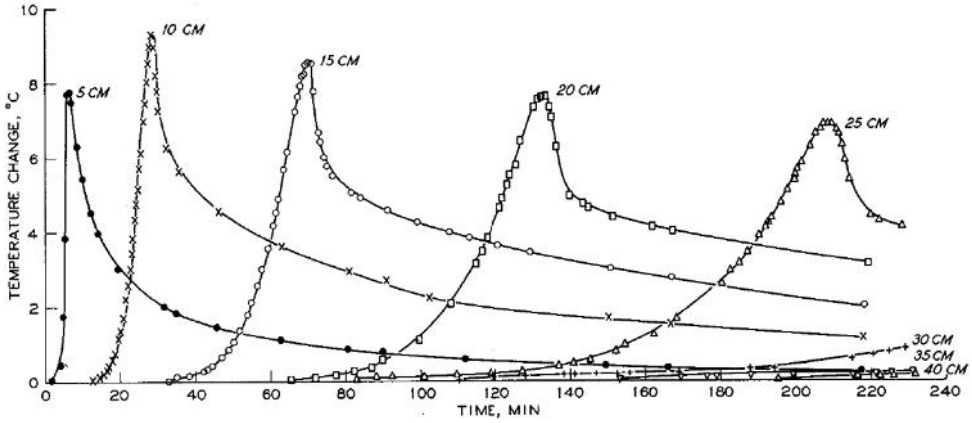

Figure 6.7 Temperature as a function of time measured at different locations in experiments of Perrier and Prakash (1977) (Perrier, E. R.; Prakash 1976)

Measurements of relative humidity transducers showed that the air humidity increased almost instantaneously from background value to 100% relative humidity (see Figure 6.8). It is clear that the temperature starts to rise much earlier than the rise of the air humidity. Perrier and Prakash (1977) (Perrier, E. R.; Prakash 1976) considered the first inflection point of the temperature profile as the position of temperature front. Because the horizontal column was made of Lucite, they could also follow the macroscopic liquid water front. They observed that the thermal peak (site of greatest temperature gradient) coincided exactly with the position of the

liquid front. "*Consequently*," they wrote, "*the thermal peak was taken to be the location of the liquid front for the data presented*." A plot of the locations of three fronts as a function of time is shown in Figure 6.9. It is evident that the vapor front arrived only slightly ahead of the water front. But, the temperature rise occurred much earlier than the change in humidity and moisture content. Perrier and Prakash (1977) (Perrier, E. R.; Prakash 1976) did not provide any explanation for this phenomenon.

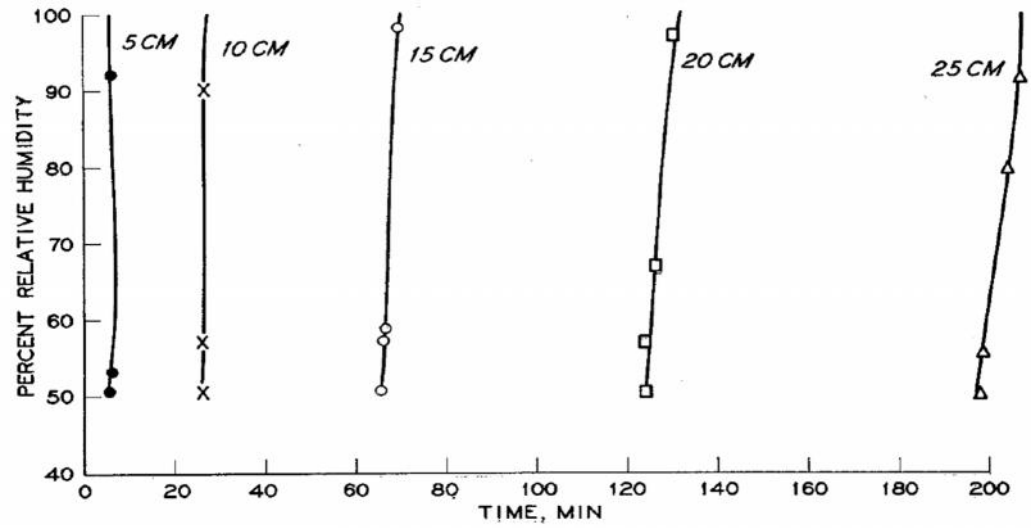

Figure 6.8 Instantaneous increase of relative humidity at various positions along the column (from Perrier and Prakash, 1977) (Perrier, E. R.; Prakash 1976)

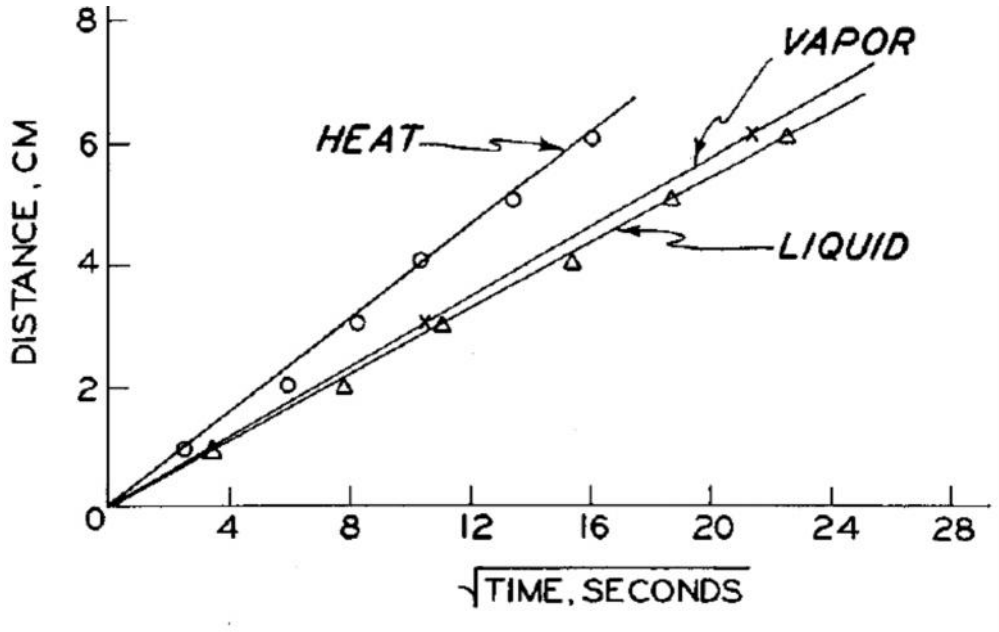

Figure 6.9 Position of temperature, humidity and water content fronts (from Perrier and Prakash, 1977) (Perrier, E. R.; Prakash 1976)

Perrier and Prakash (1977) (Perrier, E. R.; Prakash 1976) concluded the following from their experiments: "*These data show that the advance of a wetting front involves several processes: as dry soil is wetted, a large amount of heat is evolved; (b) evaporation during the wetting process supplies a vapor phase; (c) as liquid moves into dry soil, the vapor phase moves as a front immediately ahead of the wetting front; (d) a large portion of the heat evolved moves as a front well in advance of both the vapor and liquid fronts; and (e) the heat evolved subsequently heats the liquid front; however, due to evaporation and the thermal conductivity of water, the wetted soil behind the liquid front is cooled*." So, they suggested that the heat is released due to the wetting of soil and evaporation occurs afterwards as a result of this heat generation. This is opposite to the assertions of Anderson and Linville (1962) (Anderson and Linville 1962), who stated that the evaporation occurs spontaneously first and the heat is generated due to the vapor condensation on soil grain surfaces.

The hypothesis of Anderson and Linville (1962) (Anderson and Linville 1962) was also challenged by Prunty and Bell (2005) (Prunty and Bell 2005), who performed experiments similar to theirs with water flowing downward into

(partially) dry soil (see also Prunty, 2002 (Prunty 2002)). They used either Fargo silty clay or Glyndon loam, at different initial moisture values (0.00, 0.02, 0.04, and 0.06 g/g). They measured the temperature using thermocouples at six different locations along the column. For dry soil, they found temperature spikes of 5 ºC to 11 ºC, depending on soil type, initial moisture content, and the position along the column. Typical results are shown in Figure 6.10. The magnitude of temperature spikes became larger along the flow direction; this was contrary to findings of Anderson and Linville (1960) (Anderson and Linville 1960), who didn't find a change and Perrier and Prakash (1977) (Perrier, E. R.; Prakash 1976) who found a decrease along the flow direction. However, similar to Anderson and Linville (1963) (Anderson et al. 1963a), they found that the temperature rise was significantly smaller for partially wet sand. They did not observe any cooling of the medium; in any of the cases. In fact, the temperature dropped back but remained above the initial temperature. Using physical properties of the soils used in their experiments, Prunty and Bell (2005) estimated the expected temperature rise when the soils would get saturated from the oven-dry condition. They considered two different thermodynamic state changes: one when water vapor condenses on the dry surface of soil grains (with released energy being called heat of adsorption) and the other when liquid water completely covers the dry grain surfaces. They referred to the latter as the heat of wetting. They clearly showed that while the heat of wetting alone is sufficient to cause temperature rises measured in their experiments, heat of adsorption can cause only small temperature rises. They concluded that heat generated by the wetting of soil grains by liquid water is the main source of a temperature peak at the wetting front. This was in line with the conclusion of Perrier and Prakash (1977) (Perrier, E. R.; Prakash 1976).

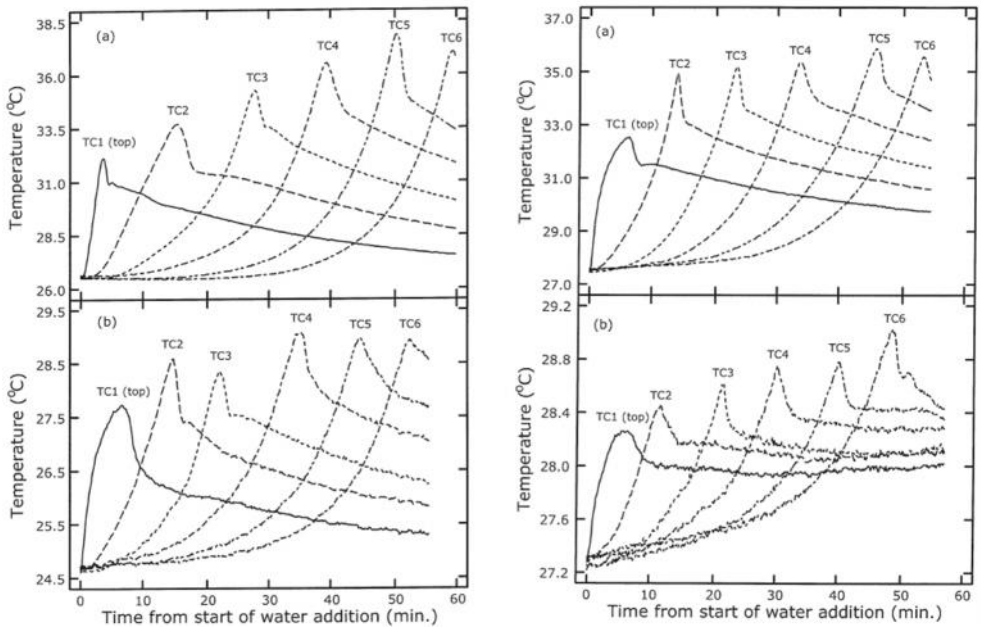

Figure 6.10. Temperature as a function of time measured at different locations in experiments of Prunty and Bell (2005) (Prunty and Bell 2005). The two plots on the left are from columns containing silty clay soil (a) dry and (b) with 0.04 g/g. Plots on the right are for loamy soil

Recently, spontaneous infiltration experiments were performed by Zoladek-Nowak et al. (2011) (Zoladek-Nowak et al. 2012), with water rising into a column by capillarity. They introduced water into the bottom reservoir of a column of dry natural zeolite grains. Water rose spontaneously in the column. The water content change in the column was monitored using neutron radiography and the temperature was recorded by thermocouples placed at four different elevations in the column. They performed many experiments at various ambient temperature and different treatments of zeolite grains. Experiments were carried out at five different constant ambient temperatures, ranging from 30 °C to 70 °C. Zeolite grains were treated at three different drying temperatures (50 °C, 100 °C, and 150 °C) for two to five weeks before packing them into the column. Typical results are shown in Figure 6.11. They found temperature spikes of 3 °C to 40 °C in various experiments, as the wetting front passed positions along the column. The largest amplitudes were for cases of higher ambient temperature and/or when zeolite grains had been treated at higher temperature. They explained that zeolite becomes more hydrophilic under those

conditions. As a result, there should be more energy released, leading to a larger temperature spike.

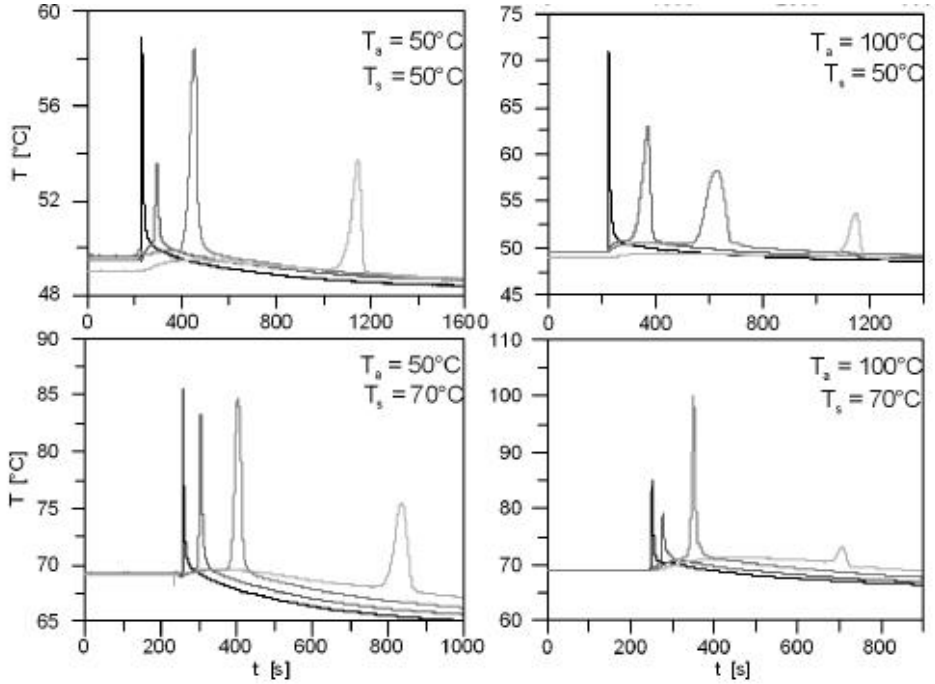

Figure 6.11. Temperature as a function of time in experiments of zoldak- Nowak et al. 2012 (Zoladek-Nowak et al. 2012). Two diagrams in the right were done on Zeolite pickings treated at 100˚C and in left at 50˚C. In both cases, ambient temperature was 50 and 70˚C.

This review shows that some of the early theories about the source of heat for temperature rise at a wetting front are questionable. In particular, the idea that the temperature rise is due to the heat of condensation of water vapor ahead of the wetting front does not hold. In fact, if temperature rise were due to the water vapor condensation on solid surface of the porous medium, it should have been observed not only at the water front but also everywhere else in the porous medium; the vapor can diffuse relatively fast in the pore space and should therefore condensate everywhere. That has not been observed. Moreover, if water vapor would wet the solid surface and reduce its surface energy, then there would remain no driving force for spontaneous imbibition to occur. That is, once the vapor diffuses into a porous medium and wets the pore surfaces, there is no thermodynamic reason for water to enter the medium, as vapor competes with its own liquid in wetting the solid

surfaces. Evidence for this statement can be found in a neat experiment reported by Bangham and Razouk (Bangham and Razouk 1937) They found that a drop of methyl alcohol spread rapidly when it was placed on freshly-split mica, when the experiment was done in air. But, when air was replaced with the saturated vapor of methyl alcohol, it did not do so; the spread film of methyl alcohol formed in air immediately gathered back into lenses when it was brought under a jet of the supersaturated vapor of the alcohol. This means that vapor condensation on surfaces of pores should actually hamper spontaneous imbibition, which we know does not occur. So, the only plausible explanation for the source of energy that causes an increase in temperature of the porous medium and the rise of water in the medium, against gravity and viscous forces, seems to be the heat of wetting; i.e., the energy released due to the spontaneous replacement of air-solid interface by the water-solid interface.

6.3 Methods

6.3.1 Paper samples

Six different paper types were used in this work including coated and uncoated papers. Five papers were made of natural cellulose fibers and one from plastic fibers. The fiber material affects the penetration of liquids into the paper significantly, even when overall porosities and mean fiber diameters are almost the same. For example, cellulose fibers consist of a bundle of fibrils (Zhao et al. 2007), which are themselves porous. Also, their surface is rough and contains nano-channels (see Figure 6.12.D). But, plastic-based fibers are usually not porous and have smooth surfaces. So, water can enter plastic-based papers only via pores formed between the fibers. While in cellulose paper, water moves not only in large pores formed between the fibers, but it also gets imbibed into individual fibers and seeps into nano-channels on the surface of fibers. Another important difference between natural and plastic fibers is in the wettability of their surfaces. Cellulose fibers have hydrogen bonds in their structure, so they are hydrophilic while plastic fibers are usually hydrophobic (Hodgson and Berg 2007). That will have a major effect on capillary suction and the amount of released heat. Figure 6.12 shows micro structures of samples of paper coating (A. surface and B. cross section) and fibrous layer (C), and the roughness on the surface of a cellulose fiber. These images were obtained by Scanning Electron Microscopy (SEM).

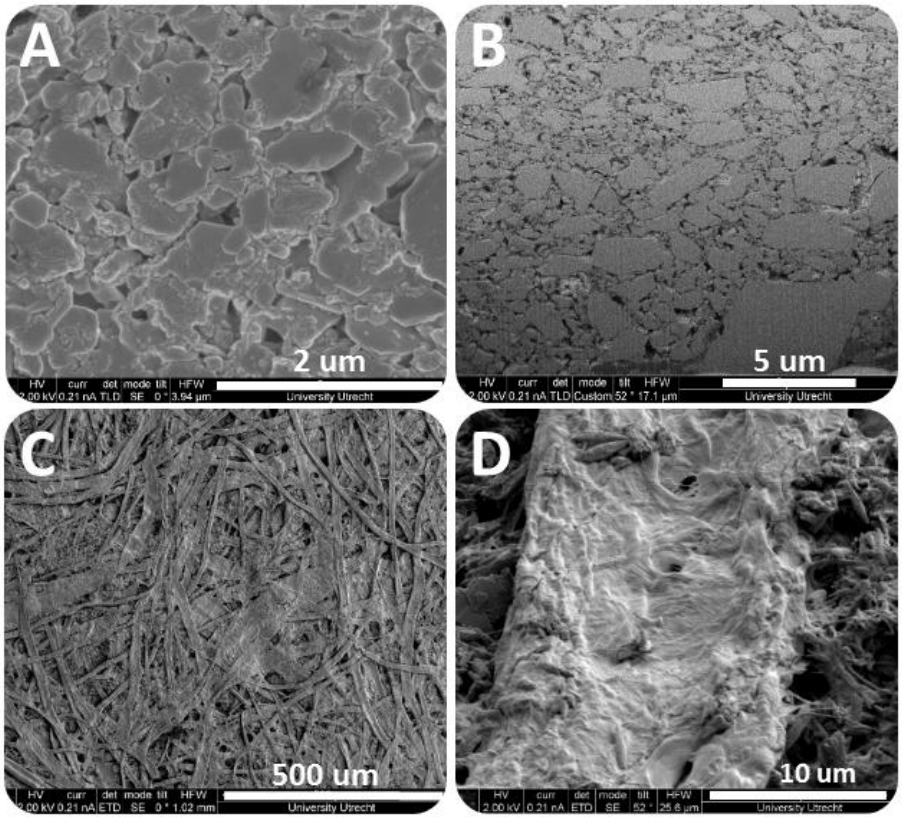

Figure 6.12. SEM images of surface and cross section of a coating layer (A, B, respectively), fibrous layer surface (C) and surface of a single fiber (D)

Specifications of the six paper types used in this study are given in Table 6-1. The Ziegler paper is like the regular papers which are used in office printers. It is an uncoated cellulose fibrous paper with a thickness of 120 µm, mean pore size of 10 µm, and a porosity of 52%. The coated paper, Magno gloss, is made of a base fibrous layer, 65 µm thick, with coating layers on both sides. Each coating layer is 10 µm thick; so, the total thickness of the paper is 85 µm. The coating layer is made of $CaCO_3$ powder, with mean pore size of 180 nm (Aslannejad et al. 2017a). The base layer is made of cellulose fibers with mean fiber diameter of 20 µm. Figure 6.13 shows capillary pressure-saturation curves for the fibrous and coating layers; obtained by simulation (ref. under review, will be added later).

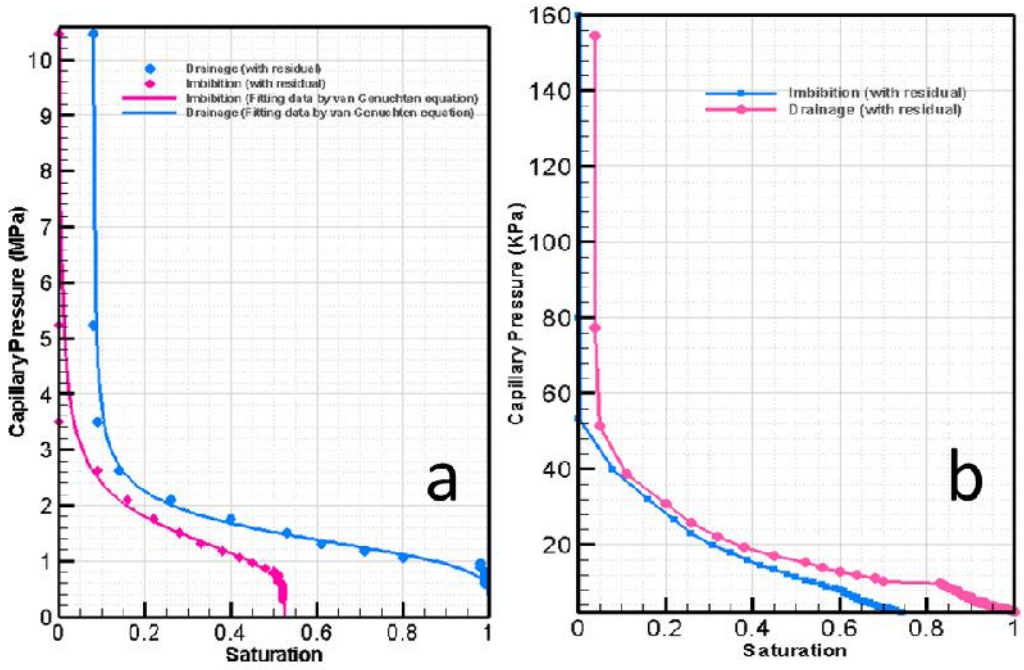

Figure 6.13. Capillary pressure curves for; a) coating layer and b) fibrous layer (Aslannejad et al. 2017a)

In addition to the Ziegler paper, we used two similar but thicker papers; RL 200 and RL professional. The material type is the same for these two papers, but the thicknesses are 260 µm and 340 µm, respectively, for RL 200 and RL professional.

Some fibrous base layers contain a filler material, made of very fine powder. The most common paper fillers are ground calcium carbonate, kaolin, precipitated calcium carbonate, talc, and titanium dioxide. The amount of fillers varies from none to at least 30% of the whole furnish. The main reasons to use them are their low cost, compared to fiber, and improvement of optical properties of the print (Brightness, Whiteness and Color) of the final product. Fillers can also improve surface properties of paper and thus have a positive effect on the printability of the final product (Gronfors 2010). Among paper samples, Plain paper, RL 200 and RL professional, have filler materials inside their fibrous layer.

The fibrous layers of Ziegler, RL 200 and RL professional papers are impregnated with mineral particles (added as fillers). We also used a sample of Prematex paper, which consists of only fibers with no mineral particles added. Its

porosity is higher (60%) relative to Ziegler paper (52%) and it has a much larger thickness.

Table 6-1 Paper sample characteristics

Paper type	porosity	Mean pore size	Material in layer(s)	Thickness
Ziegler	52%	10 µm	Cellulose	120 µm
Coated paper (Magno gloss)	-	-	-	-
Coating layer	34%	180 nm	$CaCO_3$	10 um
Fibrous layer	50%	10 um	Cellulose	65 um
RL 200	50%	12 µm	Cellulose	260 µm
RL professional	48%	12 µm	Cellulose	340 µm
Plastic based	65%	16 µm	Plastic	220 µm
Prematex	60%	20 µm	Cellulose	300 µm

6.4 Experimental setup and procedure

Four strips were cut from each paper type in order to quadruplicate the data in a single experiment. Each strip was 45 mm in length and 10 mm in width. As the fiber orientation influences the layer structure and consequently water movement, all samples were cut in the same direction (along length). In order to prevent the evaporation of water from the wet paper surface, the samples were completely covered and pressed onto a Plexiglas plate by a 62-µm-thick clear tape, which was also transparent to infrared radiation (see inset in Figure 6.14). The lower edge of the tape and the paper sample were carefully trimmed with a surgery blade to be exactly aligned with the lower edge of the Plexiglas material.

The Plexiglas plate was kept in room temperature overnight. It was fixed in the vertical position to an experimental rig. In order to increase the quality of thermal images, the Plexiglas surface was covered with a matt black adhesive ensuring a high emissivity value of 0.98. The emissivity of dry and wet paper areas was determined based on the ambient and liquid bath temperatures. The resultant emissivity for both areas was very similar, and hence, a single value of 0.9 was considered for the whole imbibition process.

A schematic representation of the setup is shown in Figure 6.14. A constant-temperature water bath was placed on a traversing stage under the Plexiglas plate. The bath was filled with distilled water. The imbibition process could be started by raising the water bath slowly until the water surface would touch the lower edge of Plexiglas and the paper strip. The temperature of the bath was set at 0.2 ◦C loTCwer

than ambient temperature in order to ensure that no heat was transferred from the water to the paper samples. Hence, any temperature variation of the paper could be attributed to the imbibition process only. The temperature of the distilled water was measured with two K-type thermocouples (TC1 and TC2 in Figure 6.14). The ambient temperature was monitored by two thermocouples positioned on the two sides of the experimental rig (TC3 and TC4) as shown in Figure 6.14.

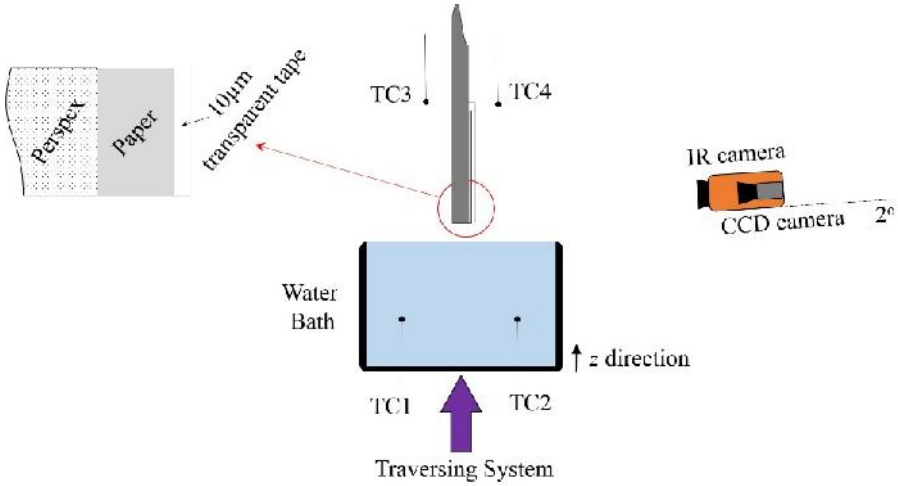

Figure 6.14. Schematic of the experimental setup

Optical and thermal cameras were installed in front of the Plexiglas plate. The spatial distribution of temperature was recorded continuously by a FLIR-SC7000C IR camera with high sensitivity, and noise levels as low as 20 mK. The IR camera had an optical lens of 25 mm with a maximum resolution of 640 × 512 pixels, which resulted in approximately 45 pixels/(mm)^2. In order to increase the quality of the infrared measurements, the backside of the experimental test rig was covered with a black curtain in order to prevent any reflection and radiation influence of the surroundings on the IR camera display. However, the top of the test rig was open and normal room illumination was provided. In addition, the CCD videos were taken with a relatively large exposure time in order to increase the contrast of the images. As the tape was transparent to infrared radiation, the IR camera actually measured the temperature of the paper surface just below the tape.

The imbibition of the water into the paper was recorded with a high definition RGB camera, model UI-3360CP, connected with a frame grabber to a 16GB-RAM computer. These hardware capabilities allowed real time image saving. Thus, images with a high spatial resolution of approximately 55 pixels/(mm)^2 could

be acquired while a KOWA LM6JC lens of 16 mm (focal lense) eliminated image distortion. Note also that the CCD camera was used in the monochrome mode in order to increase the contrast and better distinguish between wet and dry paper surfaces.

Both cameras were set to a constant frame rate typically varied between 5 Hz and 15 Hz depending on the paper sample and the associated imbibition speed. The imbibition processes typically lasted from about 2 to 12 minutes. The first frame of CCD camera was determined by small reflections of the paper on the water surface observed in the optical video, which was also used as a reference to define the beginning of the thermal recording. Hence, the start of the thermal and optical videos was synchronized with an accuracy of one frame. An example of optical and thermal images at a given instant is shown in Figure 6.15.

To start the imbibition experiment, the water bath was raised using a precise traversing system. As soon as the water covered a few mm of the Plexiglas plate holder and the paper samples, and the imbibition process started, we fixed the position of the water bath.

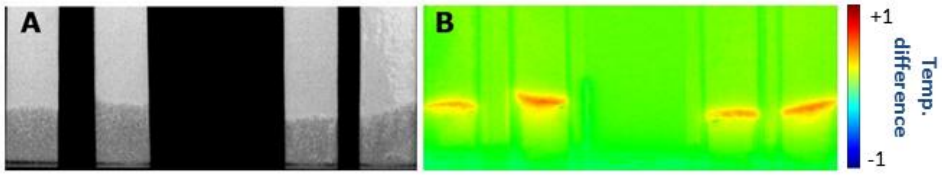

Figure 6.15 Examples of acquired images: a) optical and b) thermal

The experimental set up presented above has been recently employed by Terzis et al. (Terzis et al. 2017) in order to investigate the imbibition of a number of other liquids into paper.

6.5 Results

6.5.1 Positions of temperature and wetting fronts

Figure 6.16 shows optical and thermal images at various times during the spontaneous imbibition process, for RL 200 paper. Similar images were obtained for all other paper types. The dark-colored region in black-and-white images from CCD cameras shows the wetted part of the paper. Based on these images, profiles of gray color intensity (indicative of water distribution) and temperature at different times were obtained and are plotted in Figure 6.17. It is clear that the maximum temperature at any given point was reached when the color intensity visibly started to increase there; we refer to this point as the water front (shown by a vertical dashed line in Figure 6.17). The increase of temperature starts even earlier because it is known that precursor water films move ahead of a water front; thus, water film could cover solid surfaces and cause the release of energy and increase of temperature before any sign of moisture increase visible to the CCD camera. The temperature started to decrease and return to the ambient value as more water, which was slightly below the ambient temperature, arrived and almost fully wetted the paper.

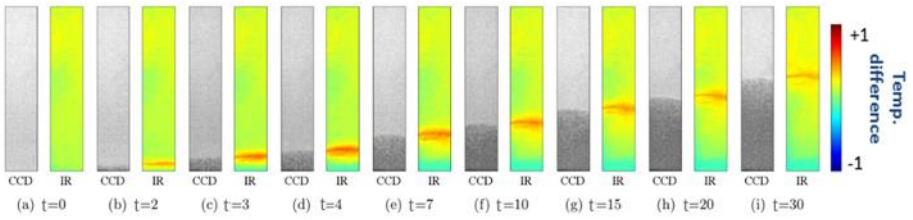

Figure 6.16 Optical and thermal images of RL 200 paper during spontaneous imbibition at various times (sec)

A plot of the positions of wetting front and temperature front (where the maximum temperature was reached) as a function of time is shown in Figure 6.18a and 6.18b, respectively, for RL professional and Prematex papers. In each case, there are six curves corresponding to the six samples of the same paper. We did not plot wetting and temperature front positions in a single graph because they would coincide and it would be hard to distinguish them. The wetting front speed was higher in the case of Prematex paper than for RL professional paper because of its significantly higher permeability.

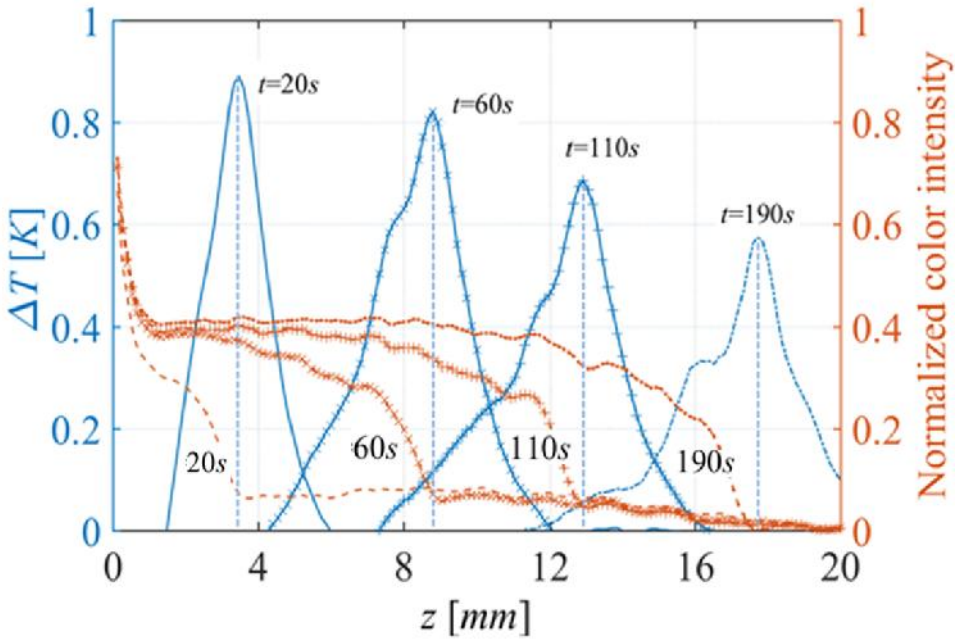

Figure 6.17 Profiles of water distribution and temperature along a sample of RL 200 paper at different times (the measured positions were in respect to the lower edge of Plexiglas plate). Vertical dashed lines indicate the positions of temperature and wetting fronts

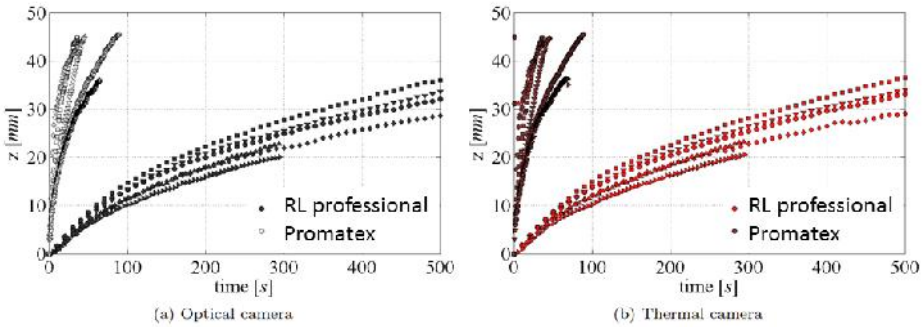

Figure 6.18 Imbibition height as a function of time for the optical and thermal image

We know that as water rises up in a porous medium spontaneously, the wetting front will become more diffuse and the corresponding maximum saturation will be lower. This means that the amount of wetted air-solid surface per unit volume

becomes less and less as the wetting front rises. This is reflected in the change of temperature with time at various positions along the paper, shown in Figure 6.19. The temperature spike at higher positions is wider (because the water front is more diffuse) and its magnitude is lower (as relatively less energy is released).

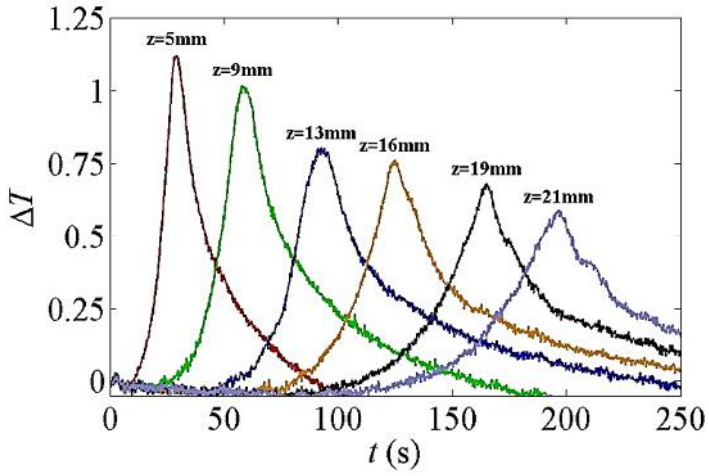

Figure 6.19 Temperature rise at various imbibition heights over time

6.5.2 Effect of paper thickness and paper type

In our setup, the released energy goes into warming up not only the paper sample but also the tape covering the paper and the Plexiglas plate behind the paper samples. So, there was significant loss of heat to the tape (and thus the air) and the Plexiglas plate. This heat loss is more or less the same for a thin paper or a thick paper. Now, for a thicker paper (or more layers of paper), there is more energy released. However, there is also a proportionally larger mass to be heated up. Nevertheless, as the heat loss remains the same, the ratio of heat loss to the released energy will decrease for thicker paper samples. So, relatively speaking, there is more energy available to thicker papers or for more layers of the same papers and this should cause a bigger rise of the observed temperature. This could be confirmed by comparing results of temperature change for RL 200 and RL professional papers. They are the same paper type but with different thicknesses, namely 260 µm and 340 µm, respectively (see Table 6-1). We also performed experiments with one, two, and three layers of the RL professional paper. Thus, the total thickness of the sample in those experiments was 340 µm, 680 µm, and 1 020 µm, respectively. The plots of temperature change with time for RL 200 and RL professional papers at the

position z=5 mm are shown in Figure 6.20a and the same for 1, 2, and 3 layers are shown Figure 6.20b. It is clear that the magnitude of temperature spike is significantly larger for more layers of the same paper or for a thicker paper.

We also investigated the influence of the paper type by performing experiments on a sample of plastic-based paper. The sample was 220 μm thick and was made of a hydrophobic non-cellulose-based material. As the solid phase is hydrophobic, it has a large solid-water interfacial tension. That means that we should expect significantly less energy released, and thus a lower temperature spike, at a wetting front, compared to a cellulose-based paper. The plots of temperature change with time for RL professional, RL 200, and plastic-based papers at the position z=5mm are shown in Figure 6.20a. It is evident that the magnitude of temperature spike for the plastic-based paper was significantly lower than for the cellulose-based papers.

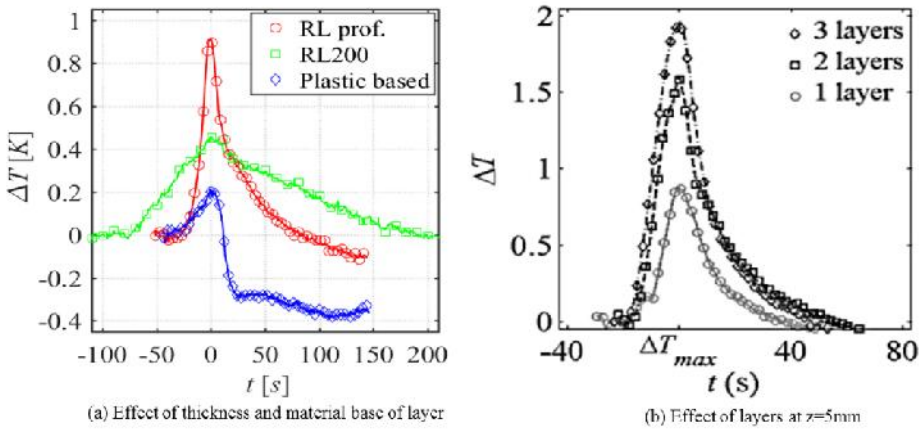

(a) Effect of thickness and material base of layer (b) Effect of layers at z=5mm

Figure 6.20 Effect of thickness and paper type on temperature rise

6.5.3 Effect of water properties

As the temperature spike is completely controlled by interfacial energies, we investigated the effect of changing water properties in order to reduce its affinity to the solid phase. We did this by dissolving salt in water creating a salty solution with the concentration of 120 g/l. The solid is known to be less wetting to saltwater compared to fresh water. In other words, the interfacial energy of salt water-solid surface is larger than that of fresh water-solid interface. Thus, one would expect less heat to be released when air-solid interface is wetted by salt water. This was clearly confirmed by the plot of temperature change with time shown in Figure 6.21; the

magnitude of temperature spike for the salt water was significantly lower than for fresh water.

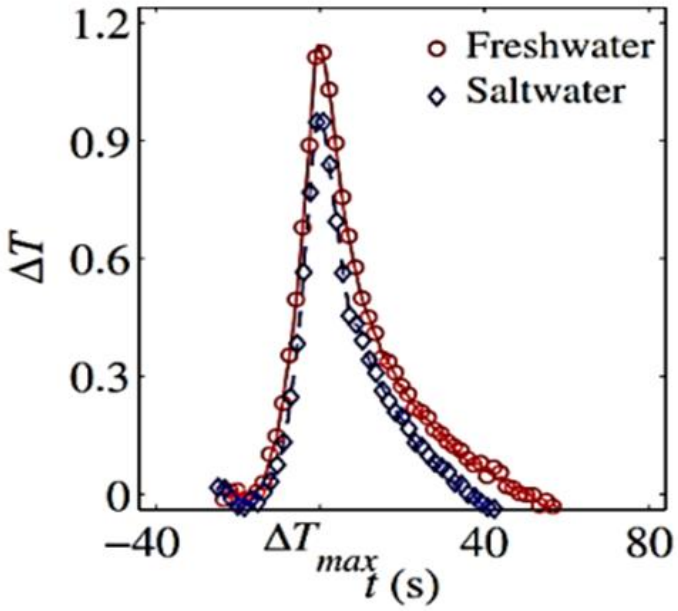

Figure 6.21 Temperature rise during water spontaneous imbibition and effect of surface tension at z=5 mm

6.5.4 Evaporation and condensation of water

As mentioned before, one of the early theories proposed for explaining the temperature spikes was based on the condensation of water vapor ahead of the wetting front. However, of course, water has to be evaporated first, and water evaporation is expected to be accompanied with cooling of the system. We looked for such a cooling effect in our observation. Indeed, at very early imbibition stages, i.e., very low imbibition heights (3-4 mm above the water source), the IR images showed a small temperature drop, which was still resolvable with IR camera. Figure 6.16 shows IR images for various time frames. Also, in Figure 6.22, we show the temperature profile with distance at very early times. Both images show that local cooling due to evaporation occurred at the very early imbibition stages. However, no cooling was observed as the imbibition process propagated.

This can be attributed to two reasons:

(a) The temperature rise caused by wetting of solid surface overcomes the evaporation cooling.

(b) The air ahead of the liquid front becomes ‘saturated’, and hence, no more evaporation occurs.

As it can be seen in videos of our experiments (see related file in Supplementary Material section), there was no temperature rise after the water front stopped. But, one would expect the evaporation of water and its condensation to occur far above the wetting front. So, the temperature rise should have been observed in the upper part of the sample even after the wetting front stopped. This was not the case.

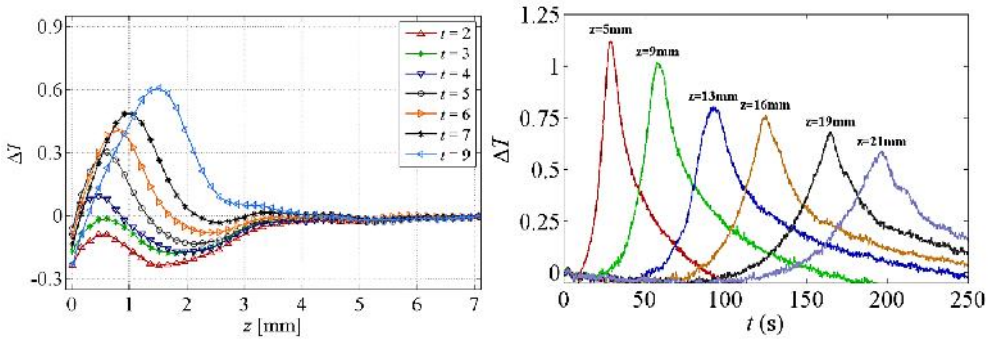

Figure 6.22. Averaged temperature distribution at various time frames at very initial imbibition stages (left)

6.6 Conclusion

There exist three interfaces in a partially-saturated porous material: air-solid, solid-liquid, and liquid-air. The surface energy of solid-air interfaces is known to be much larger than that of the water-solid interface. The spontaneous imbibition of water into a medium, such as dry paper, occurs due to the net decrease in interfacial energies of those three interfaces. The released energy is turned into heat which causes a temperature spike of the porous medium (water plus paper fibers). The magnitude of the spike depends on material, thickness, and liquid composition. Our results show that the maximum temperature at any given location occurs exactly at the time that water front arrives. Effects of various factors such as paper type, its thickness, number of layers, and liquid composition were investigated. A more extensive study of effects of different liquid on temperature rise was done recently by Terzis et al. (Terzis et al. 2017). They found that energetics of imbibition compounds are involved in temperature rise and result in electrostatic attractions as the liquid molecules are adhered on the fiber surfaces upon capillary contact.

A higher temperature rise was observed for cellulose-based samples than the plastic-based paper. For a certain paper type, thicker and more layers of paper resulted in higher temperature rise. Addition of salt to the water caused a reduction of the temperature rise. All of these observations are in line with postulation that the energy released as a result of wetting of surface of paper fibers is the source of generated heat that causes local and temporary temperature rise.

6.7 References

Alam, P., Byholm, T., Kniivilä, J., Sinervo, L., Toivakka, M.: Calculating the permeability of model paper coating structures comprising incongruent particle shapes and sizes. (2009)

Alam, P., Toivakka, M., Backfolk, K., Sirviö, P.: Impact spreading and absorption of Newtonian droplets on topographically irregular porous materials. Chem. Eng. Sci. 62, 3142–3158 (2007). doi:10.1016/j.ces.2007.03.018

Anderson, D.M., Linville, A.: Temperature Fluctuations Accompanying Water Movement through Porous Media Published by : American Association for the Advancement of Science. Am. Assoc. Adv. Sci. 131, 1370–1371 (1960)

Anderson, D.M., Linville, A.: Temperature Fluctuations at a Wetting Front: I. Characteristic Temperature-Time Curves1. Soil Sci. Soc. Am. J. 26, 14 (1962). doi:10.2136/sssaj1962.03615995002600010005x

Anderson, D.M., Linville, A., Sposito, G.: Temperature Fluctuations at a Wetting Front: III. Apparent Activation Energies for Water Movement in the Liquid and Vapor Phases1. Soil Sci. Soc. Am. J. 27, 610 (1963)(a). doi:10.2136/sssaj1963.03615995002700060014x

Anderson, D.M., Sposito, G., Linville, A.: Temperature Fluctuations at a Wetting Front: II. The Effect of Initial Water Content of the Medium on the Magnitude of the Temperature Fluctuations1. Soil Sci. Soc. Am. J. 27, 367 (1963)(b). doi:10.2136/sssaj1963.03615995002700040005x

Aronsson, M., Henningsson, O., Sävborg, Ö.: Slice-based digial volume assembly of a small paper sample. Nord. Pulp Pap. Res. J. 17, 29–33 (2001). doi:10.3183/NPPRJ-2002-17-01-p029-033

Aslannejad, H., Hassanizadeh, S.M.: Study of Hydraulic Properties of Uncoated Paper: Image Analysis and Pore-Scale Modeling. Transp. Porous Media. (2017). doi:10.1007/s11242-017-0909-x

Aslannejad, H., Hassanizadeh, S.M., Raoof, A., de Winter, D.A.M., Tomozeiu, N., van Genuchten, M.T.: Characterizing the hydraulic properties of paper coating layer using FIB-SEM tomography and 3D pore-scale modeling. Chem. Eng. Sci. 160, 275–280 (2017)(a). doi:10.1016/j.ces.2016.11.021

Aslannejad, H., Terzis, A., Hassanizadeh, S.M., Weigand, B.: Occurrence of temperature spikes at a wetting front during spontaneous imbibition. Sci. Rep. 7, 7268 (2017)(b). doi:10.1038/s41598-017-07528-7

Axelsson, M.: Image analysis for volumetric characterisation of microstructure. (2009)

Axelsson, M., Svensson, S.: 3D pore structure characterisation of paper. Pattern Anal. Appl. 13, 159–172 (2010). doi:10.1007/s10044-009-0146-1

Bangham, D.H., Razouk, R.I.: Adsorption and the wettability of solid surfaces. Trans. Faraday Soc. 33, 1459 (1937). doi:10.1039/tf9373301459

Bedram, A., Moosavi, A.: Breakup of droplets in micro and nanofluidic T-junctions. J. Appl. Fluid Mech. 6, 81–86 (2013). doi:10.4028/www.scientific.net/AMM.110-116.3673

Blumer, M.: Thermometric Monitor for Chromatographic Streams. Anal. Chem. 32, 772–776 (1960)

Bosanquet, C.H.: LV. On the flow of liquids into capillary tubes. Philos. Mag. Ser. 6. 45, 525–531 (1923). doi:10.1080/14786442308634144

Carsel, R.F., Parrish, R.S.: Developing joint probability distributions of soil water retention characteristics. Water Resour. Res. 24, 755–769 (1988)

Cheng, Kirsch, L., Wiegmann, R., Gervais, A., Bardin-Monnier, P.-C., N. Thomas, D.: PleatLab. A pleat scale simulation environment for filtration simulation. (2013)

Claxton, G.: Detector for liquid-solid chromatography. J. Chromatogr. A. 2, 136–139 (1959). doi:10.1016/S0021-9673(01)86273-7

Dalton, Preston, J.., Heard, J.., Allen, P.., Elton, G.., Husband, N..: Investigation into the distribution of ink components throughout printed coated paper. Colloids Surfaces A Physicochem. Eng. Asp. 205, 199–213 (2002). doi:10.1016/S0927-7757(02)00021-3

Das, S., Ramarao, B.V.: Inversion of lime mud and papermaking pulp filtration data to determine compressibility and permeability relationships. Sep. Purif. Technol. 28, 149–160 (2002). doi:10.1016/S1383-5866(02)00047-3

de Gans, B.-J., Duineveld, P.C., Schubert, U.S.: Inkjet Printing of Polymers: State of the Art and Future Developments. Adv. Mater. 16, 203–213 (2004). doi:10.1002/adma.200300385

Delerue, J.F., Perrier, E., Yu, Z.Y., Velde, B.: New algorithms in 3D image analysis and their application to the measurement of a spatialized pore size distribution in soils. Phys. Chem. Earth, Part A Solid Earth Geod. 24, 639–644 (1999). doi:10.1016/S1464-1895(99)00093-9

Desie, G., Deroover, G., De Voeght, F., Soucemarianadin, A.: Printing of dye and pigment-based aqueous inks onto porous substrates. J. Imaging Sci. Technol. 48, 389–397 (2004)

Do-Quang, M., Carlson, A., Amberg, G.: The impact of ink-jet droplets on a paper-like structure. Fluid Dyn. Mater. Process. 7, 389–402 (2011). doi:10.3970/fdmp.2011.007.389

Dodson, C.T.J., Sampson, W.W.: The effect of paper formation and grammage on its pore size distribution. J. pulp Pap. Sci. 22, J165–J169 (1996)

Fathi, H., Raoof, A., Mansouri, S.H.: Insights into the role of wettability in cathode catalyst layer of proton exchange membrane fuel cell; pore scale immiscible flow and transport processes. J. Power Sources. 349, 57–67 (2017). doi:10.1016/j.jpowsour.2017.03.012

Gambaryan-Roisman, T.: Liquids on porous layers: wetting, imbibition and transport processes. Curr. Opin. Colloid Interface Sci. 19, 320–335 (2014). doi:10.1016/j.cocis.2014.09.001

Gane, P., Hooper, J.: An evaluation of interactions between coating color and basepaper by coating profile analysis. Fundamentals of Papermaking. In: Trans. 9th Fundamental Reasearch Symposium, Ed. Baker and Punton, Mech. Eng. Publ., London, UK. pp. 871–893 (1989)

Gane, P.A.C.: Mottle and the influence of coating and binder migration. Pap. Technol. Ind. 30, 34–41 (1989)

Gane, P.A.C., Hooper, J.J., Baumeister, M.: The influence of furnish content on formation and basesheet profile stability during coating. Tappi J. 74, 193–201 (1991)

Gane, P.A.C., Salo, M., Kettle, J.P., Ridgway, C.J.: Comparison of Young-Laplace pore size and microscopic void area distributions in topologically similar structures: a new method for characterising connectivity in pigmented coatings. J. Mater. Sci. 44, 422–432 (2008). doi:10.1007/s10853-008-3134-8

van Genuchten, M.: A closed-form equation for predicting the hydraulic

conductivity of unsaturated soils. Soil Sci. Soc. Am. J. 44.5, 892–898. (1980)

Ghanbarian-Alavijeh, B., Liaghat, A., Huang, G.-H., van Genuchten, M.T.: Estimation of the van Genuchten soil water retention properties from soil textural data. Pedosphere. 20, 456–465 (2010)

Ghassemzadeh, J., Sahimi, M.: Pore network simulation of fluid imbibition into paper during coating—III: modelling of the two-phase flow. Chem. Eng. Sci. 59, 2281–2296 (2004)(a). doi:10.1016/j.ces.2004.01.058

Ghassemzadeh, J., Sahimi, M.: Pore network simulation of fluid imbibition into paper during coating: II. Characterization of paper's morphology and computation of its effective permeability tensor. Chem. Eng. Sci. 59, 2265–2280 (2004)(b). doi:10.1016/j.ces.2004.01.057

Girard, F., Attané, P., Morin, V.: A new analytical model for impact and spreading of one drop: Application to inkjet printing. Tappi J. 5, 24–32 (2006)

Gronfors, J.: Use of fillers in paper and paperboard grades, (2010)

Hassanizadeh, S.M., Gray, W.G.: Mechanics and thermodynamics of multiphase flow in porous media including interface boundaries. Adv. Water Resour. 13, 169–186 (1990)

Hassanizadeh, S.M., Gray, W.G.: Thermodynamic basis of capillary pressure in porous media. Water Resour. Res. 29, 3389–3405 (1993). doi:10.1029/93WR01495

Heard, P.J., Preston, J.S., Parsons, D.J., Cox, J., Allen, G.C.: Visualisation of the distribution of ink components in printed coated paper using focused ion beam techniques. Colloids Surfaces A Physicochem. Eng. Asp. 244, 67–71 (2004). doi:10.1016/j.colsurfa.2004.05.012

Hilpert, Markus, Miller, T., C.: Pore-morphology-based simulation of drainage in totally wetting porous media. Adv. Water Resour. 24, 243–255 (2001). doi:10.1016/S0309-1708(00)00056-7

Hird, K.F.: Offset lithographic technology. Goodheart-Willcox Co, Tinley Park, Illinois (2000)

Hirn, U., Schennach, R.: Comprehensive analysis of individual pulp fiber bonds quantifies the mechanisms of fiber bonding in paper. Sci. Rep. 5, 10503 (2015)

Hodgson, K.T., Berg, J.C.: Dynamic Wettability Properties of Single Wood Pulp Fibers and Their Relationship to Absorbency. Wood Fiber Sci. 20, 3–17 (2007)

Holmstad: Comparison of 3D structural characteristics of high and low resolution X-ray microtomographic images of paper. Nord. Pulp Pap. Res. J. 20, 283–288 (2005). doi:10.3183/NPPRJ-2005-20-03-p283-288

Huang, S., Goel, A., Ramaswamy, S., Ramarao, B., Choi, D.: Transverse and in-plane pore structure characterization of paper, (2002)

Hyväluoma, J., Koponen, A., Raiskinmäki, P., Timonen, J.: Droplets on inclined rough surfaces. Eur. Phys. J. E. 23, 289–293 (2007). doi:10.1140/epje/i2007-10190-7

Hyväluoma, J., Raiskinmäki, P., Jäsberg, A., Koponen, A., Kataja, M., Timonen, J.: Simulation of liquid penetration in paper. Phys. Rev. E. 73, 036705 (2006). doi:10.1103/PhysRevE.73.036705

Ingmanson, W.L., Andrews, B.D., Johnson, R.C.: Internal Pressure Distributions in Compressible Mats under Fluid Stress. TAPPI J. 42, 840–849 (1959)

Järnström, J., Väisänen, M., Lehto, R., Jäsberg, A., Timonen, J., Peltonen, J.: Effect of latex on surface structure and wetting of pigment coatings. Colloids Surfaces A Physicochem. Eng. Asp. 353, 104–116 (2010). doi:10.1016/j.colsurfa.2009.11.001

Kanit, T., Forest, S., Galliet, I., Mounoury, V., Jeulin, D.: Determination of the

size of the representative volume element for random composites: statistical and numerical approach. Int. J. Solids Struct. 40, 3647–3679 (2003). doi:10.1016/S0020-7683(03)00143-4

Karwacki, L., de Winter, D.A., Aramburo, L.R., Lebbink, M.N., Post, J.A., Drury, M.R., Weckhuysen, B.M.: Architecture-Dependent Distribution of Mesopores in Steamed Zeolite Crystals as Visualized by FIB-SEM Tomography. Angew. Chemie Int. Ed. 50, 1294–1298 (2011)

Kettle, J., Lamminmäki, T., Gane, P.: A review of modified surfaces for high speed inkjet coating. Surf. Coatings Technol. 204, 2103–2109 (2010). doi:10.1016/j.surfcoat.2009.10.035

Kuijpers, C.J., van Stiphout, T.A.P., Huinink, H.P., Tomozeiu, N., Erich, S.J.., Adan, O.C.G.: Quantitative measurements of capillary absorption in thin porous media by the Automatic Scanning Absorptometer. Chem. Eng. Sci. 178, 70–81 (2018). doi:10.1016/J.CES.2017.12.024

Lamminmäki, T., Kettle, J., Rautkoski, H., Kokko, A., Gane, P.: Limitations of Current Formulations when Decreasing the Coating Layer Thickness of Papers for Inkjet Printing. Ind. Eng. Chem. Res. 50, 7251–7263 (2011). doi:10.1021/ie102114s

Lamminmaki, T., Kettle, J.P., Puukko, P., Gane, P.A.C., Ridgway, C.: Inkjet print quality: the role of polyvinyl alcohol in speciality CaCO3 coatings. J. Pulp Pap. Sci. 35, 137–147 (2009)

Lamminmäki, T.T., Kettle, J.P., Gane, P.A.C.: Absorption and adsorption of dye-based inkjet inks by coating layer components and the implications for print quality. Colloids Surfaces A Physicochem. Eng. Asp. 380, 79–88 (2011). doi:10.1016/j.colsurfa.2011.02.015

Lamminmäki, T.T., Kettle, J.P., Puukko, P.J.T., Ridgway, C.J., Gane, P.A.C.: Short timescale inkjet ink component diffusion: an active part of the absorption mechanism into inkjet coatings. J. Colloid Interface Sci. 365, 222–235 (2012). doi:10.1016/j.jcis.2011.08.045

Le, H.P.: Progress and trends in ink-jet printing technology. J. Imaging Sci. Technol. 42, 49–62 (1998)

Lee, H.K., Joyce, M.K., Fleming, P.D., Cameron, J.H.: Production of a single coated glossy inkjet paper using conventional coating and calendering methods, https://wmich.pure.elsevier.com/en/publications/production-of-a-single-coated-glossy-inkjet-paper-using-conventio-3, (2002)

Leij, F.J., Russell, W.B., Lesch, S.M.: Closed-form expressions for water retention and conductivity data. Ground Water. 35, 848–858 (1997)

Lindsay, J.D.: The anisotropic permeability of paper: theory, measurements, and analytical tools. (1988)

Liu, G., Fu, S., Lu, Z., Zhang, M., Ridgway, C., Gane, P.: Contrasting liquid imbibition into uncoated versus pigment coated paper enables a description of imbibition into new-generation surface-filled paper. Eur. Phys. J. E. 40, 111 (2017). doi:10.1140/epje/i2017-11600-y

López-Marzo, A.M., Merkoçi, A.: Paper-based sensors and assays: A success of the engineering design and the convergence of knowledge areas, http://xlink.rsc.org/?DOI=C6LC00737F, (2016)

Luckner, L., van Genuchten, M.T., Nielsen, D.R.: A consistent set of parametric models for the two-phase flow of immiscible fluids in the subsurface. Water Resour. Res. 25, 2187–2193 (1989). doi:10.1029/WR025i010p02187

Malla, Devisetti: Novel kaolin pigment for high solids ink jet coating. Pap. Technol. 46, 17–27 (2005)

Matilainen, K., Hämäläinen, T., Savolainen, A., Sipiläinen-Malm, T., Peltonen, J., Erho, T., Smolander, M.: Performance and penetration of laccase and ABTS inks on various printing substrates. Colloids Surfaces B Biointerfaces. 90, 119–128 (2012). doi:10.1016/j.colsurfb.2011.10.015

Modaressi, H., Garnier, G.: Mechanism of wetting and absorption of water droplets on sized paper: Effects of chemical and physical heterogeneity. Langmuir. 18, 642–649 (2002). doi:10.1021/la0104931

Oce: Specificaties Océ VarioPrint i300 - Canon Nederland, https://www.canon.nl/business-printers-and-faxes/cut-sheet-colour-printers/varioprint-i300/specifications/

Oostrom, M., Dane, J.H., Lenhard, R.J.: Fluid Contents. J.H. Dane and G.C. Topp; Soil Science Society of America , Madison, WI, United States(US). (2002)

Palakurthi, N.K., Konangi, S., Ghia, U., Comer, K.: Micro-scale simulation of unidirectional capillary transport of wetting liquid through 3D fibrous porous media: Estimation of effective pore radii. Int. J. Multiph. Flow. 77, 48–57 (2015). doi:10.1016/j.ijmultiphaseflow.2015.07.010

Patrick A. Gane, †, John P. Kettle, ‡, G. Peter Matthews, * and, Ridgway, C.J.: Void Space Structure of Compressible Polymer Spheres and Consolidated Calcium Carbonate Paper-Coating Formulations. (1996). doi:10.1021/IE950413M

Perrier, E. R.; Prakash, O.M.: Heat and vapor movement during infiltration into dry soils. Soil Sci. 124, 73–73 (1976)

Podsiadlo, P., Choi, S.-Y., Shim, B., Lee, J., Cuddihy, M., Kotov, N.A.: Molecularly Engineered Nanocomposites: Layer-by-Layer Assembly of Cellulose Nanocrystals. Biomacromolecules. 6, 2914–2918 (2005). doi:10.1021/bm050333u

Prunty, L.: Thermal Transients in Closed , Unsaturated Soil Systems. Therm. Transient. 1–4 (2002)

Prunty, L., Bell, J.: Soil Temperature Change over Time during Infiltration. Soil Sci. Soc. Am. J. 69, 766 (2005). doi:10.2136/sssaj2004.0219

Ramaswamy, S., Gupta, M., Goel, A., Aaltosalmi, U., Kataja, M., Koponen, A., Ramarao, B..: The 3D structure of fabric and its relationship to liquid and vapor transport. Colloids Surfaces A Physicochem. Eng. Asp. 241, 323–333 (2004). doi:10.1016/j.colsurfa.2004.04.023

Ramaswamy, S., Huang, S., Goel, A., Cooper, A., Choi, D., Bandyopadhyay, A., Ramarao, B. V: The 3D structure of paper and its relationship to moisture transport in liquid and vapor forms. In: 12th Fundamental Research Symposium, Oxford. pp. 1289–1311 (2001)

Ridgway, C.J., Gane, P.A.C.: Controlling the absorption dynamic of water-based ink into porous pigmented coating structures to enhance print performance. Nord. Pulp Pap. Res. J. 17, 119–129 (2002)

Ridgway, C.J., Gane, P.A.C., Schoelkopf, J.: Effect of capillary element aspect ratio on the dynamic imbibition within porous networks. J. Colloid Interface Sci. 252, 373–382 (2002). doi:10.1006/jcis.2002.8468

Rolland du Roscoat, S., Decain, M., Geindreau, C., Thibault, X., Bloch, J.-F.: Microstructural Analysis of Paper Using Synchrotron X-ray Microtomography: Numerical Estimation of the Permeability and Effective Thermal Conductivity. Appita J. J. Tech. Assoc. Aust. New Zeal. Pulp Pap. Ind. 61, 286 (2008)

du Roscoat, S.R., Bloch, J.F., Thibault, X.: Characterization of the 3D paper structure with X-ray synchrotron radiation microtomography. In: The 13th FRC Symposium, Robinson College, Cambridge. pp. 901–920 (2005)

Rosenholm, J.B.: Liquid spreading on solid surfaces and penetration into porous matrices: Coated and uncoated papers. Adv. Colloid Interface Sci. 220, 8–53 (2015). doi:10.1016/j.cis.2015.01.009

Salmas, C.E., Stathopoulos, V.N., Pomonis, P.J., Rahiala, H., Rosenholm, J.B., Androutsopoulos, G.P.: An investigation of the physical structure of MCM-41 novel mesoporous materials using a corrugated pore structure model. Appl. Catal. A Gen. 216, 23–39 (2001). doi:10.1016/S0926-860X(01)00520-8

Samuelsen, E.J., Houen, P., Gregersen, Ø.W., Helle, T.: Three-dimensional imaging of paper by use of synchrotron x-ray microtomography. J. Pulp Pap. Sci. 27, 50–53 (2001)

Sappi: The Paper Making Process, https://www.youtube.com/redirect?redir_token=VEjJPq2aJlcjBgVBNfN_Rc4CZfl8MTU0MDIxMjEyMkAxNTQwMTI1NzIy&event=video_description&v=E4C3X26dxbM&q=http%3A%2F%2Fwww.na.sappi.com%2Feducation%2Flifecycle

Schoelkopf, J., Gane, P.A.., Ridgway, C.J., Matthews, G.P.: Practical observation of deviation from Lucas–Washburn scaling in porous media. Colloids Surfaces A Physicochem. Eng. Asp. 206, 445–454 (2002). doi:10.1016/S0927-7757(02)00066-3

Schoelkopf, J., Gane, P.A.C., Ridgway, C.J., Matthews, G.P.: Influence of inertia on liquid absorption into paper coating structures. Nord. Pulp Pap. Res. J. 15, 422–430 (2000)

Schulz, V.P., Wargo, E.A., Kumbur, E.C.: Pore-morphology-based simulation of drainage in porous media featuring a locally variable contact angle. Transp. Porous Media. 107, 13–25 (2014). doi:10.1007/s11242-014-0422-4

Singh, M., Haverinen, H.M., Dhagat, P., Jabbour, G.E.: Inkjet Printing-Process and Its Applications. Adv. Mater. 22, 673–685 (2010). doi:10.1002/adma.200901141

Song, Y., Davy, C.A., Bertier, P., Troadec, D.: Understanding fluid transport through claystones from their 3D nanoscopic pore network. Microporous Mesoporous Mater. 228, 64–85 (2016). doi:10.1016/j.micromeso.2016.03.023

Suffield, S., Jokar, A.: Modeling the Flow of a Liquid Droplet Diffusing Into Various Porous Media for Inkjet Printing Applications. In: Volume 10: Heat Transfer, Fluid Flows, and Thermal Systems, Parts A, B, and C. pp. 1013–1022. ASME (2008)

Tåg, C.-M., Järn, M., Granqvist, B., Järnström, J., Peltonen, J., Rosenholm, J.B.: Influence of surface structure on wetting of coated offset papers. Holzforschung. 61, 516–522 (2007). doi:10.1515/HF.2007.073

Terzis, A., Roumeli, E., Weishaupt, K., Brack, S., Aslannejad, H., Groß, J., Hassanizadeh, S.M., Helmig, R., Weigand, B.: Heat release at the wetting front during capillary filling of cellulosic micro-substrates. J. Colloid Interface Sci. 504, 751–757 (2017). doi:10.1016/j.jcis.2017.06.027

Vikman, K., Vuorinen, T.: Water fastness of ink jet prints on modified conventional coatings. 48, 138–147 (2004)

Washburn, E.W.: The Dynamics of Capillary Flow. Phys. Rev. 17, 273–283 (1921). doi:10.1103/PhysRev.17.273

Wei, H., Ramarao, B. V: Characterization of pulp slurries using a novel drainage tester. In: Tappi Engineering Conference. pp. 517–524 (1996)

Weller, H.G.: A new approach to VOF-based interface capturing methods for

incompressible and compressible flow. OpenCFD Ltd., Rep. TR/HGW/04. (2008)

Xu, L., Zhang, W.W., Nagel, S.R.: Drop splashing on a dry smooth surface. Phys. Rev. Lett. 94, 184505 (2005). doi:10.1103/PhysRevLett.94.184505

Yarin, A.L.: DROP IMPACT DYNAMICS: Splashing, Spreading, Receding, Bouncing…. Annu. Rev. Fluid Mech. 38, 159–192 (2006). doi:10.1146/annurev.fluid.38.050304.092144

Zhao, H., Kwak, J.H., Conrad Zhang, Z., Brown, H.M., Arey, B.W., Holladay, J.E.: Studying cellulose fiber structure by SEM, XRD, NMR and acid hydrolysis. Carbohydr. Polym. 68, 235–241 (2007). doi:10.1016/j.carbpol.2006.12.013

Zhu, S., Pelton, R.H., Collver, K.: Mechanistic modelling of fluid permeation through compressible fiber beds. Chem. Eng. Sci. 50, 3557–3572 (1995). doi:10.1016/0009-2509(95)00205-J

Zoladek-Nowak, J., Milczarek, J.J., Fija-Kirejczyk, I.M., Zoldek, J., Jurkowski, Z.: Transient Thermal Phenomena during Spontaneous Water Migration in Zeolite Beds. ACTA Phys. Pol. 122, 415–418 (2012)

Product information sheet Magno TM gloss Coated fine paper available in sheets and reels for offset printing Technical specifications Print recommendations Dot area Mill certifications. 2016 (2016)

Summary and Perspectives

7 Summary and Perspectives

7.1 Summary

The goal of this thesis was to understand water-based liquid transport in thin multi-layer porous materials. Existing imaging techniques were adopted in order to make it possible to image the layers and extract their three-dimensional (3D) geometrical information. The extracted geometry was then used in pore-scale modeling tools to determine main hydraulic properties of the layer. In the next step, fluid flow in porous layer modeling was carried out using open source modeling tool, OpenFOAM. Through the work packages, appropriate suggestions, regarding the digital design of layers and used liquid as liquid phase of interest, were proposed. In addition to that, the developed modeling and experimental tools were adopted in a way that they can be applied and used in a wide range of thin porous layers applications including papers, fuel cells, membranes, and catalyst layers.

Inkjet printing is attracting much attention due to its potential in the printing of graphics, 3D objects, medical applications, paper-based diagnostic devices and electronics. The inkjet printing involves ejection of a fixed amount of liquid phase from a nozzle onto a substrate; paper in case of graphics. The ejected droplet falls due to gravity. The impinged droplet spreads and penetrates into paper due to surface tension aided flow. Capillarity is the dominant force drawing ink into the pore structure of the paper. Micro capillary penetration starts typically within 0.1 ms after the droplet arrives. In order to identify and understand the main characteristics of the paper substrates used in inkjet printing, manufacturing process of a certain coated paper sample (Magno Gloss) was described. The chosen coated paper was then used later in modeling and experimental parts of the thesis.

Thin porous coating layers are widely used in industrial products to enhance their performance or to add specific feature to the product. For instance, in case of printing industry, a thin layer of $CaCO_3$ is added to certain type of papers to control ink settlement and enhance the print quality. In chapter two, the focus is on characterization of the coating layer of printing paper. As a thin porous layer, the coating layer has an average thickness of 15 μm, with mean pore size (equivalent diameter) of 180 nm. Focus Ion Beam SEM (FIB-SEM) was used to image a 3D cube of 10 x 10 x 10 μm^3. The imaged geometry was then turned into binary format and was used as an input file for modeling works. Pore-size distribution, porosity, and connectivity of the geometry were determined using image–analyzing methods. After identifying the size of Representative Elementary Volume (REV) of the layer,

pore-morphology method was used in order to obtain capillary pressure-saturation (P_c-S) curve of the layer. Pore-morphology method is based on fitting spheres in pores of the geometry and the sphere sizes are determined using Young-Laplace equation for each applied capillary pressure. In order to calculate permeability and relative permeability values, Stokes equation was solved and coupled with results of pore morphology method. Finally, van Genuchten formula was fitted to the calculated data for capillary pressure and relative permeability and van Genuchten parameters were determined.

In chapter three, the fibrous layer of paper (and uncoated paper in general) was characterized. Since the mean pore size of such a layer is 10 μm, conventional X-ray tomography could be used as the imaging technique. Results of micro computed tomography (μCT), with resolution of 0.9 μm, was analyzed further in order to calculate pore-size distribution and porosity of the layer. With the aim of determining REV size of the layer, porosity and permeability values were determined for different domain sizes. The REV size was determined to be 400 x 400 x 150 μm^3 and porosity of the layer was 50%. The fibrous layer is a relatively anisotropic layer and the permeability values were calculated for three different directions (namely machine direction, transversal to machine direction, and in depth). P_c-S curves were obtained using pore-morphology method. Almost the same P_c-S curves for different domain sizes. In the next step, the relative permeability curves were plotted and van Genuchten parameters for different domain sizes were calculated.

The effect of wetting and non-wetting phase invasion direction was studied via determination of P_c-S curves for several configurations. Later on, the impact of compression of the paper layer during printing was considered with examination of P_c-S curves for few compression values. It was concluded that compression less than 30% does not have any significant effect on P_c-S curves.

In the last stage, an experimental observation was provided, using confocal laser microscopy images, to study water-based liquids movement in fibrous layers. It was clearly seen that the liquid follows the fibers and moves in/on fibers before filling the void space between them.

Since in a stack of thin layer porous materials, there are structural differences between layers, the fluid transport differs from layer to layer. More specifically, when the fluid reaches the interfacial region between two layers, flow direction, velocity and some other properties change. Therefore, the interfacial

region needs to be studied and characterized in order to understand flow behaviour through the layer. In chapter four, the interfacial region of the coating and fibrous layers of printing paper was studied. With the purpose of calculating the coating layer thickness, a relatively long cross section (2 mm) of the coated paper was visualized with SEM imaging technique. The distribution of the coating layer thickness was determined as a function of spatial location. Furthermore, a semi-variogram was calculated to estimate the spatial correlation function. The results showed a significant spatial variability in thickness of the coating. In the light of desirable print resolution, further analysis was done to identify if the optimum coating thickness is enough to bear the applied liquid volume during the print process.

In order to study the infiltration of a single ink droplet into the fibrous layer, a pore-scale modeling study was performed using the open-source modeling code called OpenFOAM. This was presented in chapter five. The imaged geometry obtained from μCT imaging, was used as input file, and 3D simulation of two-phase flow in a porous medium was done; the two phases were an ink-like liquid and air. The modeling was done under isothermal condition assuming laminar flow. Gravity and evaporation were neglected. The liquid droplet was placed on the surface of paper and its movement into the layer was simulated. The imbibition rate, penetration depth, and lateral spreading area were calculated and later on compared with experimental results. The experimental data were obtained by imaging of the droplet movement in the fibrous layer (the same layer was imaged and used in modeling work). The comparison between modeling and experimental work showed a good agreement and therefore it was concluded that the developed modeling tool can be used in future in order to optimize ink settling process on/into the substrate during inkjet printing. For instance, the effect of contact angle and ink properties were studied on final ink fixation status. Contact angle of zero showed the largest penetration depth compared to CA60 and CA120. In the case of CA60, the liquid moved horizontally away from the jetted location. This was even more marked in the case CA120. Such behavior is not desirable in printing as it can cause blurring and low quality print. Modeling results showed that increasing the density and viscosity, all by a factor two, had insignificant effect on spreading and penetration extent. However, it took a given volume of the heavier liquid much longer to penetrate. Slower penetration means that there is more time for the liquid to evaporate near the surface of the paper.

Chapter 7

During the experimental part of this research, it was found that the temperature of samples rise, in a range of 0.5-2°C, during liquid infiltration. Since the temperature of the paper and liquid samples were all the same, a question rose that "why temperature is rising right at the liquid front?"

In order to answer this question, a systematic experiment was designed and conducted. Several paper types were chosen. Water and salty water were selected as the liquid. For temperature measurements, an IR camera setup was used to measure temperature rise of the paper sample during liquid infiltration. The paper samples were placed on an insulated vertical stage and then liquid was provided to lower edge of the sample. An IR and a CCD camera were installed in a certain configuration, which enabled simultaneous recording of the temperature and liquid front rise. There has been a relation between sample type and amount of the temperature rise. In addition, the liquid composition was also playing a role since changing water with salty water resulted in different temperature rises.

Since the temperature rise was happening exactly at the liquid front (this was confirmed via conformity of the IR and CCD camera images), it was concluded that the wetting of solid phase, i.e. replacing the air-solid interface with liquid-solid interface was the cause of the temperature rise. The surface energy of hydrophilic solid-air interfaces is known to be much larger than that of the water-solid interface. The spontaneous imbibition of water into a medium, such as dry paper, occurs due to the net decrease in internal energies of the system mainly those of the two interfaces. The released energy is turned into heat, which causes a temperature spike of the porous medium (water plus paper fibers).

7.2 Perspectives

Pore-scale imaging and modeling provides valuable insights into processes that occur in thin porous layers. In this research, various aspects were studied but there are still many remaining open questions regarding structural change of the layers during imbibition, evaporation of the liquid during imbibition, and how to visualize the dynamic imbibition into a thin layer.

In the work presented in this PhD thesis, the sample liquid was not containing any solid particles. However, in real inkjet process, pigment-based inks are often used. The ink then contains some solid particles, which should be considered; phenomena like clogging during ink infiltration. The clogging will cause blockage of coating layer pores, which will totally change the ink infiltration patterns into the layer. This will cause different spreading area and penetration depth in comparison with a case study where the sample liquid does not contain any particles.

Another open question about ink impact on paper is the ink arrival velocity on paper. In modeling part of our work, we assumed that the ink droplet is placed on paper surface with velocity zero. Then, the infiltration of the droplet into the fibrous layer was the point of interest. However, in real printing processes, the ink droplets are ejected from the dispenser, which is normally located higher than paper surface. The ink droplet falls onto the paper surface after traveling a distance between the dispenser and the paper substrate. Therefore, the liquid droplet arrives on paper surface with a velocity, which should be considered in modeling works. Hence, in further studies, the developed modeling tools in this thesis should be extended by adding the effect of impact velocity.

In addition to that, another important phenomenon, especially in the case of uncoated paper, is the evaporation of liquid. The water-based ink used in inkjet printing contains a significant amount of water and some other solvents, which are volatile. Thus, from the moment that a droplet leaves the dispenser, evaporation starts and the liquid part of the droplet starts to vaporize. This occurs even when the liquid enters the porous layer and is located inside pores. Therefore, the inclusion of evaporation in future modeling work is advised.

As previously mentioned in chapter one, the surface of paper fiber (and standard coating) is naturally anionic, i.e. negatively charged. Inkjet ink dye is also commonly anionic, and so also negatively charged. To enhance fixation of the dye the fiber matrix is often treated with cationic starch (or the coating on paper is

converted to have a cationic charge) to capture the dye. Consequently, for a comprehensive understanding of ink fixation on surface of printing paper, the charge interaction should be considered. This was out of focus of this thesis since here we just used water-based ink (pH7) and the paper surface charge was not changed.

As stated in the beginning of this section, structural changes could be considerable depending on the substrate type and the amount of liquid provided. For instance, in the case of cellulose fibers, if their surface is not treated chemically and enough liquid is provided to them, they start to swell. As a result, the diameter of fibers increases and may cause paper deformation. However, the focus of this thesis was on single droplet imbibition into the fibrous layer. As the size of droplet was very small (about 200 pL) in comparison with the size of one single fiber, the swelling was negligible. In cases that the amount of liquid is substantially comparable with the size of fibers (and fibrous layer), structural changes due to swelling become important and should be included in the modeling works.

Finally, the dynamic imbibition visualization, which was done in this work on fibrous layer, is not applicable to the coating layer. The coating layer has pores in the range of few tens of nanometers and the resolution of the confocal microscopy is not high enough to capture any dynamic information there. Similarly, μCT facilities currently available do not have enough resolution to image liquid infiltration into the coating layer. But in case a technique eventually becomes available for capturing details of ink movement inside the coating layer, then the modeling work can lead to better understanding of the imbibition process and it would be possible to perform optimization studies in order to achieve a better print quality.

8 Samenvatting

Deze dissertatie beschrijft het onderzoekswerk en de resultaten voor een verbeterd begrip van transport van waterige vloeistoffen door meerdere lagen dun poreus materiaal. Hiervoor is een multidisciplinaire ‘workflow’ ontwikkeld. Bestaande beeldvormingstechnieken zijn waar nodig aangepast, waardoor het mogelijk werd om de poreuze lagen in beeld te brengen en de driedimensionale geometrie te karakteriseren. De gevonden 3D structuur is vervolgens toegepast in porie schaal computermodellen waarmee de geometrische eigenschappen in verder detail bestudeerd konden worden. Ook de voornaamste hydraulische eigenschappen konden per laag worden vastgesteld. Vervolgens zijn vloeistofstromen door de poreuze lagen gemodelleerd met behulp van het vrij toegankelijke (‘open access’) software pakket OpenFOAM.

De ontwikkelde multidisciplinaire workflow is geschikt voor het analyseren van dunne poreuze lagen, bijvoorbeeld papier, brandstofcellen, membranen en katalysatoren. Het onderzoek beschreven in deze dissertatie concentreert zich op papier en de coating van papier, met inktjet printen als toepassing.

Inktjet printen staat in de belangstelling wegens de toepassingen bij hoge resolutie printen, 3D printen, medische applicaties en het printen van elektronische apparaten rechtstreeks op papier, waaronder diagnostieke elektronica. Het inktjet principe begint bij het mondstuk van waaruit een druppel inkt met specifiek volume zich richting het papier begeeft. De druppel valt richting het papier door de zwaartekracht. Op het papier verspreidt de druppel zich over het oppervlak en tegelijkertijd dringt het door in het papier. Papier bestaat uit willekeurig gestapelde vezels met veel poriën tussen de vezels. Daardoor kan de inkt eenvoudig het papier in worden getrokken door capillaire krachten. De micro-capillaire penetratie van inkt in papier begint zo’n 0.1 milliseconde nadat de druppel het papier heeft geraakt.

Om de resolutie van inktjetprinters te vergroten, wordt er een coating ($CaCO_3$) aangebracht op het papier. Deze coating heeft een veel kleinere porie-grootte, waardoor de laterale spreiding wordt beperkt. De stipjes blijven kleiner en daardoor de resolutie hoger. In deze dissertatie is uitgegaan van één type gecoat papier, Magno Gloss. Meer details over inktjet printen staan in het eerste hoofdstuk.

In het tweede hoofdstuk ligt de focus op het karakteriseren van de coatinglaag. De coating is een dunne laag met een gemiddelde dikte van 15 µm en een gemiddelde poriediameter van 180 nm. De driedimensionale structuur van een klein stukje coating (10 x 10 x 10 μm^3) werd in beeld gebracht door de Focused Ion

Beam – Scanning Electron Microscope (FIB-SEM). De beelden zijn verwerkt tot binaire data (2 fases: Vaste materie en tussenliggende poriën). De binaire data is vervolgens gebruikt voor computermodellen. Beeldanalyse resulteerde in een porie grootte verdeling, de porositeit en de onderlinge verbondenheid van de poriën. Allereerst is een Representatief Elementair Volume (REV) vastgesteld. Dit is een minimaal volume waarbij kleine lokale variaties worden uitgemiddeld. De "Pore-morphology" methode is toegepast om de capillaire druk-saturatie (PC-S) kromme van de laag te bepalen. Deze methode probeert de grootst mogelijke bollen in de poriën te passen. Met behulp van de Young-Laplace vergelijking kan de capillaire druk worden berekend op basis van de gevonden maximale boldiameter. Om het mogelijk te maken om de permeabiliteit en de relatieve permeabiliteit te bepalen, zijn de numerieke Stokes oplossing gekoppeld aan de Pore-morphology methode in combinatie met de wet van Darcy. Tot slot is de Van Genuchten vergelijking passend gemaakt op de verkregen data, waarmee de Van Genuchten parameters zijn bepaald.

In hoofdstuk drie staat beschreven hoe de vezelstructuur van lagen papier (zonder coating) is gekarakteriseerd. De gemiddelde porie-grootte van zulke lagen is 10 µm. Daardoor is het mogelijk om standaard X-ray tomografie (oplossend vermogen 0.9 µm) te gebruiken voor de beeldvorming. De resultaten van micro-CT (µCT) zijn geanalyseerd om de porie-grootte verdeling en de algemene porositeit te bepalen. Om een REV te bepalen, zijn de porositeit en de permeabiliteit bepaald voor verschillende domein groottes. De gevonden REV van papier is 400 x 400 x 150 µm3 met een porositeit van 0.5 (50%). Omdat de vezellagen betrekkelijk heterogeen zijn, is de permeabiliteit in drie richtingen bepaald (fabricagerichting, haaks op de fabricagerichting en in de diepte). De bepaling van de Pc-S krommes is gedaan met behulp van de Pore-morphology methode. De berekeningen van de Pc-S krommes voor de verschillende domeingroottes resulteerden in vrijwel overeenkomende krommes.

De invloed van fases die bevochtigen of juist niet bevochtigen en de stroomrichting zijn bepaald via de Pc-S kromme voor verschillende configuraties. In een vervolgstap is de invloed van compressie onderzocht door bestudering van de Pc-S krommes bij bepaalde compressiewaarden. Het is gebleken dat een compressie van minder dan 30% geen significant effect heeft op de Pc-S kromme.

Naast de numerieke karakterisering op basis van X-ray beelden, zijn er ook experimentele observaties gedaan met behulp van confocaal microscopie, waarmee de beweging van waterige vloeistoffen door de vezelstructuur kon worden gevolgd.

Het was duidelijk waarneembaar dat de vloeistof eerst de individuele vezels volgde, alvorens de poriën te vullen.

In stapelingen van verschillende dunne lagen poreuze materialen kan het transport van vloeistoffen per laag en richting verschillen door de structurele verschillen van elke laag. In het bijzonder zijn daarbij de grensvlakken tussen twee lagen interessant, omdat daar de stroomrichting, snelheid en andere eigenschappen van de vloeistof veranderen. In hoofdstuk vier is daarom het grensvlak bestudeerd tussen de coating en de vezel structuur van papier. Een dwarsdoorsnede van 2 mm breed is bekeken met de SEM om de gemiddelde dikte van de coating te kunnen vaststellen. De verdeling van de dikte van de coating is bepaald als functie van plaats. Bovendien is een semi-variogram berekend voor een ruimtelijke correlatie functie. De resultaten tonen aan dat er een significante variatie bestaat in dikte. Indachtig de resolutie van de printer is verdere analyse gedaan om te bepalen of de coating dik genoeg is om de vloeistof van de printer te kunnen bevatten. Daarvoor is een OpenFOAM computersimulatie opgezet om de infiltratie van een enkele druppel inkt in de vezellaag te bestuderen. Dit staat beschreven in hoofdstuk vijf. De µCT beelden leverden de geometrie van het model en een 3D simulatie van twee-fase stroming door poreuze materialen is uitgevoerd. De twee fases zijn een inktachtige vloeistof en lucht. Het dynamische model gaat uit van isothermische condities en een niet-comprimeerbare laminaire stroming. Zwaartekracht en verdamping zijn verwaarloosbaar.

De vloeistofdruppel is op het papieroppervlak geplaatst en de beweging het papier in werd gevolgd in de tijd. De imbibitiesnelheid, de penetratiediepte en de laterale spreiding zijn vastgelegd ter vergelijking met experimentele observaties. De experimentele observaties zijn verkregen door het in beeld brengen van de beweging van kleine druppels door een reeds eerder beschreven laag papier. De experimentele resultaten zijn goed vergelijkbaar met de simulaties. Daarmee is aangetoond dat de ontwikkelde simulatie geschikt is om in de toekomst onderzoek te doen naar het optimaliseren van het afzetten van inkt in papier voor de invloed van verschillende eigenschappen van inkt op de verdeling van inkt in het papier. Als voorbeeld is de invloed van de contacthoek onderzocht.

Een contacthoek van 0° resulteerde in de grootste penetratie diepte in vergelijking tot een hoek van 60° en 120°. De vloeistof bewoog over het coatingoppervlak horizontaal weg van de jet in het geval van een contacthoek van 60°. Dit effect was nog significanter bij een hoek van 120°. Dit is onwenselijk in het geval van printen, omdat daarmee geprinte afbeelding minder scherp wordt.

Computermodellen tonen aan dat een grotere dichtheid en viscositeit (beide een factor 2 groter) geen significant effect hebben op de laterale spreiding en penetratiediepte. Echter, eenzelfde volume met grotere dichtheid heeft veel meer tijd nodig om de coating binnen te dringen, waardoor er meer tijd aan het oppervlak is voor het verdampen.

Tijdens het experimentele werk bleek dat de temperatuur van de papieren monsters stijgt gedurende de vloeistofinfiltratie, ondanks dat zowel de vloeistof en het papier dezelfde temperatuur hadden. Daardoor kwam de vraag op: “waarom stijgt de temperatuur bij een vloeistoffront?”

Systematische experimenten zijn opgezet en uitgevoerd om deze vraag te beantwoorden. Verschillende types papier en verschillende variaties vloeistof (kraanwater, zout water) zijn getest, waarbij de temperatuur contactloos werd geregistreerd. Het is gelukt om de temperatuur te meten met behulp van een infrarood camera tijdens de infiltratie van vloeistof. Papieren monsters werden op een geïsoleerde houder geplaatst, waarna een vloeistof van onderaf werd aangevoerd. De infrarood en CCD camera’s waren dusdanig gericht dat ze gelijktijdig het vloeistoffront konden volgen.

De temperatuurstijging kon worden gerelateerd aan het type papier gedurende de infiltratie. Ook de samenstelling van de vloeistof speelt een rol. Omdat de temperatuurstijging plaats vindt precies op het voortbewegende front, is geconcludeerd dat het vervangen van een lucht-vaste stof grensvlak door een vloeistof-vaste stof grensvlak de oorzaak is van de temperatuurstijging. Het is bekend dat de oppervlakte energie van lucht-vaste stof veel groter is dan die van water-vaste stof. De spontane imbibitie van water in een medium, zoals droog papier, gebeurt door een netto reductie van de oppervlakte energieën van die drie grensvlakken (lucht-vloeistof is het derde grensvlak). De vrijgekomen energie komt vrij in de vorm van warmte.